

Contrails

CONFIDENTIAL

SELF-ADAPTIVE FLIGHT CONTROL BY MULTIVARIABLE PARAMETER IDENTIFICATION

*P. P. SHIPLEY
A. G. ENGEL, JR.
J. W. HUNG*

NORTH AMERICAN AVIATION, INC.

FOREWORD

This report was prepared by the Space and Information Systems Division of North American Aviation, Inc., under Air Force Contract AF 33(615)-1882, Refine Process Identification and Controller Synthesis Techniques. The contract was initiated under Project No. 8225, Task No. 822501. The work was administered under the direction of the Control Elements Branch, Flight Control Division, AF Flight Dynamics Laboratory, Research and Technology Division. Mr. Charles J. Harmon and Captain Robert Rankine were the project engineers.

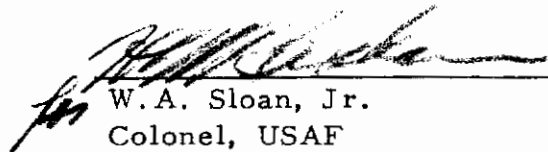
This report covers work conducted from 1 June 1964 to 1 July 1965 under the direction of Mr. K. W. Nielsen, Program Manager.

The process identification technique defined in this report was developed by Mr. P. P. Shipley, Project Engineer and principal contributor. Significant contributions were also made by Mr. A. G. Engel, Jr. on the analysis and simulation and Dr. J. W. Hung on the error analysis and digital computer evaluation. Acknowledgement is also made to Messrs. R. J. Gibson and Y. N. Chang for valuable assistance. Special thanks is given to Miss M. E. Shanhart. All contributors are from the Information Systems Division of S&ID, Downey, California.

This report is identified at the Space and Information Systems Division of North American Aviation, Inc., under publication number SID 65-697.

Manuscript of this report released by the authors May 1965 for publication as an RTD technical report.

This technical report has been reviewed and is approved.


W. A. Sloan, Jr.
Colonel, USAF
Chief, Flight Control Division
AF Flight Dynamics Laboratory

ABSTRACT

Described in this report is an approach to adaptive flight control which uses outputs from a relatively simple parameter tracking computer to adjust flight control system parameters. A unique characteristic of the parameter tracking mechanism is the ability to function with almost any type of disturbance as an input, including normal pilot activity, wind turbulence, and oscillations due to control loop instability. This may be accomplished without special test inputs or limit cycles.

The ability to function with almost any type of input is a direct consequence of the fact that the airframe is represented in its true form as a multivariable system, thereby accounting for all inputs and outputs. One of the most common reasons for failure of adaptive flight control systems to function properly is that wind turbulence is ignored in performing identification of airframe dynamics. Even if this problem could be ignored, many approaches would still be limited in application because of the difficulty involved in extending basic concepts to coupled axes, such as the lateral axes of an airframe.

Stability of the parameter adjustments is verified analytically, and simulation results show that convergence is smooth and fast (about five seconds) in all axes.

Contrails

CONTENTS

Section		Page
1	Introduction	1
2	The Problem of Identifying Vehicle Dynamics	3
3	The S&ID Approach to Parameter Identification	7
	Application to the Pitch Axis	8
	Parameter Identification Refinements	18
4	Pitch Axis	21
	System Design	21
	Analog Computer Simulation Results	49
5	Lateral Axes	69
	Theoretical Justification for Treating Loops Separately	69
	Analog Computer Simulation Results	81
6	Digital Implementation Requirements	93
	Computer Requirements	93
	Stability Analysis	96
	References	109
	Appendixes	
	I. Optimum Correlation Time	111
	II. A Comparative Treatment of Certain Techniques for Parameter Identification Based on the State Space Approach	113
	III. Noise Analysis	131

ILLUSTRATIONS

Figure		Page
1	Pitch Axis with Single Input	3
2	Pitch Rate Damper Configuration	4
3	Signal Flow Equivalent of Equation (13)	10
4	Geometrical Interpretation of Equation (18)	12
5	Implementation of Equation (16)	13
6	Pitch Axis AGC	19
7	Pitch Axis Input Filters	20
8	Asymptotic Bode Gain of Typical Aircraft Pitch Axis Dynamics	22
9	Pitch SAS Block Diagram	27
10	$G_2G_3P(s)$ Gain Ratio, FC 5	28
11	$G_2G_3P(s)$ Gain Ratio, FC 13	29
12	$G_2G_3P(s)$ Gain Ratio, FC 17	30
13	$G_2G_3P(s)$ Gain Ratio, FC 28	31
14	$G_2G_3P(s)$ Gain Ratio, FC 32	32
15	Argument $G_2G_3P(s)$, FC 5	33
16	Argument $G_2G_3P(s)$, FC 13	34
17	Argument $G_2G_3P(s)$, FC 17	35
18	Argument $G_2G_3P(s)$, FC 28	36
19	Argument $G_2G_3P(s)$, FC 32	37
20	Bode Gain/Phase $G_2G_3P(j\omega)$, FC 5	38
21	Bode Gain/Phase $G_2G_3P(j\omega)$, FC 13	39
22	Bode Gain/Phase $G_2G_3P(j\omega)$, FC 17	40
23	Bode Gain/Phase $G_2G_3P(j\omega)$, FC 28	41
24	Bode Gain/Phase $G_2G_3P(j\omega)$, FC 32	42
25	SAS Autopilot Root Locus, FC 5	43
26	SAS Autopilot Root Locus, FC 13	44
27	SAS Autopilot Root Locus, FC 17	45
28	SAS Autopilot Root Locus, FC 28	46
29	SAS Autopilot Root Locus, FC 32	47
30	Typical Pitch SIDAC Response, FC 17, SIDAC Parameters and Model Error.	50
31	Typical Pitch SIDAC Response, FC 17, Aircraft Variables and Pitch Damper Adaptive Gain.	51
32	Typical X-15 Flight Conditions	52
33	Typical X-15 Flight Conditions in Terms of SIDAC Parameters	53
34	SIDAC Block Diagram	55

Figure		Page
35	Pitch SIDAC Identification Times	56
36	Identification on Pilot Inputs	58
37	Effects of Input Filtering on Identification	59
38	Effects of Sensor Noise	60
39	Effects of Real Sensors	61
40	Effects of Pilot Inputs	63
41	Typical Response Time Variation with Wind Turbulence Level for Three SIDAC Configurations	65
42	Typical Identification Response with SGN Error SIDAC	66
43	Basic Control System for Lateral Axes	73
44	Roll/Yaw Damper Gain Interaction at Crossover (FC 28)	75
45	Roll Stability Augmentation System	82
46	Yaw Stability Augmentation System	83
47	Typical Roll SIDAC Response FC 21	84
48	Typical Yaw SIDAC Response FC 21	87
49	Roll SIDAC Identification Times	90
50	Yaw SIDAC Identification Times	91
51	Pitch Axis Flow Chart	94
52	Rectangular Integration Based on Past Input	100
53	Rectangular Integration Based on Present Input	100
54	Trapezoidal Integration	100
55	Integrator	105
56	Linear Input Prediction	105
57	Root Locus for Rectangular Integration with Input Prediction	105
58	Analog Counterpart of Equation (II-2a)	114
59	Analog Counterpart of Equation (II-4a)	115
60	Model Equivalent to Equation (II-37)	121
61	Contours of Constant Mean-Squared Error	124
62	Rotated and Translated E Contours	125
63	E Contours After Scaling	125
64	SIDAC Model (Pitch Axis)	132

SYMBOLS

φ, θ, ψ	Eulerian roll, yaw, pitch angles
$\dot{\varphi}, \dot{\theta}, \dot{\psi}$	Eulerian roll, yaw, pitch rates
p, q, r	body roll, yaw, pitch rates
$\delta_a, \delta_e, \delta_r$	aileron, elevator, rudder deflections
$n(t), w_g$	wind gust or turbulence
$D(s), G(s), H(s),$ $T(s), F(s), P(s)$	transfer functions (see text)
a_z, a_y	vertical, lateral accelerations
α	angle of attack with respect to smooth air
α_g	angle of attack due to wind turbulence
$\alpha_p = \alpha + \alpha_g$	total angle of attack
β	total sideslip
β_g	sideslip due to wind turbulence
$\hat{p}, \hat{q}, \hat{r}, \hat{\alpha}_p, \hat{\beta}, \hat{a}_z, \hat{a}_y$	outputs of sensors measuring $p, q, r, \alpha_p, \beta, a_z, a_y$ respectively
l_z, l_x, l_b	distance forward of C. G. for mounting a_z, a_y, β sensors
$\varphi_o, \theta_o, \alpha_o$	steady state roll angle, pitch angle, angle of attack
x_i	i'th input to SIDAC model
b_i^*	gain of i'th channel in SIDAC model
b_i	correct setting of b_i^*

e	output (error) of SIDAC model
E	mean-squared value of e
V	Lyapunov function
K_q, K_p, K_r	adaptive gain in pitch, roll, yaw control loops
K_{q_m}, K_{q_n}	maximum stable, nominal ($\frac{1}{2} K_{q_m}$) value of K_q
K_i	gain of i'th parameter adjustment loop
$M_\delta, 1/T_a, \zeta_a, \omega_a, \sigma_a/c$	pitch short period gain, zero, damping ratio, frequency, closed loop damping
$\dot{\theta}_M$	output of pitch rate command prefilter
n_{δ_e}	noise in δ_e sensor
K_M	AGC gain
V_c	integrator clamping voltage
L'_s, N'_s	modified stability derivatives defined by equation (57).

Contrails

SECTION 1

INTRODUCTION

An approach to adaptive flight control has been developed (Reference 1) which promises to be of fundamental importance in overcoming basic deficiencies common to earlier techniques. Outputs from a relatively simple parameter tracking computer are used to adjust parameters in a flight control system, thereby compensating for variations in airframe dynamics. This is accomplished without special test inputs (Reference 2) or limit cycles (Reference 3). Results obtained from past simulations indicate that the parameter tracking computer is capable of rapidly and accurately identifying airframe dynamics from conventional sensor data using normal airframe disturbances. These disturbances may include any or all of the following:

1. Pilot activity
2. Wind turbulence
3. Guidance loop commands
4. Oscillations due to control loop instability
5. Special test inputs

The unique characteristics of the S&ID adaptive control (SIDAC) system is its ability to function with almost any type of disturbance. This is a direct consequence of the fact that the airframe is represented in its true form as a multivariable system, thereby accounting for all inputs and outputs. The multivariable approach is easily accomplished by the simple expedient of directly utilizing the basic differential equations of motion, rather than working in terms of transfer functions which are valid only for single input/single output systems. Although transfer functions are useful models of system dynamics for control loop design, the complete differential equations of motion are required for effective parameter identification.

In contrast to the S&ID approach, each of various approaches to the adaptive flight control problem developed to date has utilized only one type of disturbance to identify or otherwise infer some aspect of vehicle dynamics as a basis for initiating control action. In such cases, when two or more types of disturbance exist simultaneously, all but one are treated as noise to be removed by filtering, or by statistical averaging or correlation. Unfortunately, an airframe is normally subjected to more than one type of

Manuscript released by authors 10 June 1965 for publication as an RTD Technical Documentary Report.

disturbance for a substantial portion of the flight regime. Under these conditions, ignoring all but one type of disturbance may result in serious degradation of performance.

In general, one of the most common reasons for failure of adaptive flight control systems to function properly is that wind turbulence is ignored in performing identification of airframe dynamics. It has been demonstrated in flight tests (Reference 2) that removing the effects of turbulence by correlation of the input and output requires harsh commands and excessive averaging time. These conclusions were later verified analytically by Lindenlaub and Cooper (Reference 4), showing that even an ideal identifier could do no better (Appendix I).

By using the S&ID approach to adaptive control, parameter tracking may be performed effectively, using data obtained from wind turbulence alone or in the presence of normal command inputs, without the necessity of special test inputs. When correlation is used, turbulence presents a formidable problem, even with large test inputs.

Even if the turbulence problem could be ignored, most approaches to parameter identification would still be limited in application because of the difficulty involved in extending basic concepts to coupled axes. However, the treatment of coupled axes is considerably simplified by using the basic differential equations of motion. This allows the lateral airframe dynamics to be described by multivariable relations, involving wind turbulence, rudder deflection and aileron deflection as system inputs, and roll, yaw, lateral acceleration, and sideslip as system outputs. Under these conditions, data sensing and processing problems are minimized, while retaining a correct and adequate mathematical representation of airframe dynamics.

Although additional sensors are required for mechanization of a parameter identification flight control system by the multivariable approach, in many cases the additional sensors may already be on board the aerospace vehicle fulfilling other data requirements, such as outer loop feedback control or energy management.

SECTION 2

THE PROBLEM OF IDENTIFYING VEHICLE DYNAMICS

Most approaches to the problem of adaptive control of aerospace vehicles are based upon single variable concepts. Usually, the problem requires an estimate of system dynamics from measurements of a single input and a single output. This is illustrated in Figure 1 for the pitch axis.



Figure 1. Pitch Axis with Single Input

The vehicle dynamics are usually represented in linear fashion, either as a transfer function, or as an impulsive response.

If the airframe is disturbed by wind turbulence, there exists a component of the output which is not due to the measured input. This component is treated as contaminating noise which must be averaged out by correlation. Successful identification requires existence of some input which is not correlated with the turbulence, and which disturbs the airframe severely enough to permit rapid averaging of the contaminated data. Such an input must be derived from one of the following two sources:

1. Normal maneuvering commands required to successfully accomplish a mission
2. Special test inputs.

It is not possible to rely upon maneuvering commands because they are frequently of insufficient amplitude to provide rapid and accurate identification in the presence of moderate or heavy turbulence. Worse yet, when a smooth trajectory is flown, maneuvering commands may almost disappear or become highly correlated with turbulence. For example, if a pilot injects commands to maintain steady flight in turbulent air, his actions are a direct consequence of motion due to turbulence. The same thing is true of information fed back through a control loop, such as the pitch rate damper illustrated in Figure 2.

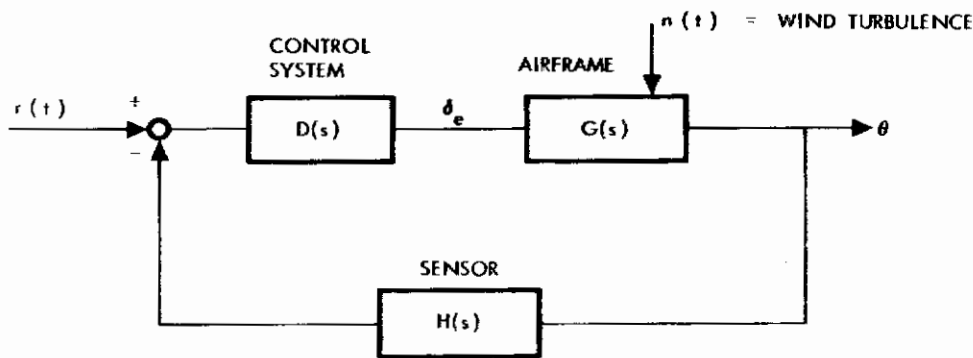


Figure 2. Pitch Rate Damper Configuration

If $r(t)$ is nonzero and $n(t)$ is zero, Figure 2 yields the airframe transfer function $G(s)$ without difficulty as equation (1).

$$\dot{\theta}/\delta_e = G(s) \quad (1)$$

However, if $r(t)$ is zero and $n(t)$ is nonzero, the only input to the system is wind turbulence. Equation (2) describes the relationship between control surface deflection and pitch rate.

$$\delta_e = -D(s)H(s)\dot{\theta} \quad (2)$$

The apparent airframe transfer function is given by equation (3).

$$\dot{\theta}/\delta_e = -1/D(s)H(s) \quad (3)$$

This transfer function is independent of the vehicle dynamics represented by $G(s)$. Hence, in this case, it is impossible to deduce anything about changes in vehicle dynamics from the relationship between control deflection and pitch rate.

If both inputs are present simultaneously, the results will be some compromise between equations (1) and (3) unless the effect of noise $n(t)$ is eliminated by some means, such as correlation. In any case, it is clear that signals obtained from a feedback loop do not necessarily help solve the identification problem.

Referring to the second alternative (special test inputs), attempts were made (Reference 2) to perform identification based upon special test inputs. The general result has been that test inputs of sufficient amplitude to provide rapid and accurate identification produced objectionable airframe motion.

As a result of additional studies (Reference 4) (see Appendix I) a definite lower bound on identification time was discovered, and the results

Contrails

were just as discouraging as those obtained during flight tests. Moreover, it was learned that the correlation technique used in the flight test program provided the optimum processing of available sensor data (i. e., the identification time, while being too long to be practical, was as short as possible using correlation techniques).

Contrails

SECTION 3

THE S&ID APPROACH TO PARAMETER IDENTIFICATION

In view of the severe shortcomings of any approach to identification of airframe dynamics based upon correlation, an alternate solution was required. Reflection on the foregoing observations led to the conclusion that the information content obtained from measurements made upon a single input and a single output was totally inadequate. The logical solution was to obtain data from additional sensors, and dispense with correlation entirely. This led to a multivariable approach (Reference 1) to parameter identification.

Using the multivariable approach, selection of additional variables is not critical, but they should be easily sensed. Data already required for other control functions, or for other applications such as energy management, are desirable. Implementation of the multivariable approach proceeds as follows:

1. The differential equations describing airframe motion are written in conventional form.
2. All inputs and outputs which are not easily measured are eliminated algebraically. The result is one or more equations involving only measurable quantities. All terms are transferred to one side of the equal sign, obtaining an expression equal to zero for each equation.
3. An error expression of the same form as the foregoing expression is defined. If the unknown coefficients of the error expression are adjusted to their true values, the error becomes zero.
4. The coefficient of each of the measured variables is adjusted automatically by a standard gradient approach to drive the error toward zero. As the error approaches zero, the parameters approach the correct values.
5. The parameter values are then used to adjust gain and compensation of the control loop. One technique for gain adjustment utilizes the fact that the product of the high frequency gain of the control loop and the control surface effectiveness is approximately constant at

the stability boundary. Because one of the parameters obtained in the identification is directly proportional to control surface effectiveness, gain times surface effectiveness can be maintained at some percentage of critical value. In pitch axis simulations (Section 4), maximum damping was obtained at all flight conditions if loop gain was about 50 percent of critical.

APPLICATION TO THE PITCH AXIS

The five steps in implementation will now be described in detail for the pitch axis.

Write Equations of Motion

Assuming constant airspeed, the pitch stability axis equations of motion are given by equations (II-63) of Reference 5 essentially as follows:

$$a_z = U_0 (\dot{\alpha} - \dot{\theta}) + g \sin \theta_0 = U_0 Z_w \alpha_p + Z_{\delta_e} \delta_e \quad (4a)$$

$$\dot{q} - M_q q - U_0 (M_w \dot{\alpha} + M_w \alpha_p) = M_{\delta_e} \delta_e \quad (4b)$$

where

$$\alpha_p = \alpha + \alpha_g \quad (4c)$$

α = angle of attack with respect to smooth air

α_g = angle of attack due to wind turbulence

α_p = total measurable angle of attack

The output from an angle of attack sensor mounted a distance ℓ_a ahead of the center of gravity is given by equation (5).

$$\hat{\alpha}_p = \alpha_p - \ell_a q / U_0 \quad (5)$$

The output from an accelerometer mounted a distance ℓ_z ahead of the center of gravity is given by equation (6).

$$\hat{a}_z = a_z - \ell_z \dot{q} \quad (6)$$

Substituting equations (5) and (6) into equations (4a) and (4b) yields equations (7a) and (7b), respectively.

$$\begin{aligned}\hat{a}_z + \ell_z \dot{q} &= U_0 (\dot{\alpha} - \dot{\theta}) + g \theta \sin \theta_0 \\ &= Z_w (U_0 \hat{\alpha}_p + \ell_a q) + Z_{\delta_e} \delta_e\end{aligned}\quad (7a)$$

$$\dot{q} - (M_q + \ell_a M_w) q - U_0 (M_w \dot{\alpha} + M_w \hat{\alpha}_p) = M_{\delta_e} \delta_e \quad (7b)$$

Eliminate All Except Measurable Quantities

The only variable in equations (7a) and (7b) which cannot be sensed directly is $\dot{\alpha}$. Elimination between these two equations yields equation (8) in terms of measurable quantities only.

$$\begin{aligned}\dot{q} - (M_q + \ell_a (M_w + Z_w M_w)) q - U_0 M_w \dot{\theta} + M_w g \theta \sin \theta_0 \\ - U_0 (M_w + Z_w M_w) \hat{\alpha}_p - (M_{\delta_e} + Z_{\delta_e} M_w) \delta_e = 0\end{aligned}\quad (8)$$

Equation (8) is in a suitable form for parameter identification. However, it is usually possible to make simplifications. Assuming small steady state roll angle, equation (II-38) of Reference 5 yields equation (9).

$$\dot{\theta} = q \cos \phi_0 - r \sin \phi_0 \approx q \quad (9)$$

The stability derivative M_w arises due to downwash from the wing to the tail, and is normally quite small, so that θ need not be measured. Equation (8) now simplifies to equation (10).

$$\begin{aligned}\dot{q} - (M_q + U_0 M_w + \ell_a (M_w + Z_w M_w)) q - U_0 (M_w + Z_w M_w) \hat{\alpha}_p \\ - (M_{\delta_e} + Z_{\delta_e} M_w) \delta_e = 0.\end{aligned}\quad (10)$$

For convenience, the various quantities in equation (10) are redefined as follows:

$$x_0 = \dot{q}, \quad x_1 = \hat{\alpha}_p, \quad x_2 = q, \quad x_3 = \delta_e \quad (11a, b, c)$$

$$b_1 = -U_0 (M_w + Z_w M_w) \quad (11d)$$

$$b_2 = - (M_q + U_0 M_w + \ell_a (M_w + Z_w M_w)) = - (M_q + U_0 M_w) + \ell_a b_1 / U_0 \quad (11e)$$

$$b_3 = - (M_{\delta_e} + Z_{\delta_e} M_w) \quad (11f)$$

Equation (10) may now be written as equation (12).

$$x_0 + \sum_i b_i x_i = 0 \quad (12)$$

Write Error Expression

During parameter adjustment, the current estimate of the i 'th parameter b_i will be designated by b_i^* . An error is defined by equation (13).

$$e = x_0 + \sum_i b_i^* x_i \quad (13)$$

Subtracting equation (12) from (13) yields (14).

$$e = \sum_i (b_i^* - b_i) x_i \quad (14)$$

An analog model capable of computing the error from equation (13) appears in Figure 3.

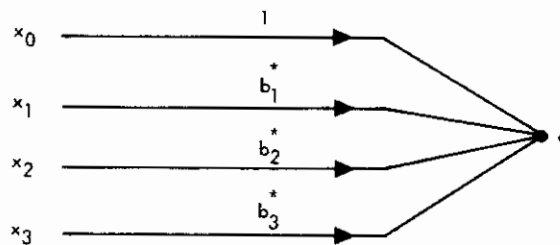


Figure 3. Signal Flow Equivalent of Equation (13)

Parameter Adjustment

The parameter in this circuit could be adjusted manually, simply by feeding the error into an rms voltmeter and adjusting each parameter in turn to obtain a minimum. After several repetitions, a null should be obtained.

From equation (12), it is seen that the four inputs to the model in Figure 3 form a linearly dependent set. However, any three of these four

variables are linearly independent except in special cases. Hence, convergence of the error to zero normally requires that the coefficient of every input variable in equation (14) approach zero. Equating each coefficient to zero requires that the i 'th estimated coefficient b_i^* converge to the true value b_i .

Automatic coefficient adjustment is achieved with a gradient technique due to Clymer (Reference 6) to reduce squared error. Differentiating squared error by the chain rule yields equation (15).

$$\frac{d}{dt} e^2 = 2e\dot{e} = 2e \left(\sum_i \frac{\partial e}{\partial b_i^*} \dot{b}_i^* + \frac{\partial e}{\partial t} \right) = 2e \left(\sum_i x_i \dot{b}_i^* + \frac{\partial e}{\partial t} \right) \quad (15)$$

Adjusting the parameters will not directly affect the final term in equation (15). However, it is possible to make the other terms negative, thereby tending to reduce squared error. One way to accomplish this is to implement steepest descent using equation (16), where K is a positive constant.

$$\dot{b}_i^* = -K \partial e^2 / \partial b_i^* = -2Ke \partial e / \partial b_i^* = -2Kex_i \quad (16)$$

Substituting equation (16) into equation (15) yields equation (17).

$$\frac{d}{dt} e^2 = -4Ke^2 \sum_i x_i^2 + 2e \partial e / \partial t \quad (17)$$

If it were not for the final term in equation (17), convergence of squared error toward zero could be assured. This would show that the parameter adjustment scheme was stable.

Miller (Reference 7) has shown that stability of the adjustments may be verified using Lyapunov's Second Method. A Lyapunov function V is defined in terms of deviations of the estimated parameters from the true parameters by equation (18).

$$V = \sum_i (b_i^* - b_i)^2 \quad (18)$$

If the rate of change of V with respect to time can be made negative or zero at all times, the adjustments are said to be stable in the sense of Lyapunov. Differentiating equation (18) with respect to time yields equation (19).

$$\dot{V} = 2 \sum_i (b_i^* - b_i) (\dot{b}_i^* - \dot{b}_i) \quad (19)$$

Substituting the control law from equation (16) into (19) yields equation (20).

$$\dot{V} = -4Ke \sum_i (b_i^* - b_i) x_i - 2 \sum_i (b_i^* - b_i) \dot{b}_i \quad (20)$$

Substituting equation (14) into (20) yields equation (21).

$$\dot{V} = -4Ke^2 - 2 \sum_i (b_i^* - b_i) \dot{b}_i \quad (21)$$

If the true parameters are stationary, \dot{V} is always negative whenever any error exists in the model, and the adjustments are stable.

A geometrical interpretation of the foregoing results, shown in Figure 4, adds clarity to the analysis. Equation (18) defines a circle, sphere, or hypersphere in parameter space for two, three, or more parameter adjustments respectively. For simplicity, the two parameter case will be considered. Equation (18) becomes equation (22), where r is the radius of the circle.

$$V = r^2 = (b_1^* - b_1)^2 + (b_2^* - b_2)^2 \quad (22)$$

This circle is centered at the true parameter settings b_1 and b_2 , and V is the square of the radius, as shown in Figure 4.

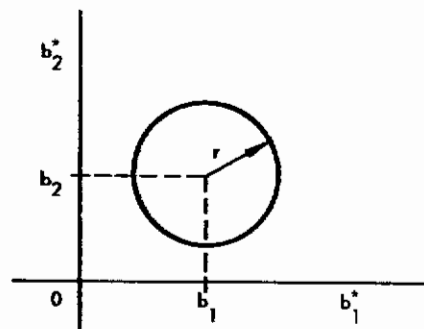


Figure 4. Geometrical Interpretation of Equation (18)

If \dot{V} is always negative, as indicated by the first term of equation (21), the radius of the circle in Figure 4 is continually shrinking. Because the parameters lie on the circumference of the circle, they will be drawn steadily in the direction of the correct solution. However, if the true parameters change, the center of the circle will move, resulting in a change in radius.

This is responsible for the right hand expression in equation (21). Inasmuch as this term is associated only with tracking error due to changes in the solution being sought, the system may be considered stable on the basis of the expression on the left of equation (21). Moreover, if tracking error were to become excessive, the error would increase, and the expression on the left would eventually dominate, forcing \dot{V} negative.

The basic parameter adjustment mechanism is simple. All that is required is the model shown in Figure 3 and the implementation of equation (16), shown in Figure 5.

In obtaining the foregoing results, it was assumed that both pitch acceleration \dot{q} and angle of attack $\hat{\alpha}_p$ could be measured or calculated from measured data. In general, this assumption may not always be valid. Hence, the possibility of using model equations other than (10) will be considered. Another reason for investigating other configurations is that the parameters obtained are generally different. Simultaneous use of two or more models provides more information about airframe dynamics than does a single model, but at the price of additional data sensing and processing.

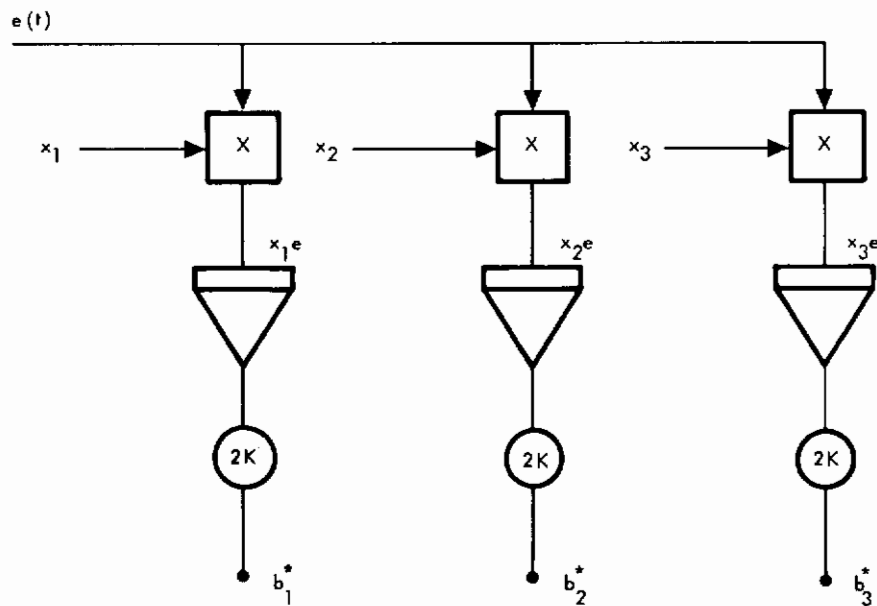


Figure 5. Implementation of Equation (16)

One new model equation is obtained by substituting equation (10) into equation (7a) to eliminate \dot{q} , then substituting equations (11d), (11e), and (11f).

$$\hat{a}_z - (U_0 Z_w + b_1) \hat{\alpha}_p - (\ell_a Z_w + \ell_z b_2) q - (Z_{\delta_e} + \ell_z b_3) \delta_e = 0 \quad (23)$$

Equation (23) is of the same form as equation (12). The following parameters may be identified:

$$b_4 = - (U_0 Z_w + \ell_z b_1) \quad (24a)$$

$$b_5 = - \ell_a (Z_w + \ell_z b_2) \quad (24b)$$

$$b_6 = - (Z_{\delta_e} + \ell_z b_3) \quad (24c)$$

A third model may be obtained by eliminating $\hat{\alpha}_p$ between equations (10) and (7a), resulting in

$$\begin{aligned} (1 - \ell_z (M_w / Z_w + M_w^*)) \dot{q} - (M_q + U_0 M_w^*) q - (M_w / Z_w + M_w^*) \hat{a}_z \\ - (M_{\delta_e} - M_w Z_{\delta_e} / Z_w) \delta_e = 0 \end{aligned} \quad (25)$$

Equation (25) is of the same form as equation (12). The following parameters may be identified:

$$b_7 = - (M_q + U_0 M_w^*) / d_1 \quad (26a)$$

$$b_8 = - (M_w / Z_w + M_w^*) / d_1 \quad (26b)$$

$$b_9 = - (M_{\delta_e} - M_w Z_{\delta_e} / Z_w) / d_1 \quad (26c)$$

where

$$d_1 = 1 - \ell_z (M_w / Z_w + M_w^*) \quad (26d)$$

Control Loop Adjustments

Once a method has been derived for obtaining information about airframe dynamics from sensor data, the next problem is to improve stability and control. It is helpful to consider aircraft transfer functions associated with

whatever control loops are used to enhance response. For a pitch rate damper, the pitch rate transfer function is considered. For normal acceleration, the acceleration transfer function is used.

The pitch rate transfer function is derived from equations (4a) and (4b). Equation (9) is substituted into equation (4a) and θ_0 assumed zero. Omitting turbulence, equations (4a) and (4b) reduce to equations (27a) and (27b), respectively.

$$U_0 (s - Z_w) \alpha - U_0 q = Z_{\delta_e} \delta_e \quad (27a)$$

$$- U_0 (sM_w^* + M_w) \alpha + (s - M_q) q = M_{\delta_e} \delta_e \quad (27b)$$

Solving equations (27a) and (27b) by Cramer's rule yields the pitch rate transfer function, as expressed by

$$\begin{aligned} \frac{q}{\delta_e} &= \frac{\begin{vmatrix} U_0 (s - Z_w) & Z_{\delta_e} \\ - U_0 (sM_w^* + M_w) & M_{\delta_e} \end{vmatrix}}{\begin{vmatrix} U_0 (s - Z_w) & - U_0 \\ - U_0 (sM_w^* + M_w) & (s - M_q) \end{vmatrix}} \\ &= \frac{(M_{\delta_e} + Z_{\delta_e} M_w^*) s + (Z_{\delta_e} M_w - Z_w M_{\delta_e})}{s^2 - (Z_w + M_q + U_0 M_w^*) s + Z_w M_q - U_0 M_w} \quad (28) \end{aligned}$$

One technique (Reference 3) for gain adjustment in the control loop utilizes the fact that the total loop gain which just produces instability is approximately constant at high frequencies. This is true provided enough lead compensation is included to overcome lags introduced by the servo, actuator, and sensor up to frequencies well beyond the short period natural frequency. The high frequency gain of the airframe pitch rate transfer function is obtained as a limiting case of equation (28), producing

$$\lim_{s \rightarrow \infty} \dot{q} / \delta_e = M_{\delta_e} + Z_{\delta_e} M_w^* \quad (29)$$

Referring to equation (11f), it is seen that this gain is obtained directly from the parameter identification. A constant gain criterion may now be mechanized to maintain total loop gain at some percentage of the constant critical value. If the variable gain in the control loop is designated by K_q , the adjustment proceeds according to equation (30), where K is a constant.

$$K_q = K/b_3^* \approx -K/(M_{\delta_e} + Z_{\delta_e} \dot{M}_w) \quad (30)$$

Analog and digital studies of an X-15 pitch axis controller indicated that maximum damping was obtained at all flight conditions with a loop gain of about one-half of the critical value (Section 4).

If angle of attack is not measured, an approximation is required. If Z_{δ_e} and l_z are relatively small, equation (26c) may be used in place of equation (11f), leading to

$$K_q = K/b_9 \quad (31)$$

The zero of the pitch rate transfer function of equation (28) is also of special interest in designing an adaptive flight control system. Usually, a closed loop pole appears near this zero. Inasmuch as the magnitude of the zero is generally quite small, the nearby pole has a long time constant, resulting in a very long tail on the step response. In order to get the step response to approach final value within a reasonable period of time, it is sometimes desirable to track this zero so that it may be cancelled. If Z_{δ_e} is again assumed to be relatively small, the zero is obtained from equations (28) and (24a) as

$$1/T_a \approx -Z_w \approx b_4/U_0 \quad (32)$$

In the event independent gain adjustment of a normal acceleration loop is required, the high frequency gain of the acceleration transfer function may be used. If equations (4a) and (4b) are simulated on an analog computer, q and α are obtained as integrator outputs, and do not play a role in determining high-frequency gains. At high frequencies, equation (4a) reduces to

$$a_z \approx Z_{\delta_e} \delta_e \quad (33)$$

Substituting equations (33) and (29) into (6) yields

$$\hat{a}_z \approx Z_{\delta_e} \delta_e - l_z \dot{q} \approx Z_{\delta_e} \delta_e - l_z (M_{\delta_e} + Z_{\delta_e} \dot{M}_w) \delta_e \quad (34)$$

Substituting equations (11f), (24a), and (24d) into equation (34) yields the required high-frequency gain as expressed by

$$\lim_{s \rightarrow \infty} \hat{a}_z / \delta_e = -b_6 \quad (35)$$

If pitch rate and normal acceleration are fed back through the control loop, the elevator deflection is of the form given by

$$\delta_e = a_1 q + a_2 \hat{a}_z + \delta_{e_c} = a_1 q + a_2 (a_z - l_z \dot{q}) + \delta_{e_c} \quad (36)$$

At high frequencies, if a_2 contains appreciable lag (as is true in the present system), equation (36) degenerates to

$$\delta_e \approx \delta_{e_c} \quad (37)$$

Substituting equation (37) into equations (29) and (34) yields

$$\lim_{s \rightarrow \infty} \frac{\dot{q}}{\delta_{e_c}} = M_{\delta_e} + M_w^* Z_{\delta_e} \quad (38a)$$

$$\lim_{s \rightarrow \infty} \frac{a_z}{\delta_{e_c}} = Z_{\delta_e} - l_z (M_{\delta_e} + M_w^* Z_{\delta_e}) \quad (38b)$$

Hence, the high-frequency loop gains are independent of each other if sufficient lag is designed into the acceleration loop. This independence is advantageous in the sense that the pitch rate damper gain may be adjusted independently of the acceleration loop gain.

It may be concluded from the foregoing results that if angle of attack is sensed and used by the SIDAC computer for parameter adjustment, the high frequency gains for the control loops will be obtained correctly without modification, provided the same sensors are used for both identification and control. However, if the SIDAC computer utilizes only inertial data (acceleration and angular rates), corrections may be required to compensate for accelerometer locations other than the center of gravity, as well as for the fact that the stability derivative Z_{δ_e} may not be negligible.

Similar conclusions are drawn in Section 5 of this report for the lateral axes, and are verified by simulation results.

Although the remaining parameters in the pitch rate transfer function are of secondary importance, it is possible to obtain approximations for them as simple functions of the identified parameters. The complete transfer function would be useful in establishing more complex control laws, such as complete specification of closed loop poles (Reference 8) or complete optimal control (Reference 9). Implementation of such control laws is not contemplated at present, but equations (39) and (40) give approximations for the remaining coefficients to illustrate future potential of the approach.

$$-(Z_w + M_q + U_0 M_{\dot{w}}) \approx b_4/U_0 + b_2 \approx b_4/U_0 \quad (39)$$

$$Z_w M_q - U_0 M_w \approx b_2 b_4/U_0 + b_1 \approx b_1 \quad (40)$$

The b_1 coefficient is also useful in determining minimum gain required to stabilize an unstable airframe, such as a missile.

PARAMETER IDENTIFICATION REFINEMENTS

Although parameter adjustments based upon equation (16) and implemented as in Figure 5 are fast and stable, certain refinements are advantageous.

In the first place, equation (16) can be generalized considerably, as may also the Lyapunov function specified by equation (18). For example, equation (18) may be replaced by the more general form

$$V = \sum_i (b_i^* - b_i)^2 / K_i \quad (41)$$

It is easy to show by the method used previously that the system is stable if the parameter adjustment equation specified by equation (16) is replaced by

$$\dot{b}_i^* = -K_i \left| f(e, x_1, x_2, \dots, x_N, b_1^*, b_2^*, \dots, b_N^*) \right| \text{ex}_i \quad (42)$$

This reduces to various special cases:

$$\dot{b}_i^* = -K_i \text{ex}_i \quad (43a)$$

$$\dot{b}_i^* = -K_i \text{ex}_i / \left| e \right| = -K_i \text{sgne } x_i \quad (43b)$$

Equation (43a) permits unequal integrator gains, which speed convergence in some cases. Equation (43b) permits replacing multipliers by relays in analog

circuitry. Both of these modifications have been quite effective in simulations. It is clear from equation (42) that limiting or deadband in the error channel may also be used if desired.

Conditions have also been derived under which integrator inputs may be cross coupled to compensate for interaction between adjustment rates of individual parameters (Appendix II). However, parameter interaction has never been severe enough in past simulations to justify the extra complexity of cross coupling.

Parameter adjustment schemes discussed so far are highly input sensitive. For example, equation (21) indicates that adjustment rates are proportional to the square of the error. The error intensity is in turn proportional to input intensity. For an airplane flying in turbulent air, adjustment rates would be strongly influenced by prevailing weather conditions. This effect may be greatly ameliorated by means of an AGC circuit, as illustrated in Figure 6 for the control law of equation (43a).

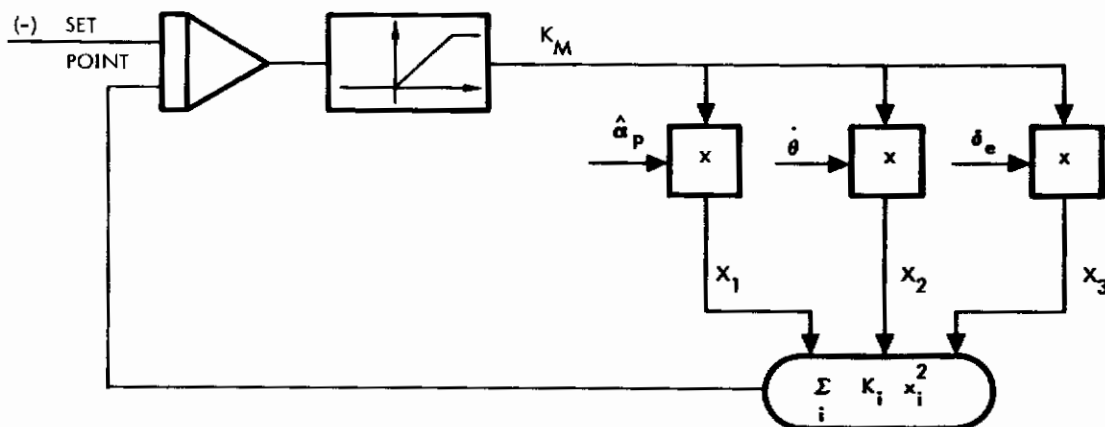


Figure 6. Pitch Axis AGC

It may be shown (Section 6) that the configuration of Figure 6 has the added advantage that instability due to sampling lags in a digital implementation may be avoided.

Another refinement to the basic parameter adjustment mechanism is the use of input filters. Because the equations of airframe motion (equations 4a and 4b) are linearized about steady state values, such steady state values should not be fed into the model inputs. An easy way to accomplish this, as well as to remove sensor bias, is to pass each input through a washout (high-pass) filter. Frequency sensitive filters may be used to remove noise from data, provided the frequency content of the noise differs from that of the normal signal.

If the parameters being tracked are slowly varying, it can be shown that passing all inputs through identical filters does not alter the form of the model, nor does it change the values to which the parameters converge. This may be demonstrated by multiplying equation (12) by the transfer function $F(s)$ of an arbitrary filter, provided initial conditions in the filters are zero so that transfer functions are valid. (Nonzero initial conditions eventually decay out for stable filters.)

$$F(s) (x_0 + \sum_i b_i x_i) = 0 \quad (44)$$

For example, consider a low pass filter applied to equation (10), as in

$$\frac{c}{s+c} (sq + b_1 \alpha_p + b_2 q + b_3 \delta_e) = 0 \quad (45)$$

Equation (45) may be implemented without measuring \dot{q} as shown in Figure 7.

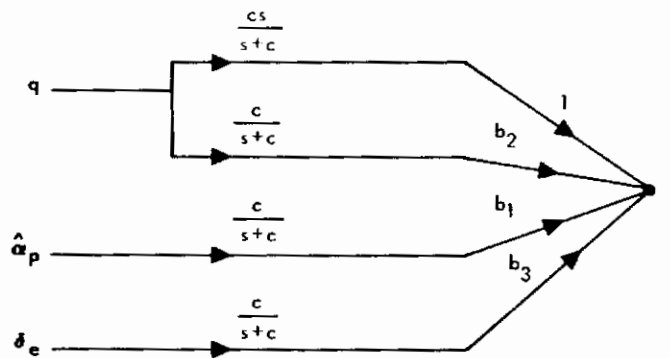


Figure 7. Pitch Axis Input Filters

SECTION 4

PITCH AXIS

SYSTEM DESIGN

In designing the pitch axis control system, emphasis was placed upon choosing a configuration capable of good damping over a wide range of flight conditions, even without adaptive control. This serves two main purposes:

1. In the event of failure of the SIDAC computer, the linear portion of the control system may be used as an ordinary fixed gain system until completion of the mission. The result is an effective increase in reliability.
2. Accuracy requirements on parameter estimation are less critical if the linear portion of the system is well designed. Hence, the system should be less affected by sensor noise, flexible modes, nonlinearities, and other effects not explicitly described by the SIDAC equations.

The basic philosophy of the design procedure is similar to that introduced by Horowitz (Reference 10). However, the design differs substantially from that of Horowitz in two respects:

1. An upper limit of about 10 rad/sec is imposed upon the bandwidth of the closed-loop system to prevent excitation of control surface flutter, the 25 rad/sec first bending mode, the tail-wags-dog effect, and to prevent excess limit cycling due to component nonlinearities.
2. Design is restricted to simple compensation networks, three dipoles in this case. The more elaborate networks suggested by Horowitz provide exact cancellation of vehicle dynamics at a single flight condition, but do not appear to be justified over the remainder of the flight regime.

The basic design philosophy for the pitch axis may be illustrated by referring to Figure 8, where the asymptotic frequency response of the vehicle dynamics, together with a second order lag to represent higher

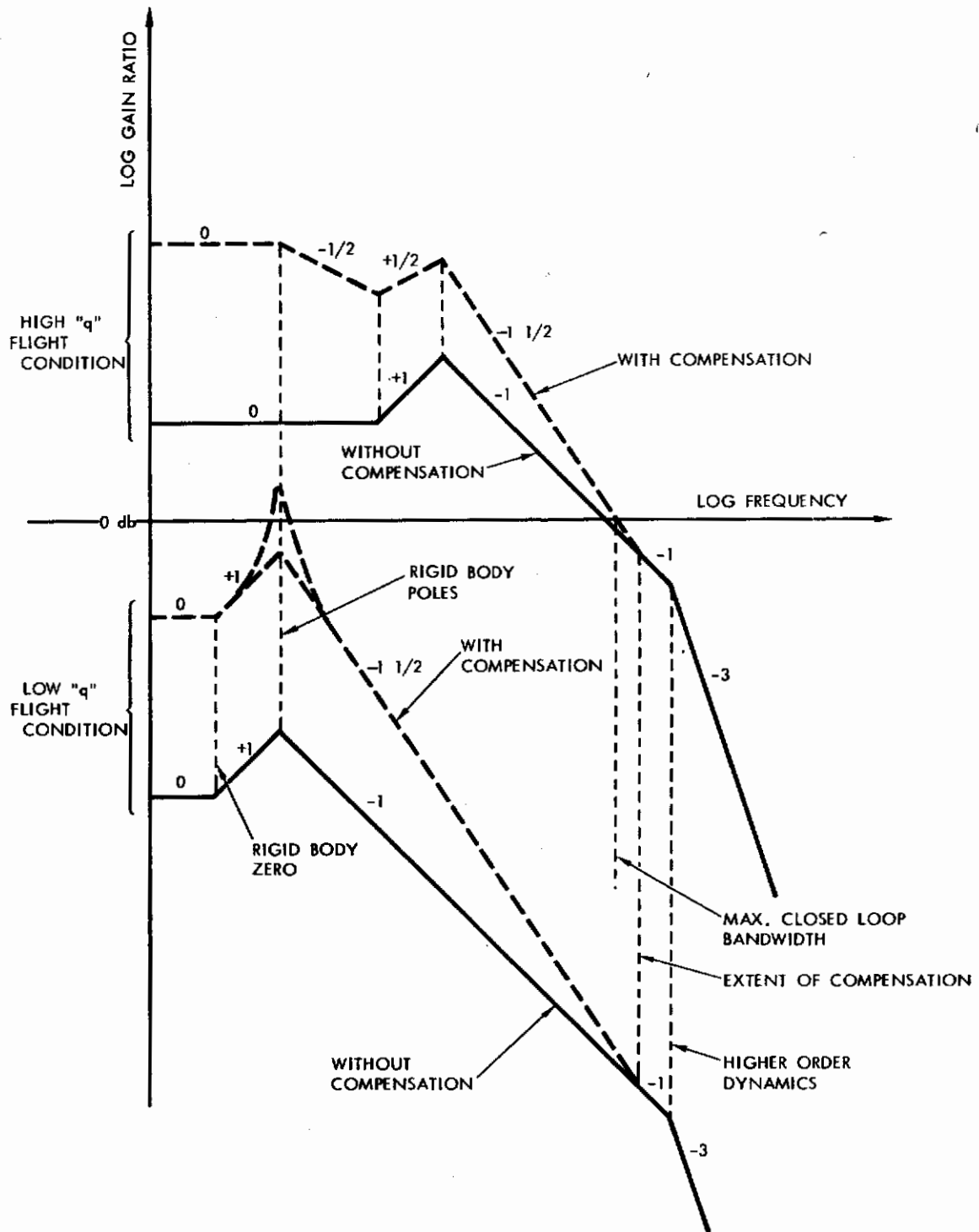


Figure 8. Asymptotic Bode Gain of Typical Aircraft Pitch Axis Dynamics

frequency dynamics of control system components, is sketched for both maximum q and minimum q flight conditions. The design procedure is basically as follows:

1. A constraint is placed upon the maximum allowable closed-loop bandwidth to prevent excitation of structural resonances, tail-wags-dog effect, and to minimize limit cycling due to nonlinearities. In the case of the X-15 pitch axis, 10 rad/sec was chosen.
2. The control loop gain is adjusted at the maximum q condition such that the zero db (unity gain) level crosses the open-loop frequency response at the maximum allowable closed-loop bandwidth frequency. Below this frequency, the closed-loop transfer function $T(s)$ for Figure 2 is approximately (assuming unity feedback)

$$T(s) = \frac{D(s)G(s)}{1 + D(s)G(s)} \approx 1 \quad (46)$$

and for higher frequencies,

$$T(s) \approx D(s)G(s) \quad (47)$$

The closed-loop transfer function has unity gain at frequencies below where the open-loop transfer function crosses the zero db line, and is essentially the same as the open-loop at higher frequencies. Hence, the closed-loop bandwidth is approximately equal to the frequency at which the open-loop gain drops below unity.

3. To ensure that phase margin will be adequate at all flight conditions, the open-loop gain curves must be shaped in such a manner that phase shift is less than 180 degrees by an amount equal to the minimum allowable phase margin at all frequencies at which the zero db line may cross the open-loop frequency response. Generally speaking, this means frequencies below the maximum bandwidth frequency previously chosen. It is well known that a definite relationship exists between gain and phase curves for minimum phase systems, so that in general, the steeper the gain curve, the greater is the negative phase shift, and the less is the phase margin. For example, if the logarithm of gain is plotted against the logarithm of frequency, a slope of zero corresponds to zero phase shift or 180-degree phase margin, a slope of -1 corresponds to a -90-degree phase shift or 90-degree phase

margin, and a slope of -2 corresponds to a -180-degree phase shift or zero phase margin. Hence, phase margin at a given frequency is approximately (where m denotes the slope of the gain curve)

$$PM = (2 + m) 90 \text{ deg} \quad (48)$$

For an average phase margin of 45 degrees, the average slope of the gain curve, throughout the region where the unity gain line may cross the gain curve is $-1-1/2$, as illustrated in Figure 8. If one were to choose to maximize phase margin, it would appear to be desirable to reduce the negative slope of the gain curve as much as possible. However, it is apparent from Figure 8 that if compensation were introduced to flatten the gain curves, the low q gain would be far below unity at all frequencies, thereby preventing effective damping of the rigid body. This is apparent from equation (47), where it is observed that if the gain at the peaking frequency of the rigid body is far below unity, the shape of the peak will not be modified appreciably, and the control system will be ineffective as far as stability augmentation is concerned. On the other hand, damping may be increased by increasing the slope of the gain curve with compensation, thereby raising the rigid body peak to near the unity gain level.

It now becomes apparent that a compromise in design is required. Maximum stability requires that negative slope in the gain curve be kept small to increase phase margin; whereas if large variations in control surface effectiveness are to be handled (corresponding to large displacement between the frequency response plots at high frequencies for various flight conditions), the gain curve should be as steep as possible. For an average phase margin of 45 degrees, the average slope of $-1-1/2$ is somewhat steeper than the -1 slope associated with a simple damper configuration, as illustrated in Figure 8. Three specific advantages may be cited for this type of design: (1) Decreased sensitivity to gain variations; (2) maximization of bandwidth at all flight conditions. This is made apparent by observing in Figure 8 that with the negative slope of the gain curve maximized, the loss in closed-loop bandwidth as a function of decreasing open-loop gain (in turn a function of control surface effectiveness for various flight conditions) is minimized; and (3) maximum disturbance attenuation. It is observed in Figure 8 that maximizing negative slope also maximizes low-frequency gain. Hence, disturbance attenuation is enhanced.

Pitch Axis Design Details

X-15 pitch axis data for several flight conditions appears in Table 1. The details of a preliminary pitch axis design are presented in Figure 9. Two modifications in the basic design procedure are immediately apparent:

1. An integrated servo is included to reduce steady state error to zero in response to a step input. This is important if an outer attitude loop is used in the control system. Otherwise, pitch angle would change as a function of flight condition whenever attitude hold was engaged.
2. Inasmuch as it is not possible to achieve a slope of $-1-1/2$ in the gain curve with simple physical networks, three dipoles are used to provide shaping on an approximate basis.

Figures 10 through 24 show open-loop frequency response data for the final design obtained from an IBM 7094 digital computer run. A 30-degree phase margin was used instead of 45 degrees.

The corresponding root loci appear in Figures 25 through 29. The critical gain K_{qm} is identified for each flight condition, and also the nominal operation gain $K_{qn} = K_{qm}/2$. It is readily seen that this gain setting gives very nearly maximum damping for each flight condition. The damping coefficient σ_a/c is defined as the negative of the real components of the complex short period poles, and is seen to be nearly constant for all flight conditions, as revealed by Table 2. This means that the time required to damp disturbances is nearly invariant throughout the flight regime. If heavier damping is required, increasing the phase margin requirements from 30 degrees to 45 degrees should suffice.

Invariant damping may also be predicted analytically. Consider the characteristic equation for simple rate feedback:

$$\begin{aligned}
 0 &= 1 + K_{qn} \frac{M_\delta (s + 1/T_a)}{s^2 + 2\zeta_a \omega_a s + \omega_a^2} \\
 &= \frac{s^2 + 2(\zeta_a \omega_a + K_{qn} M_\delta / 2T_a) s + (\omega_a^2 + K_{qn} M_\delta / T_a)}{s^2 + 2\zeta_a \omega_a s + \omega_a^2} \quad (49)
 \end{aligned}$$

The closed-loop damping is given by one half of the coefficient of the s in the numerator.

TABLE 1.
X-15 FLIGHT DATA

Flight Condition	h (1000s of ft)	\bar{q} (psf)	M	u (fps)	$M_{\delta e}^2$ (sec ⁻²)	ω_a (rad/sec)	ζ_a	$1/T_a$ (rad/sec)
5	40	274	1	969	9.7589	2.7697	0.1352	0.20588
13	100	253	4	4018	2.2394	1.9197	0.0206	0.03663
17	120	241	6	6027	1.5506	1.2033	0.0158	0.01836
21	60	2622	5	4843	20.859	4.3270	0.0752	0.3245
25	80	160	2	1937	3.0819	2.4016	0.0398	0.0947
28	10	1467	1.2	1078	52.946	7.4924	0.3325	2.0708
31	5	444	0.6	659	16.293	2.5505	0.4373	1.1644
32a	0	59	0.2	223	0.2193	1.5111	0.0997	0.035638
32b	0	59	0.2	223	0.2193	0.5111	0.0997	0.035638

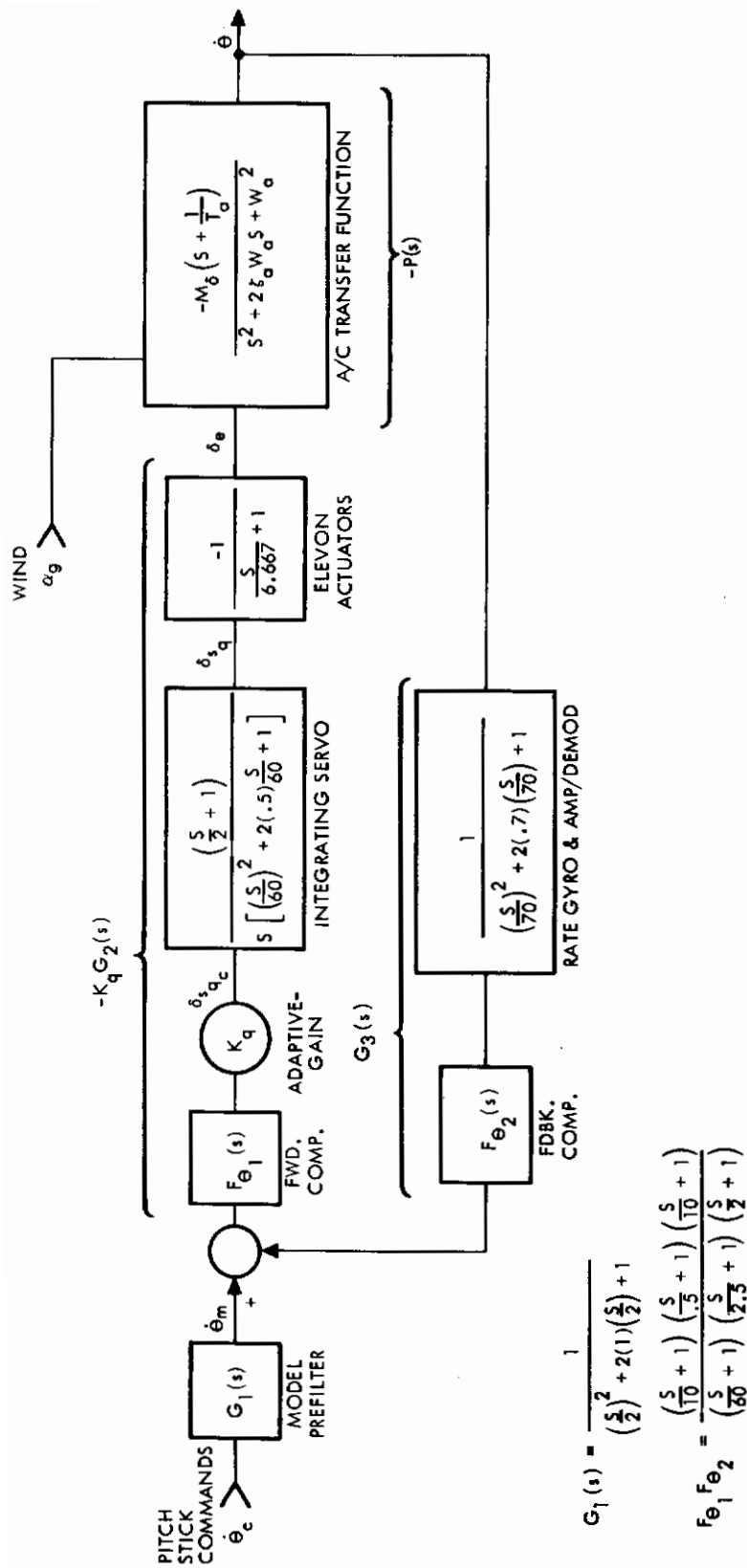


Figure 9. Pitch SAS Block Diagram

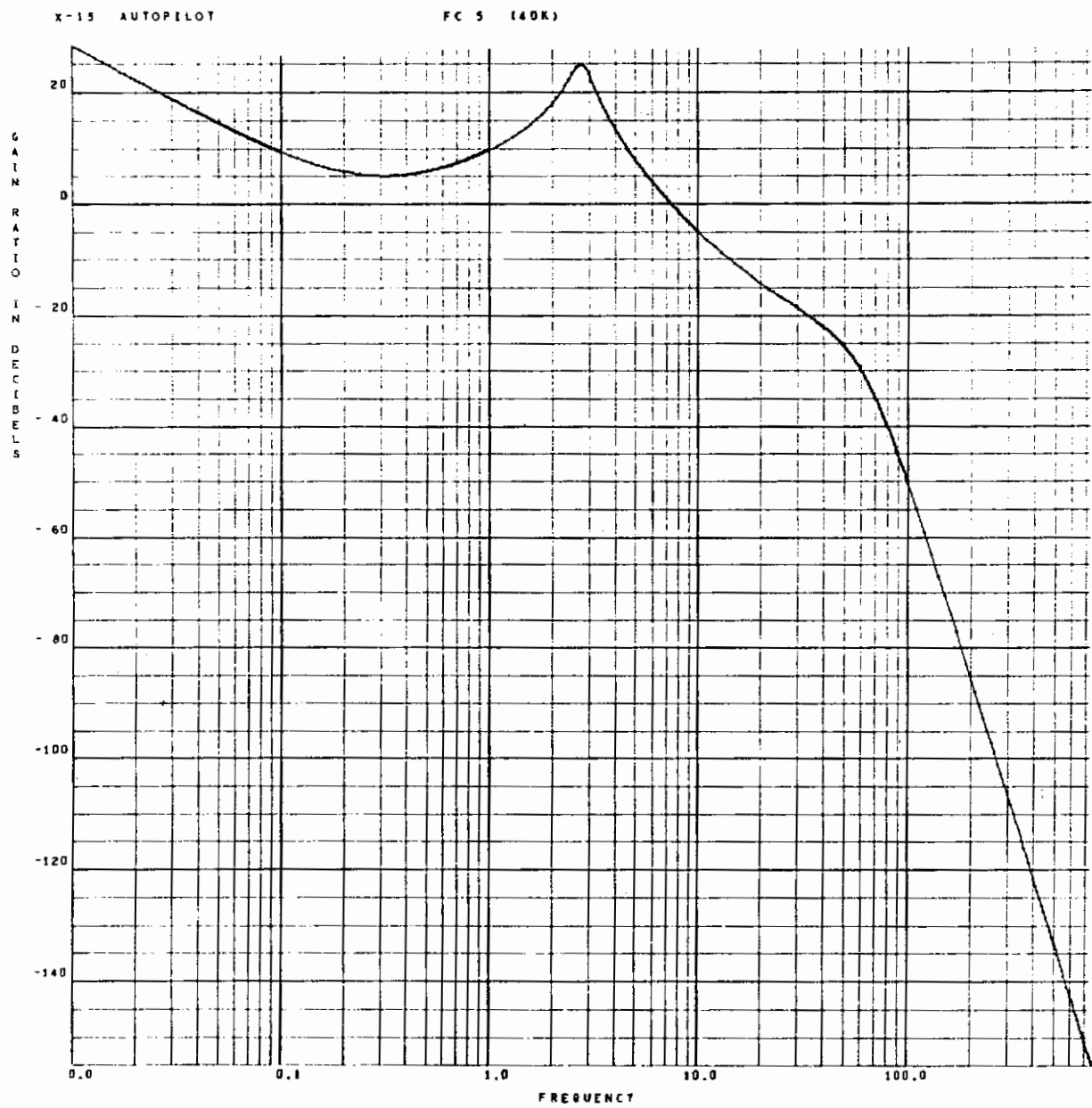


Figure 10. $G_2G_3P(s)$ Gain Ratio, FC 5

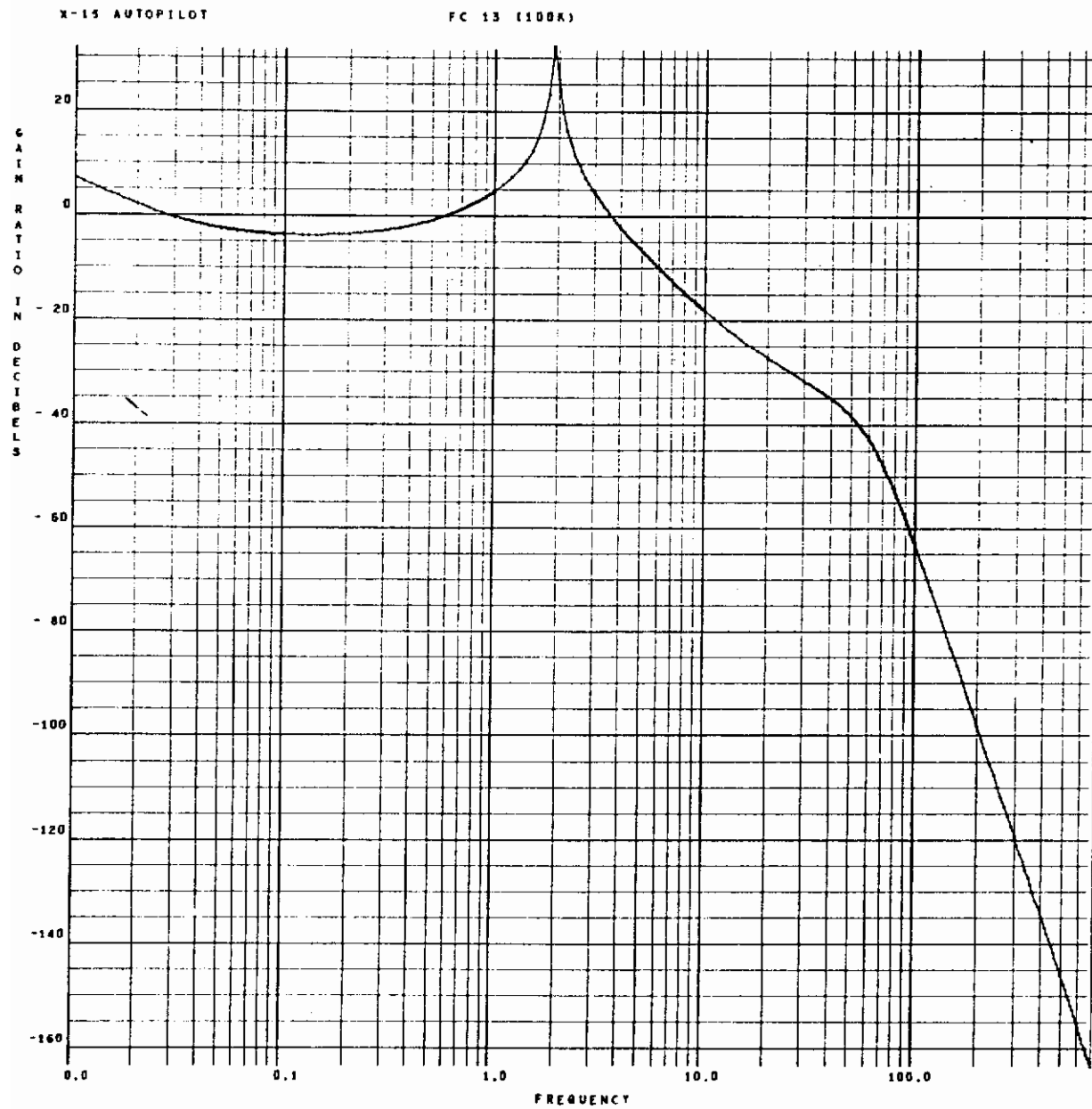


Figure 11. $G_2G_3P(s)$ Gain Ratio, FC 13

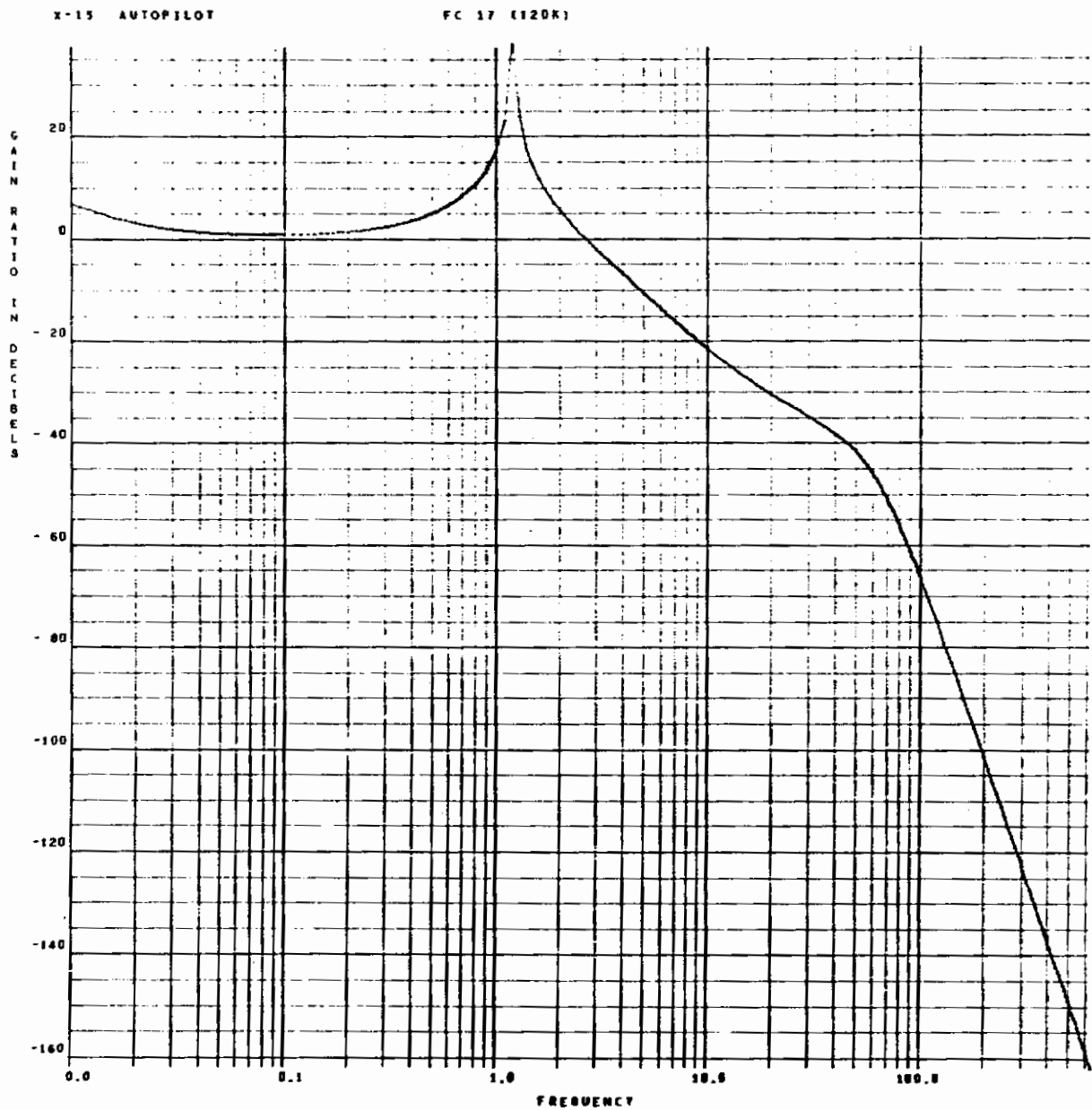


Figure 12. $G_2G_3P(s)$ Gain Ratio, FC 17

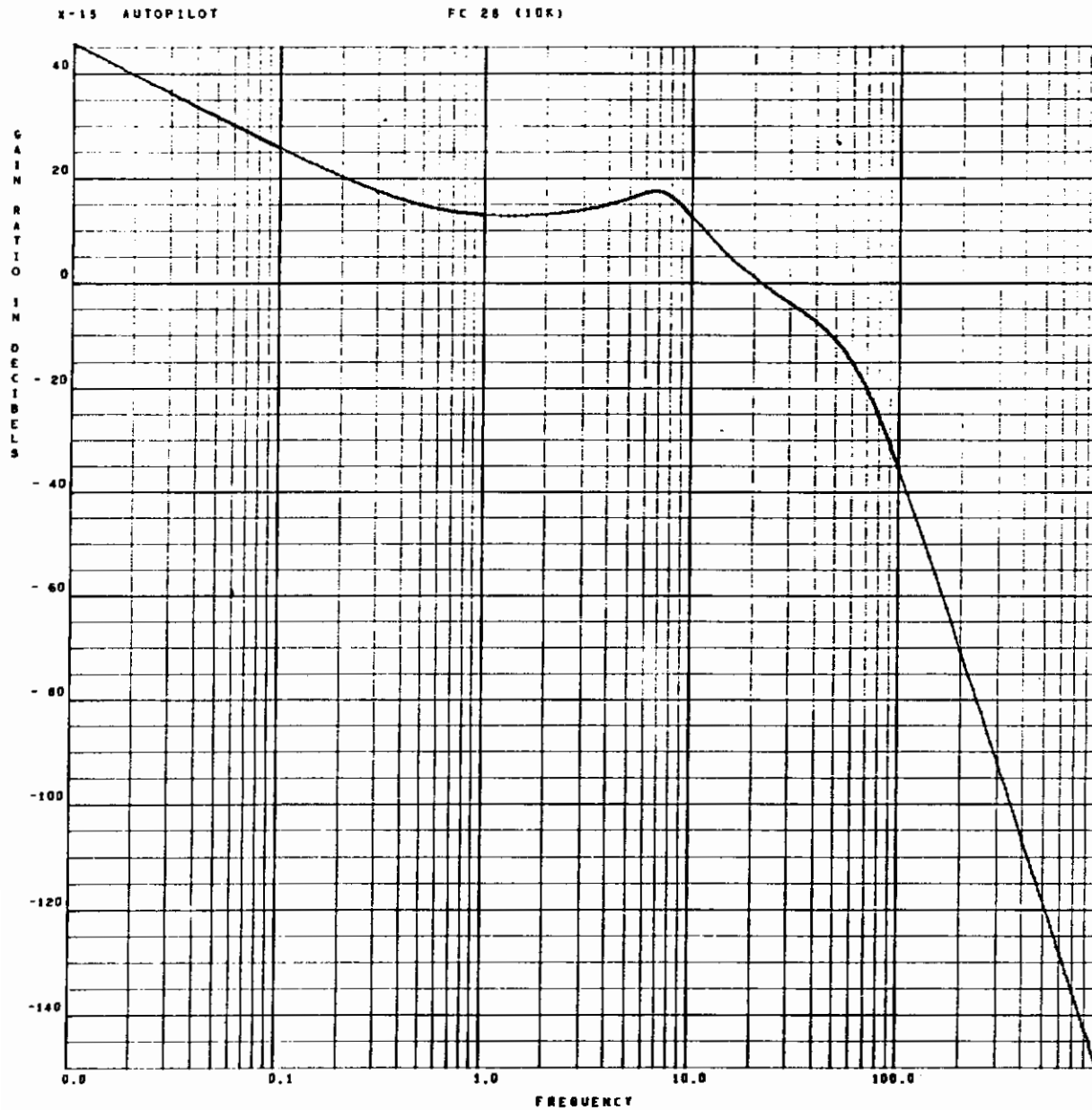


Figure 13. $G_2G_3P(s)$ Gain Ratio, FC 28

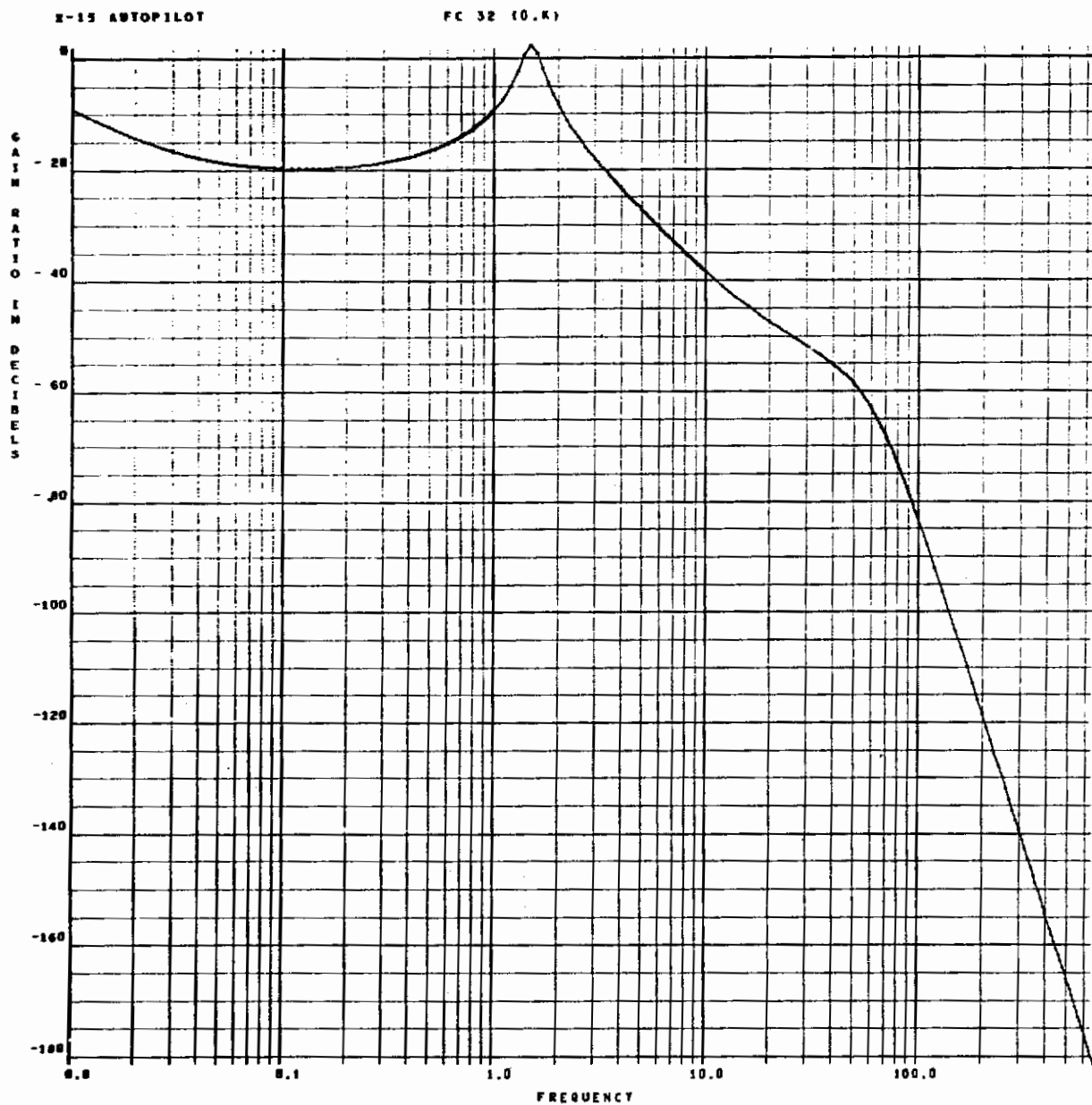


Figure 14. $G_2G_3P(s)$ Gain Ratio, FC 32

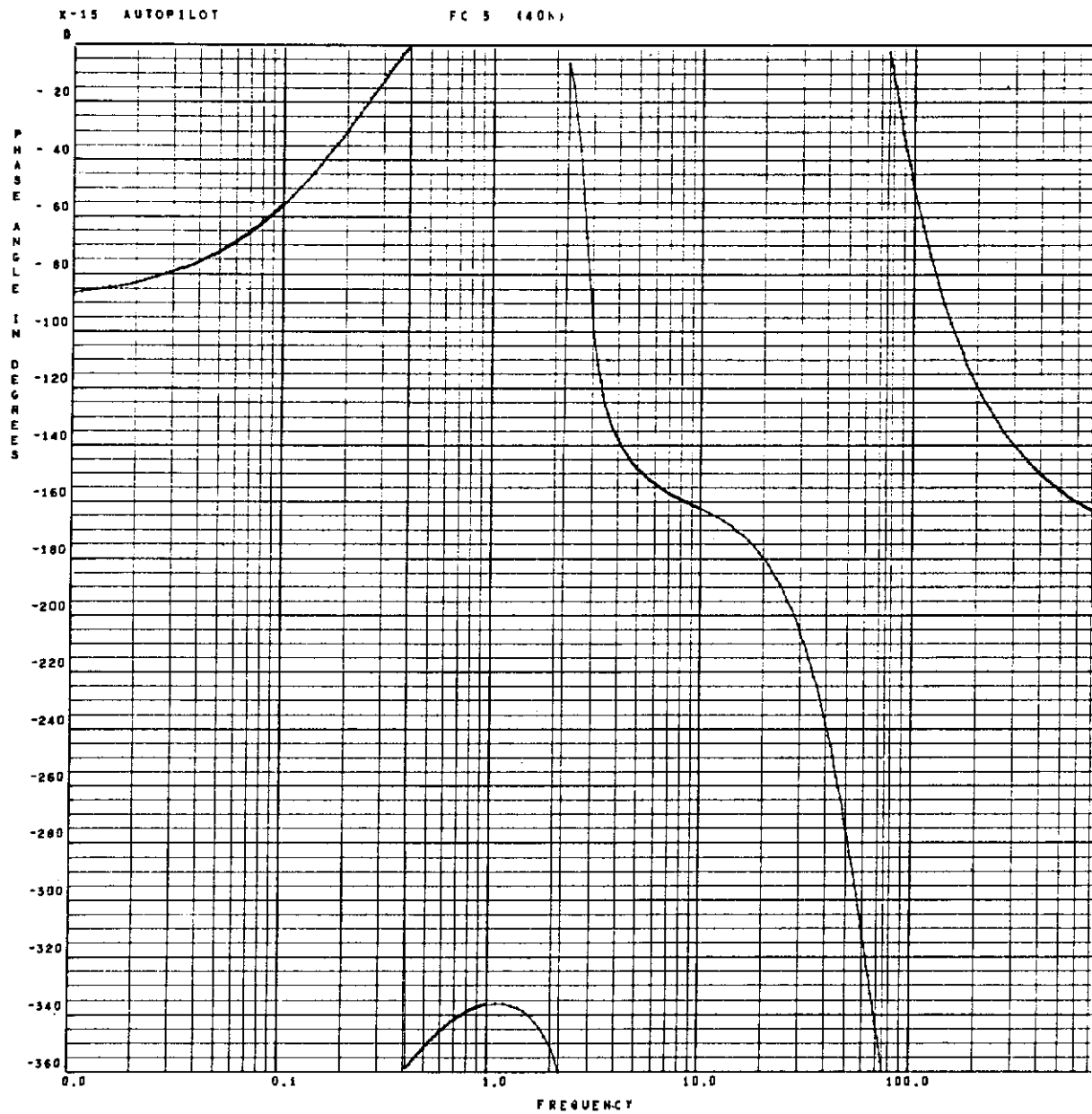


Figure 15. Argument $G_2G_3P(s)$, FC 5

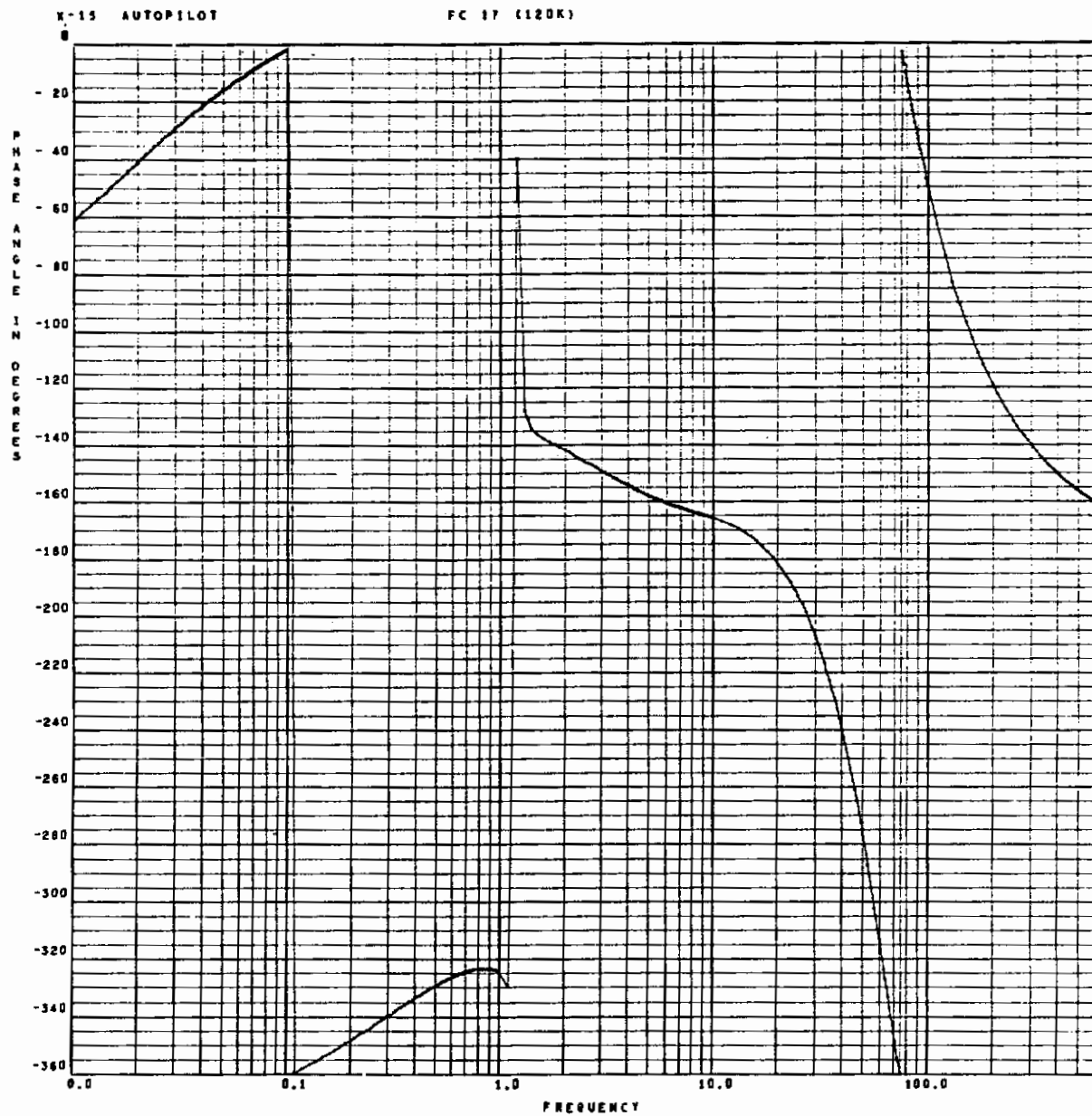


Figure 16. Argument $G_2G_3P(s)$, FC 13

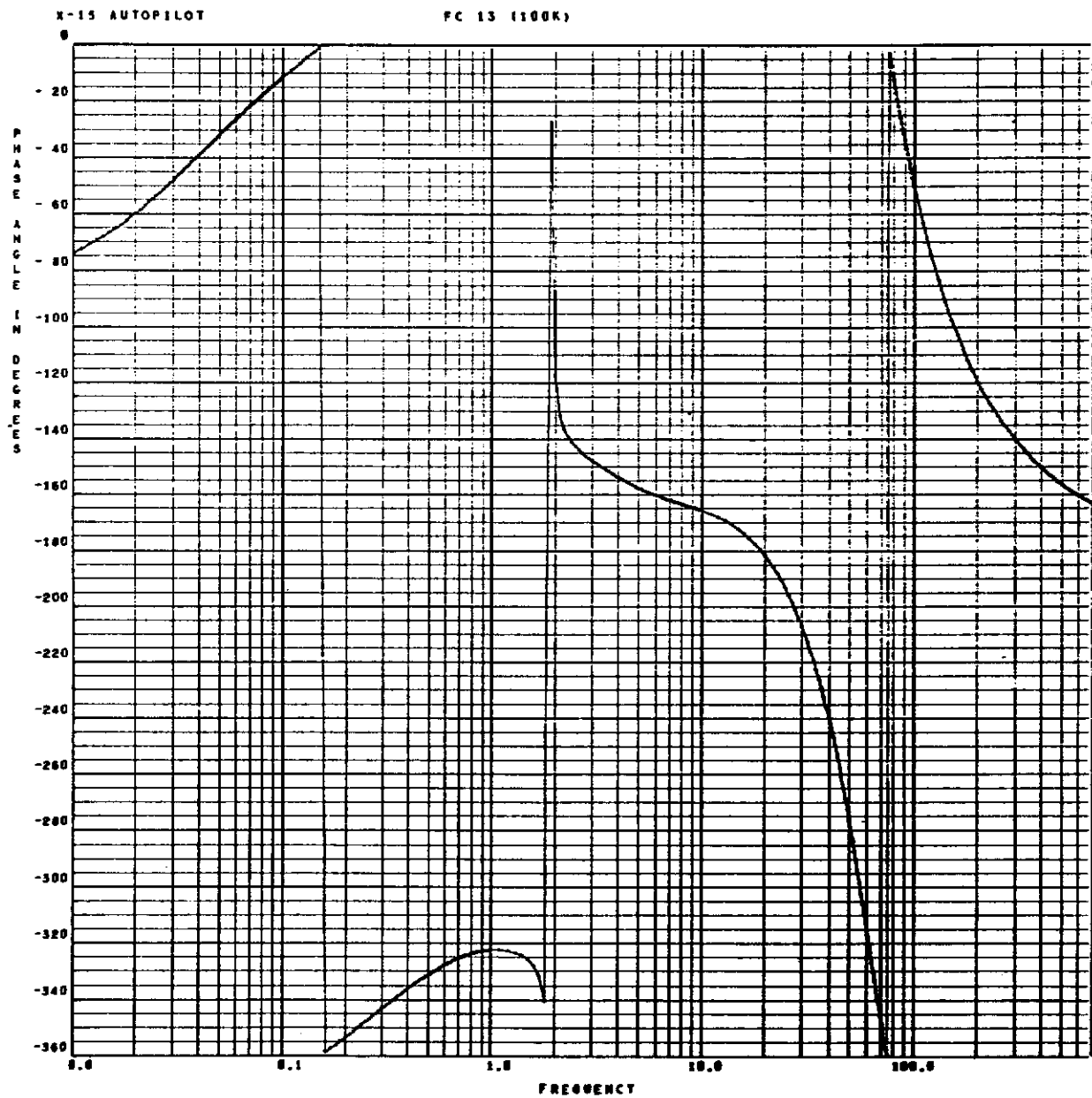


Figure 17. Argument $G_2G_3P(s)$, FC 17

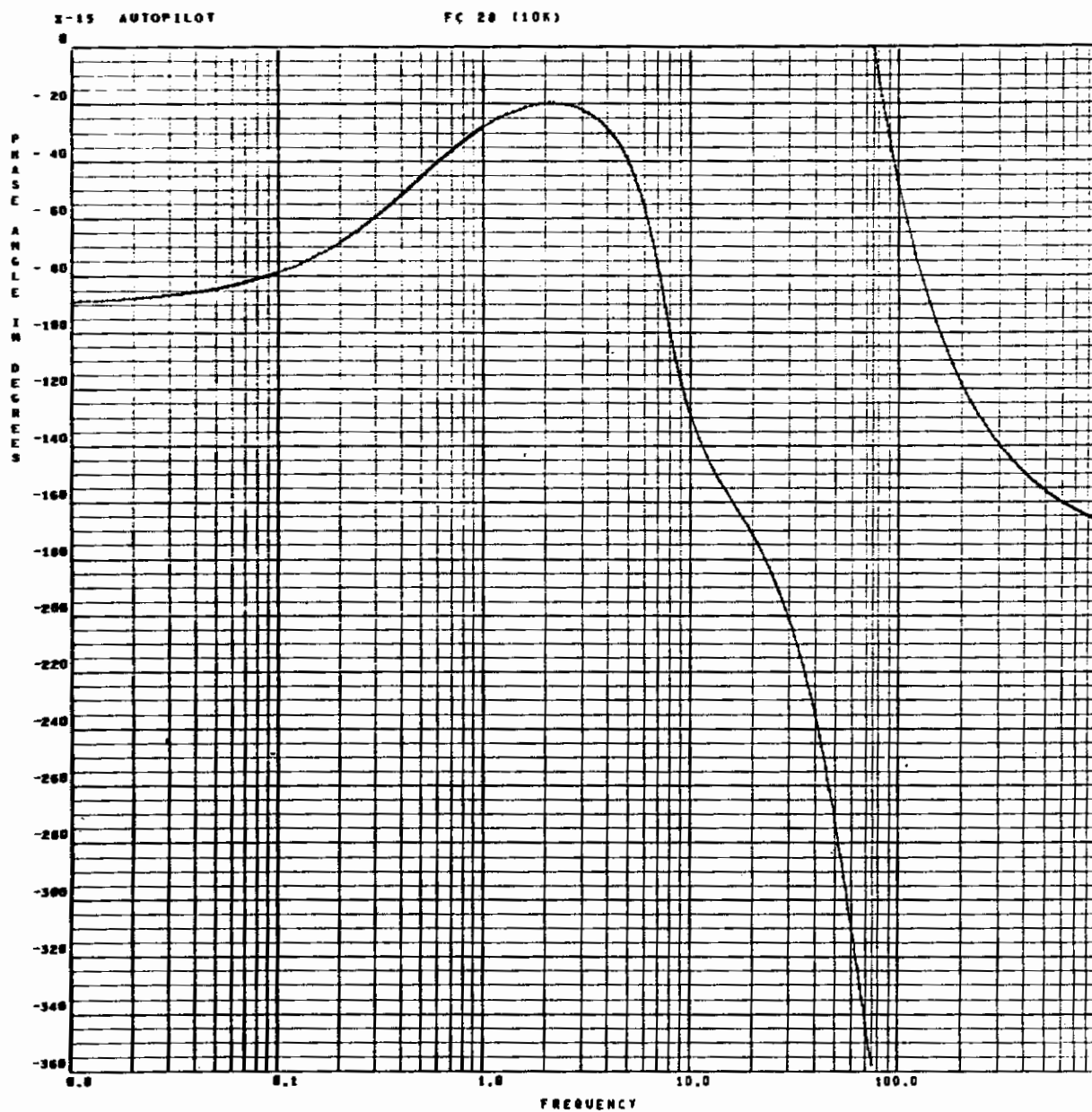


Figure 18. Argument $G_2G_3P(s)$, FC 28

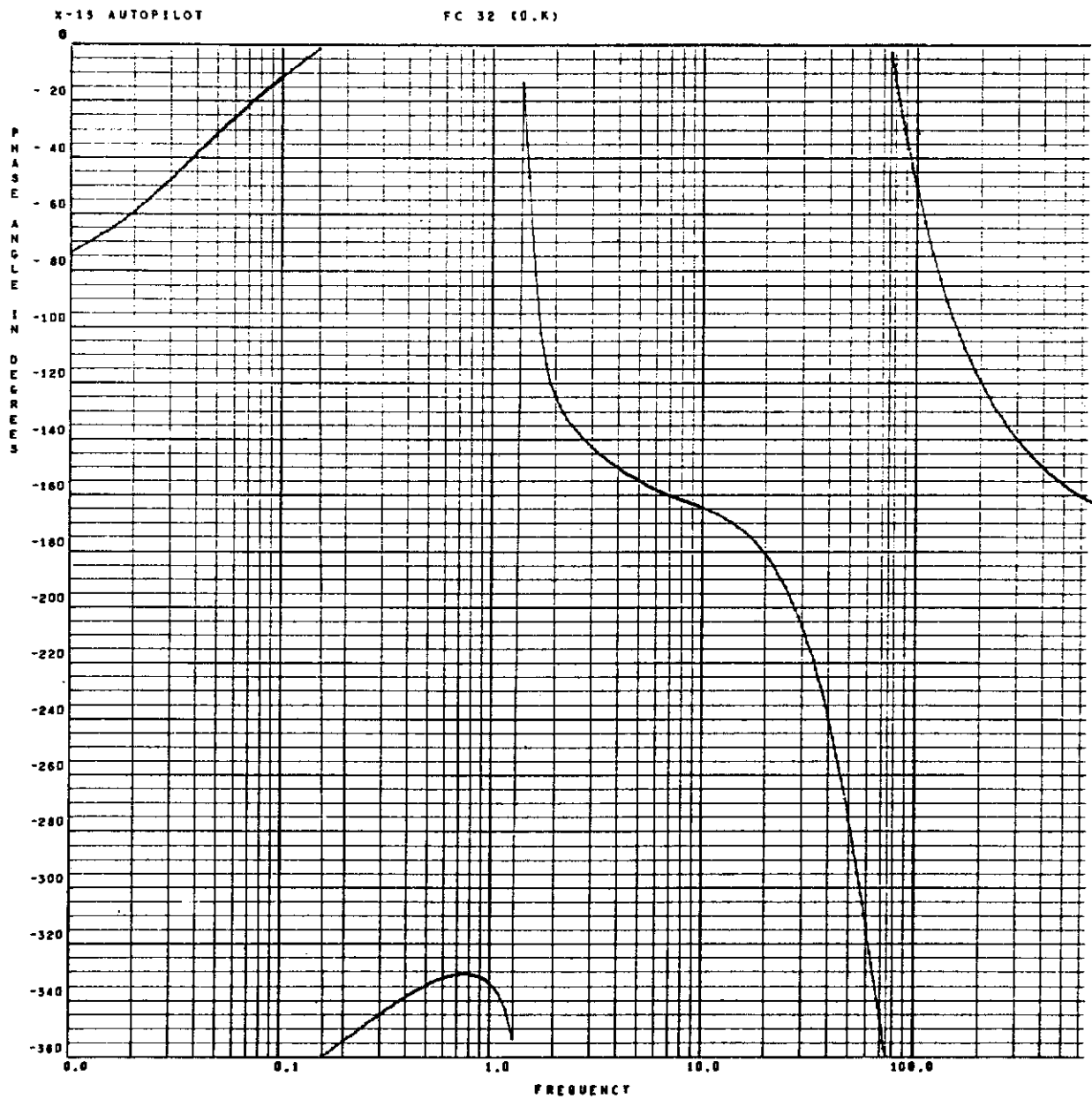


Figure 19. Argument $G_2G_3P(s)$, FC 32

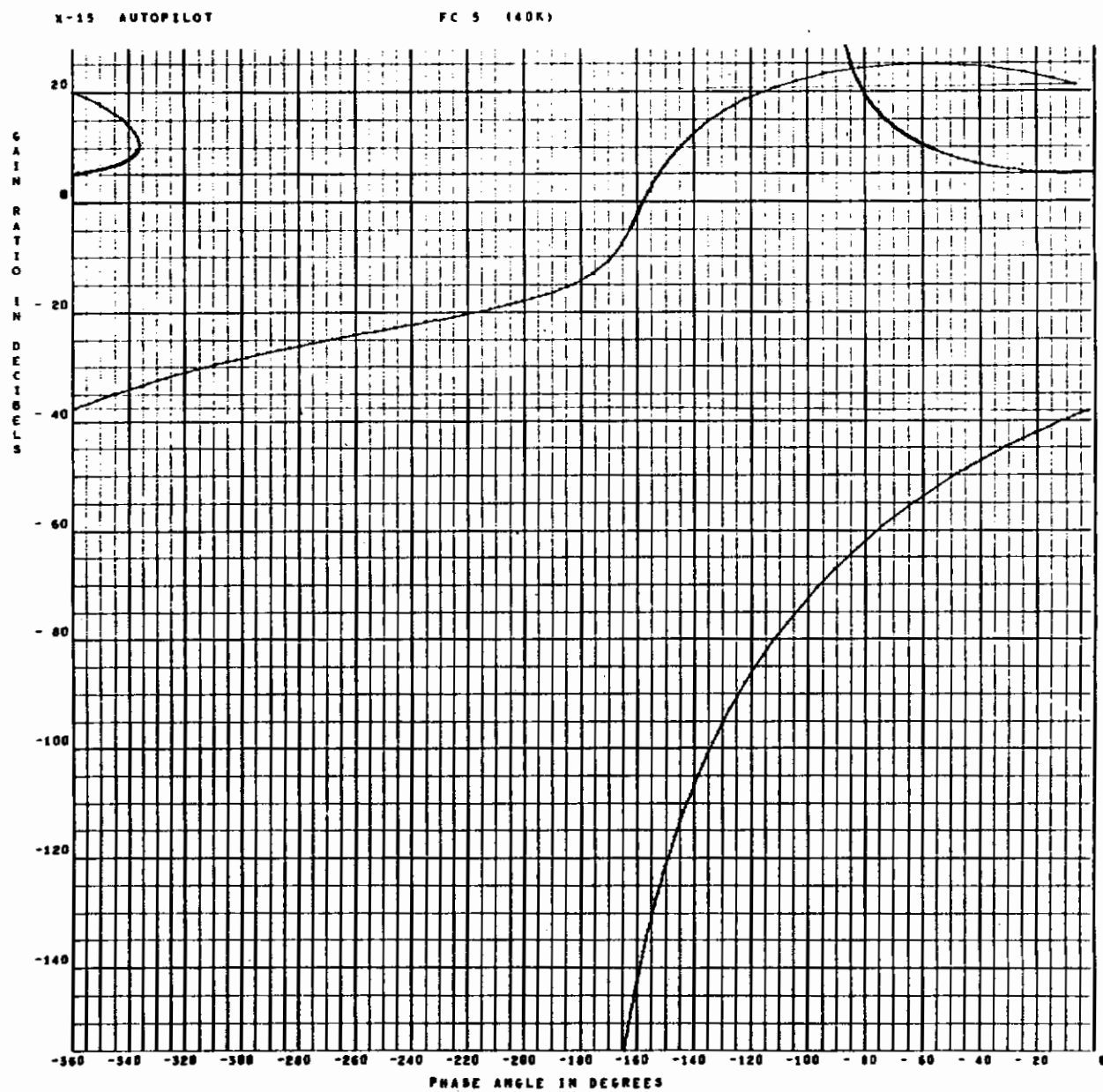


Figure 20. Bode Gain/Phase $G_2G_3P(j\omega)$, FC 5

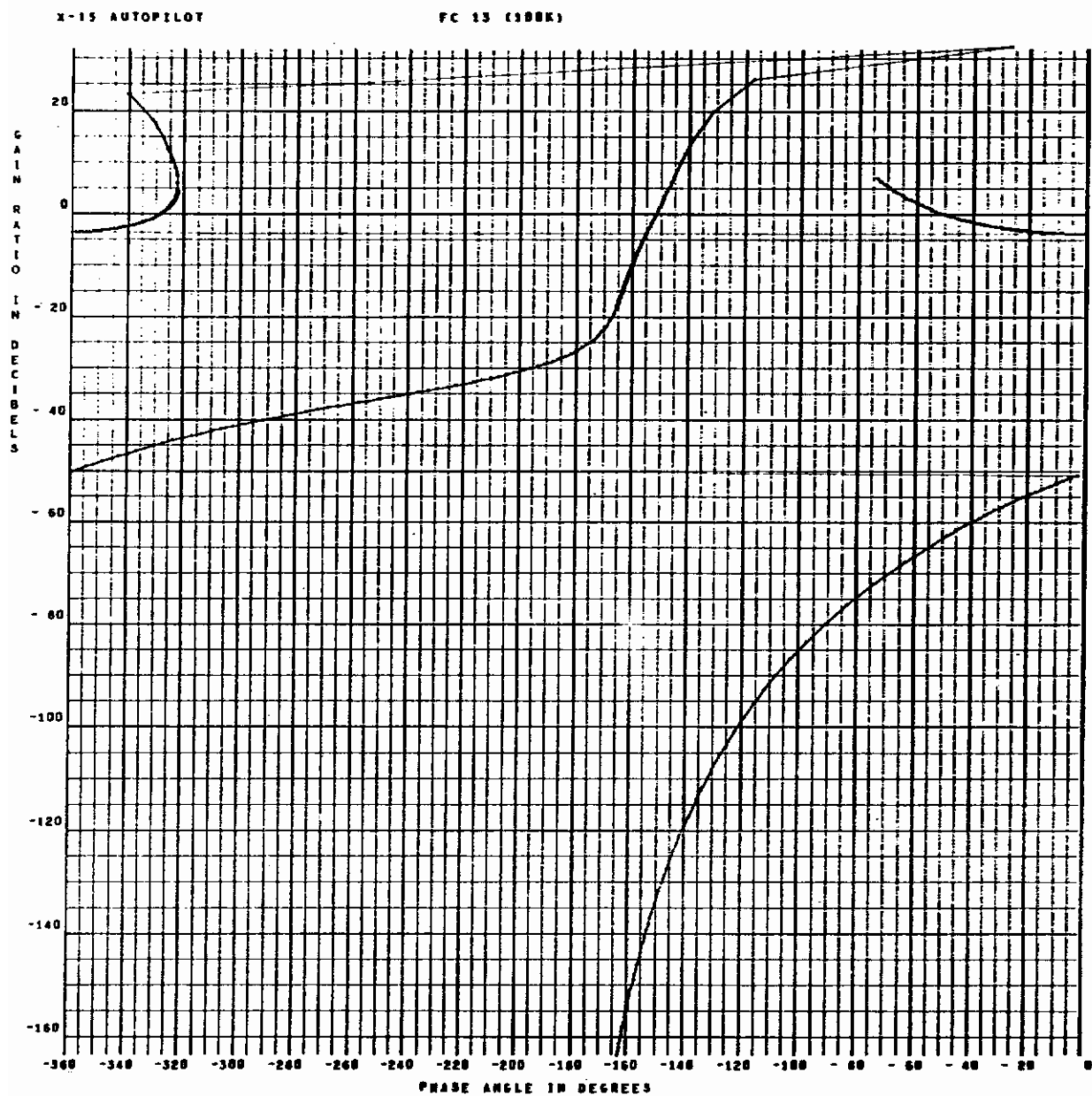


Figure 21. Bode Gain/Phase $G_2G_3P(j\omega)$, FC 13

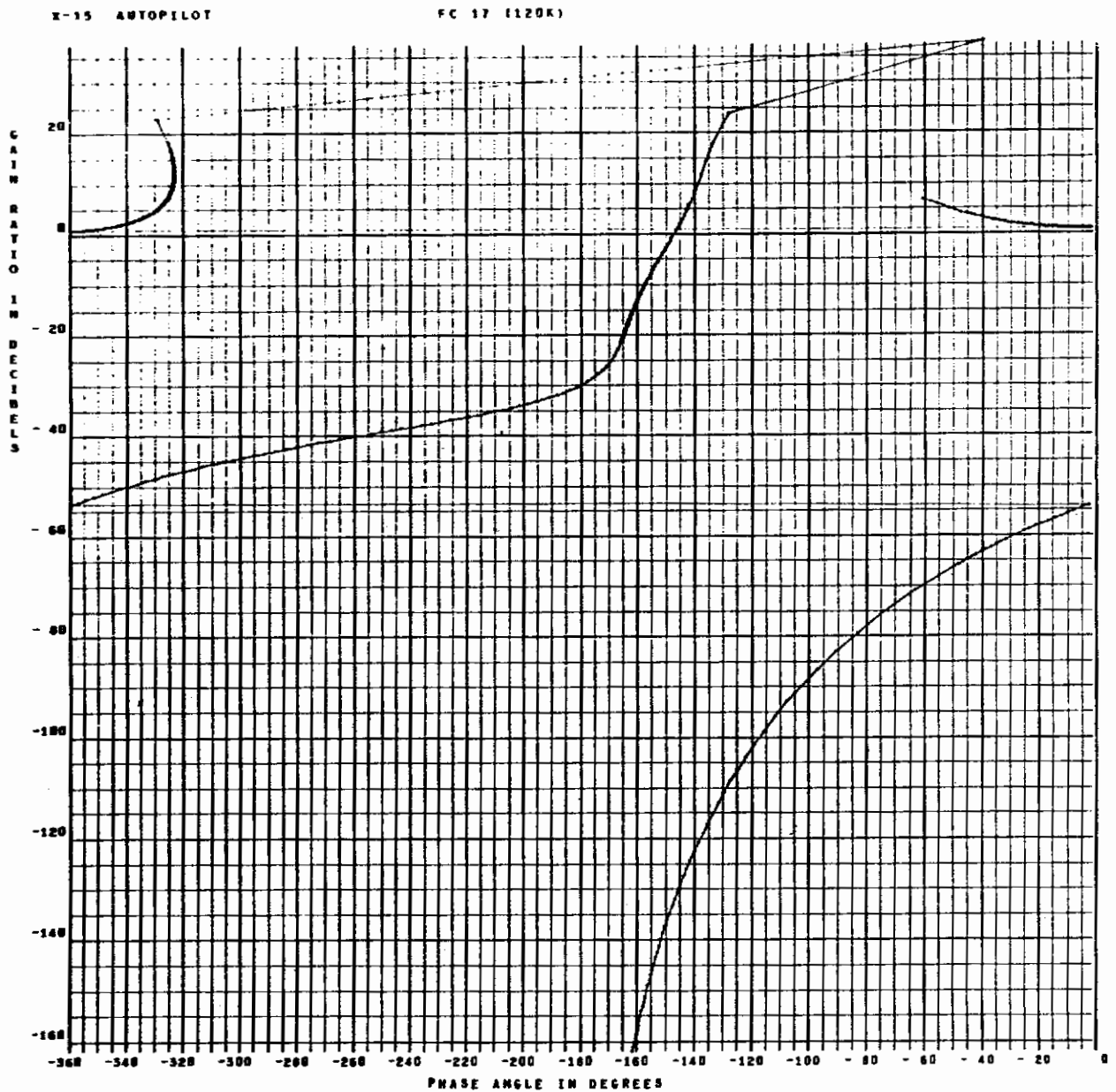


Figure 22. Bode Gain/Phase $G_2G_3P(j\omega)$, FC 17

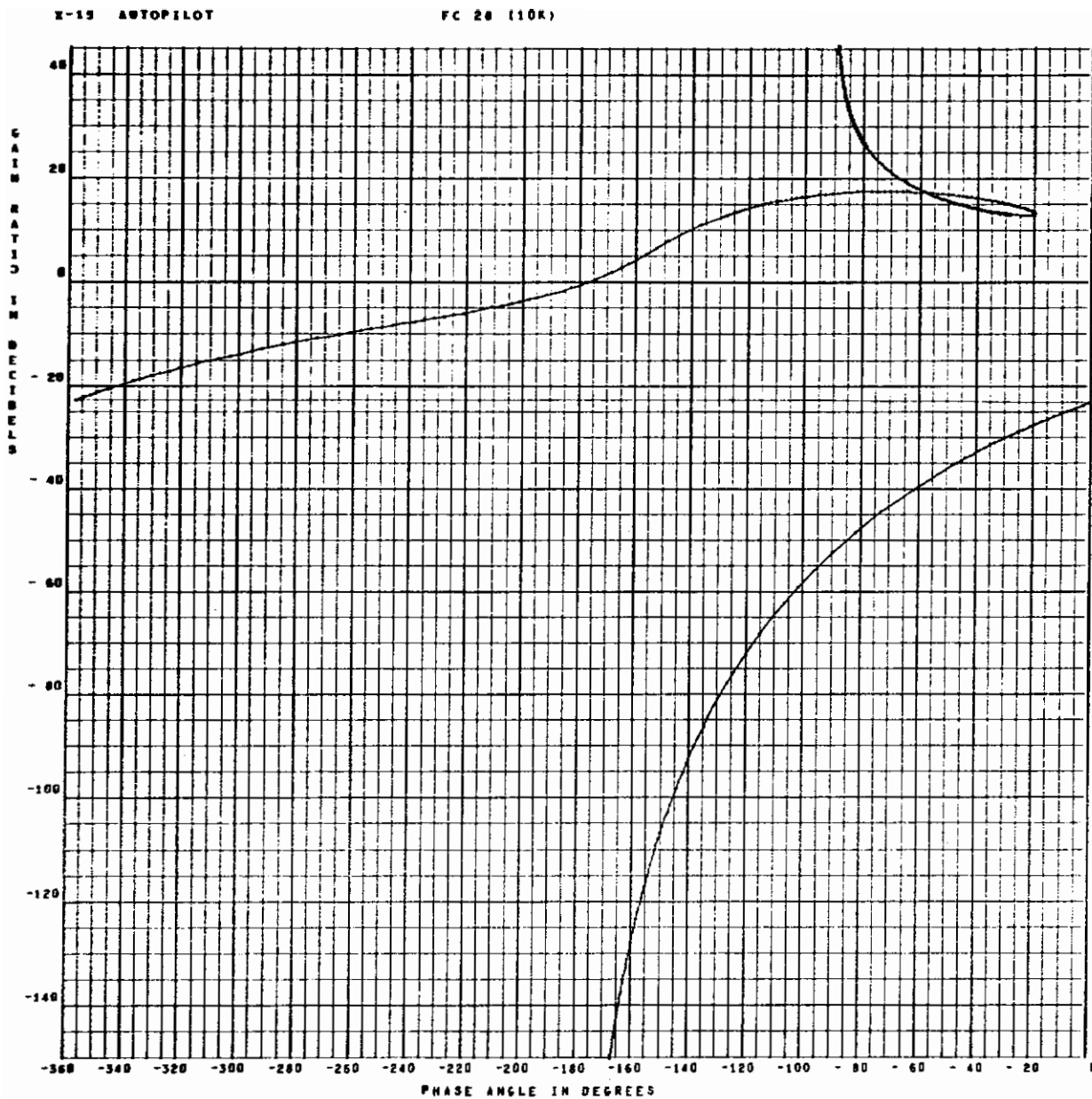


Figure 23. Bode Gain/Phase $G_2G_3P(j\omega)$, FC 28

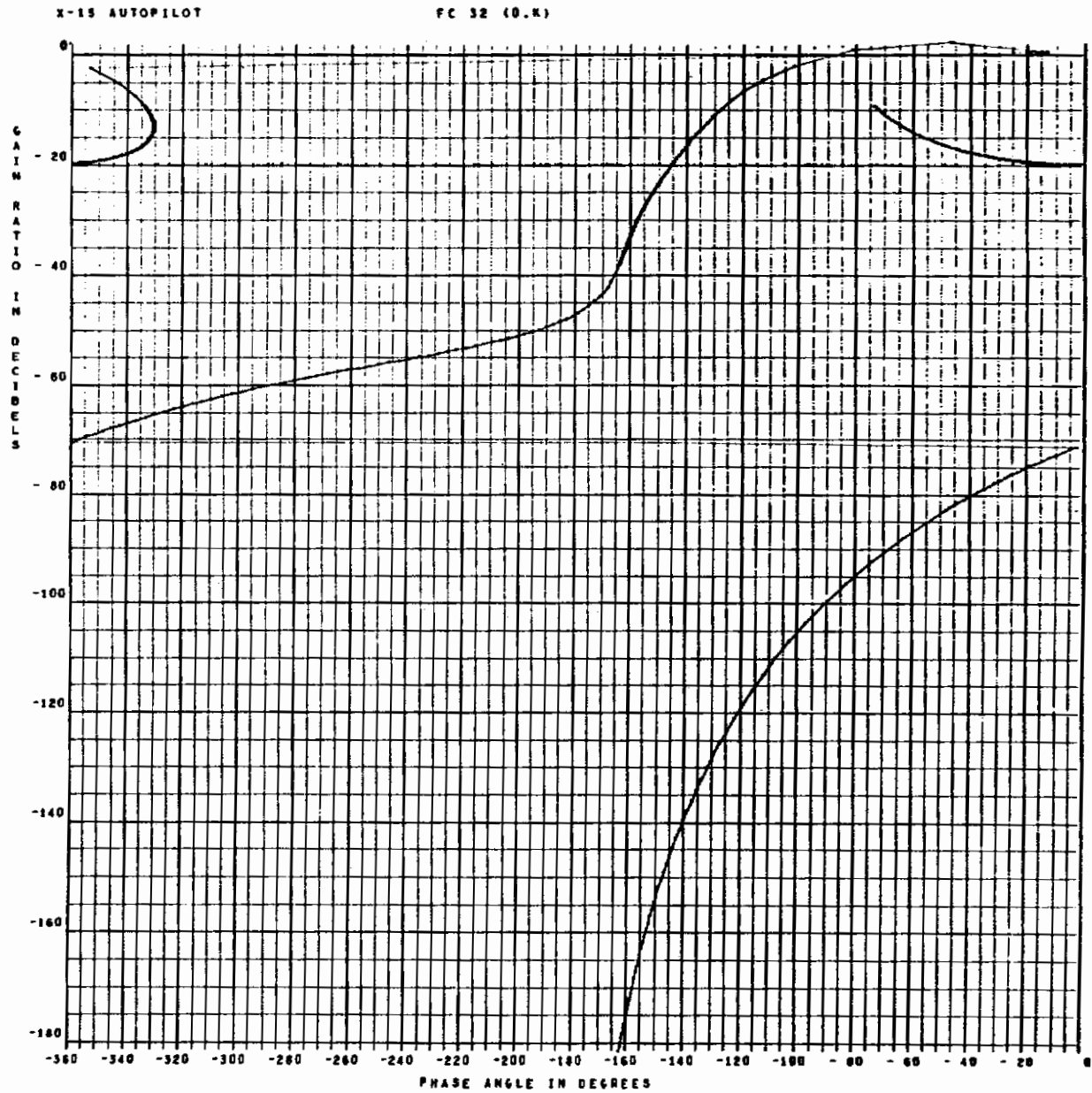


Figure 24. Bode Gain/Phase $G_2G_3P(j\omega)$, FC 32

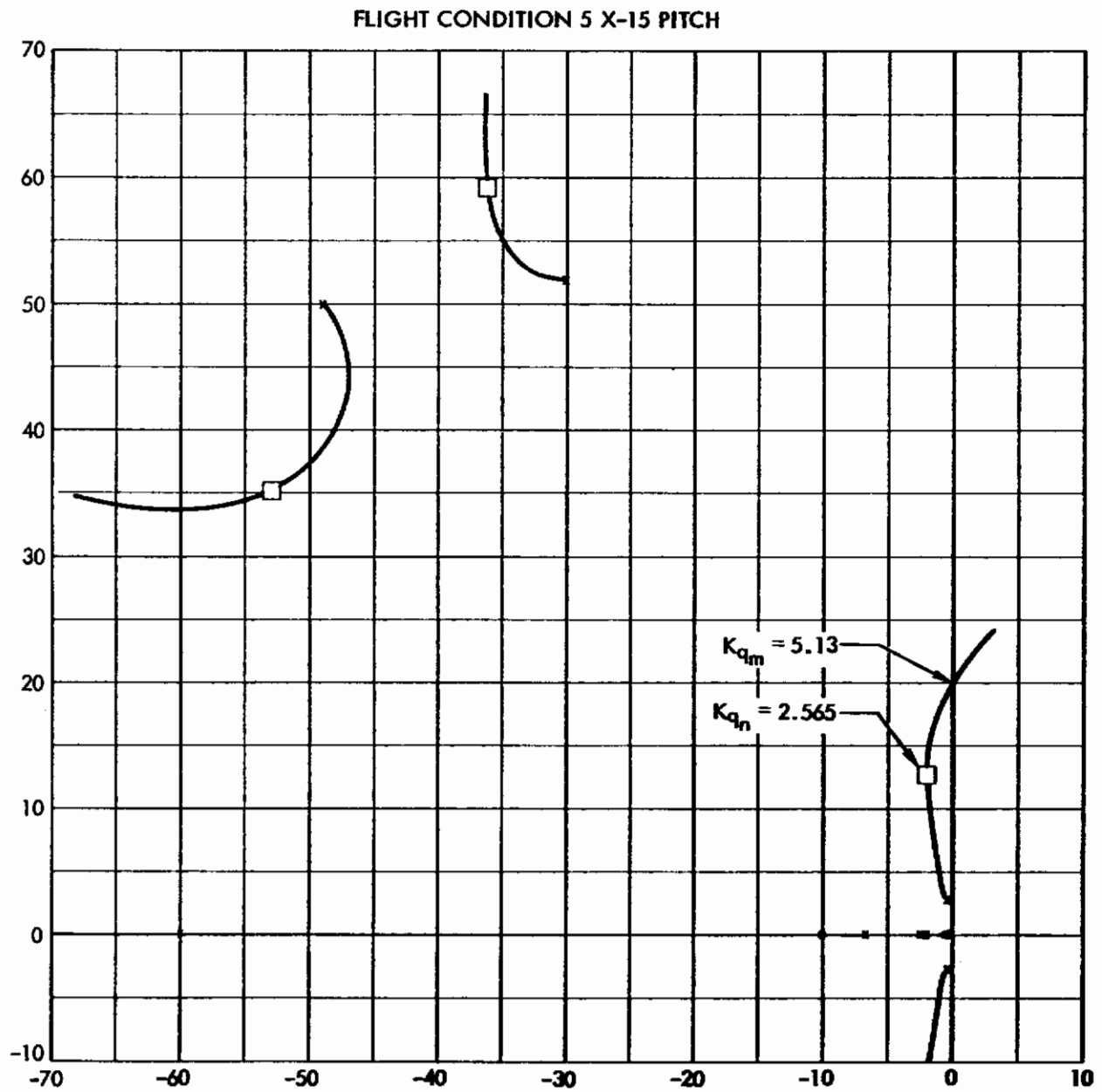


Figure 25. SAS Autopilot Root Locus, FC 5

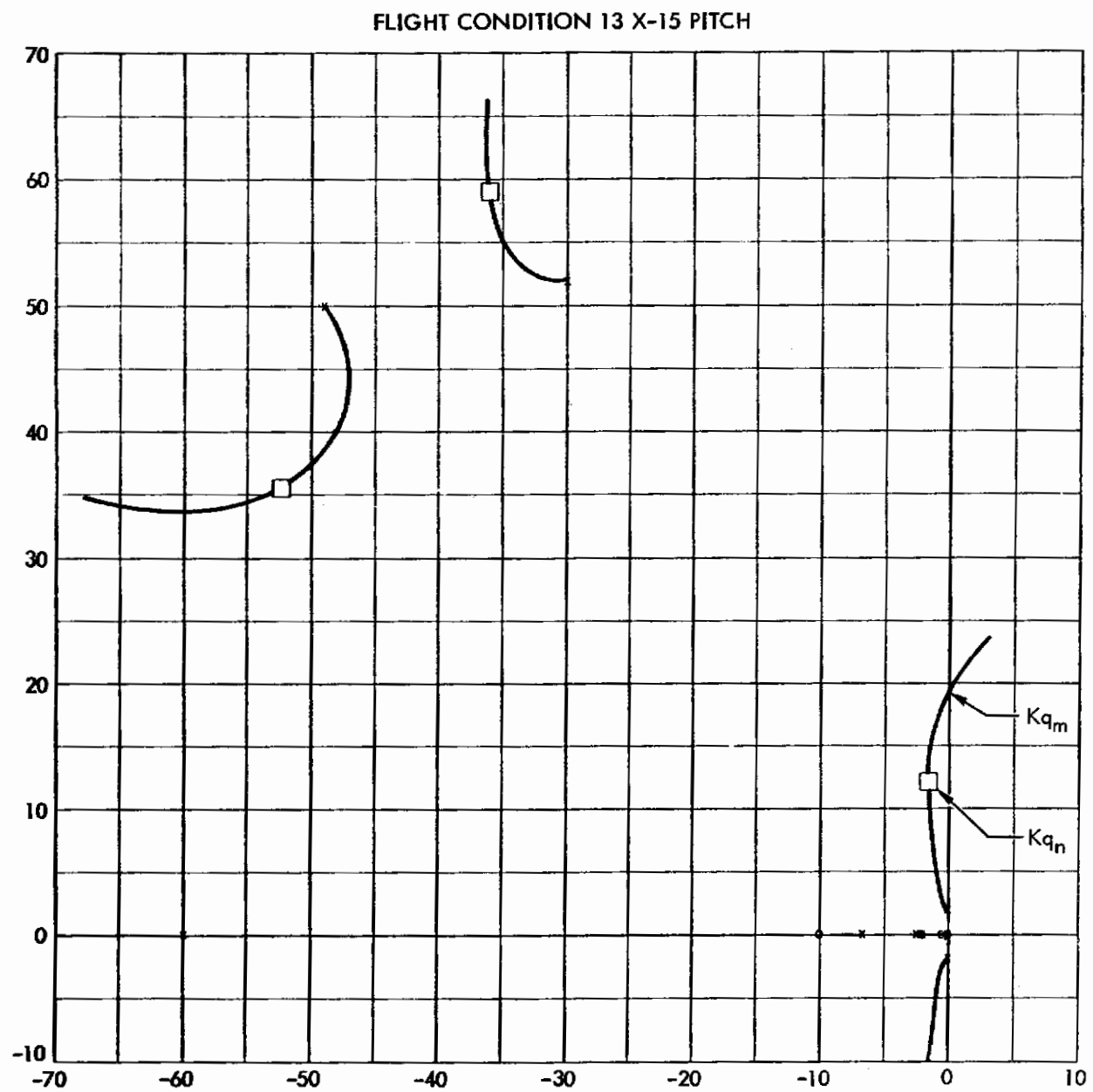
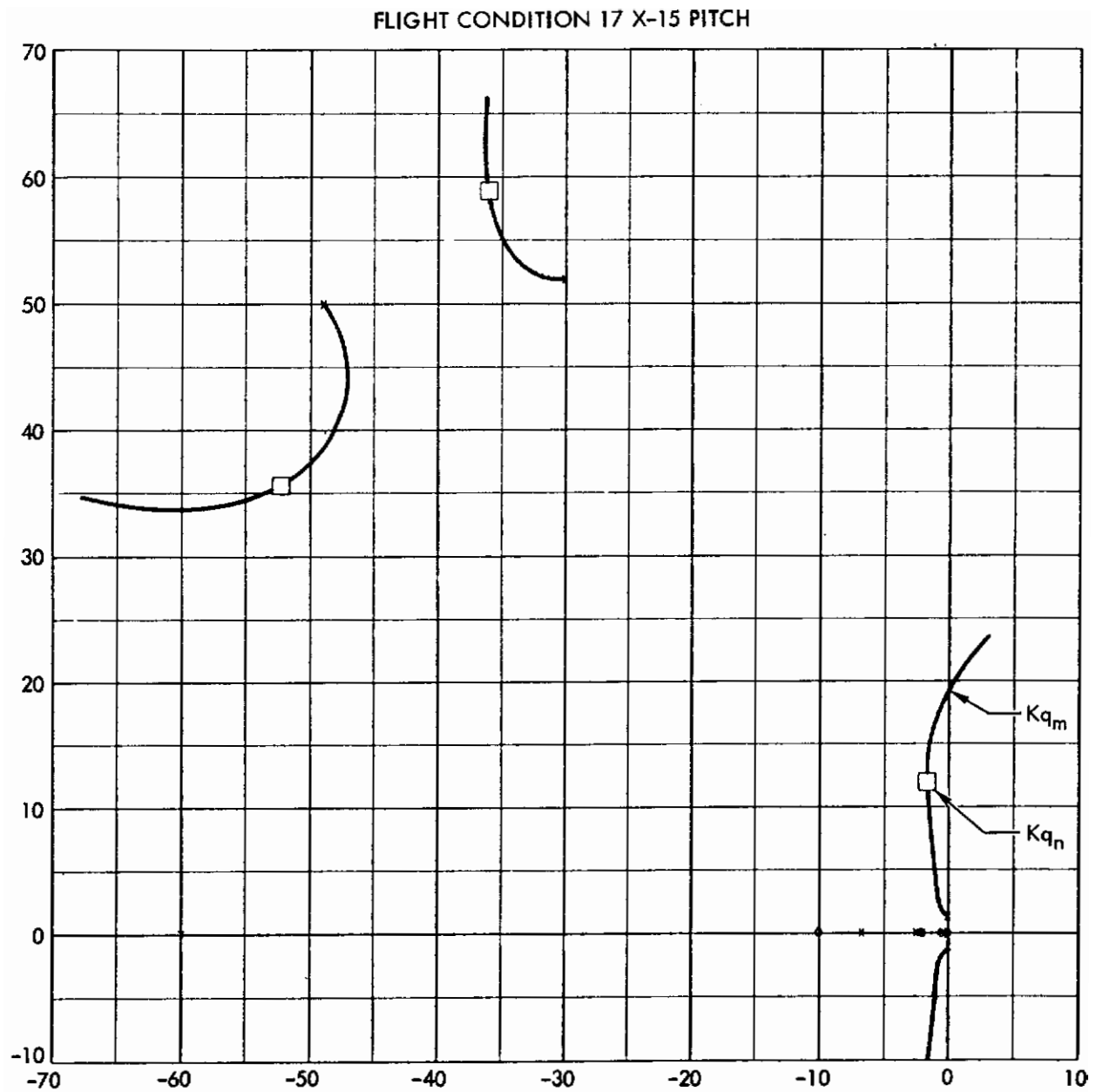


Figure 26. SAS Autopilot Root Locus, FC 13



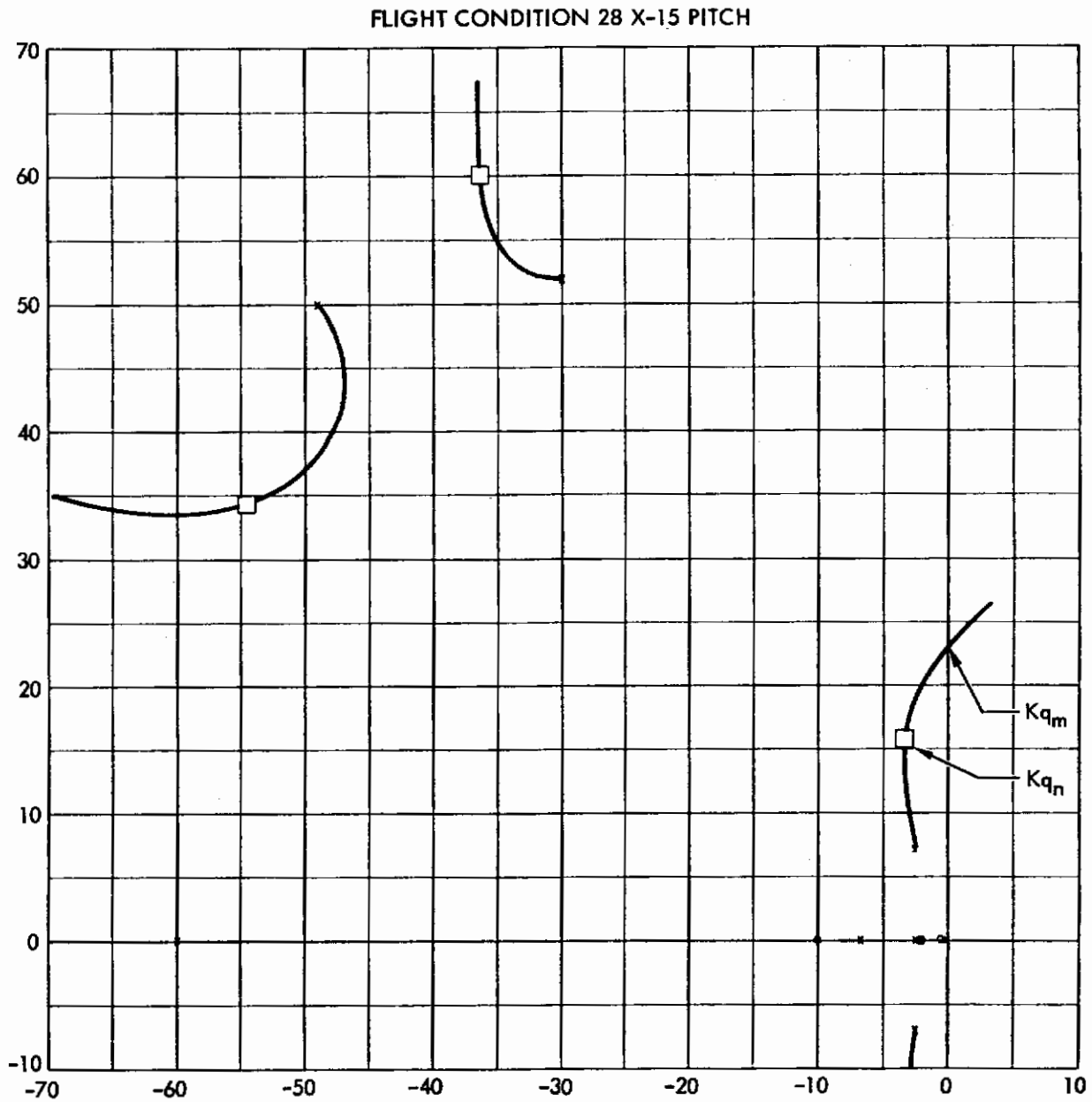


Figure 28. SAS Autopilot Root Locus, FC 28

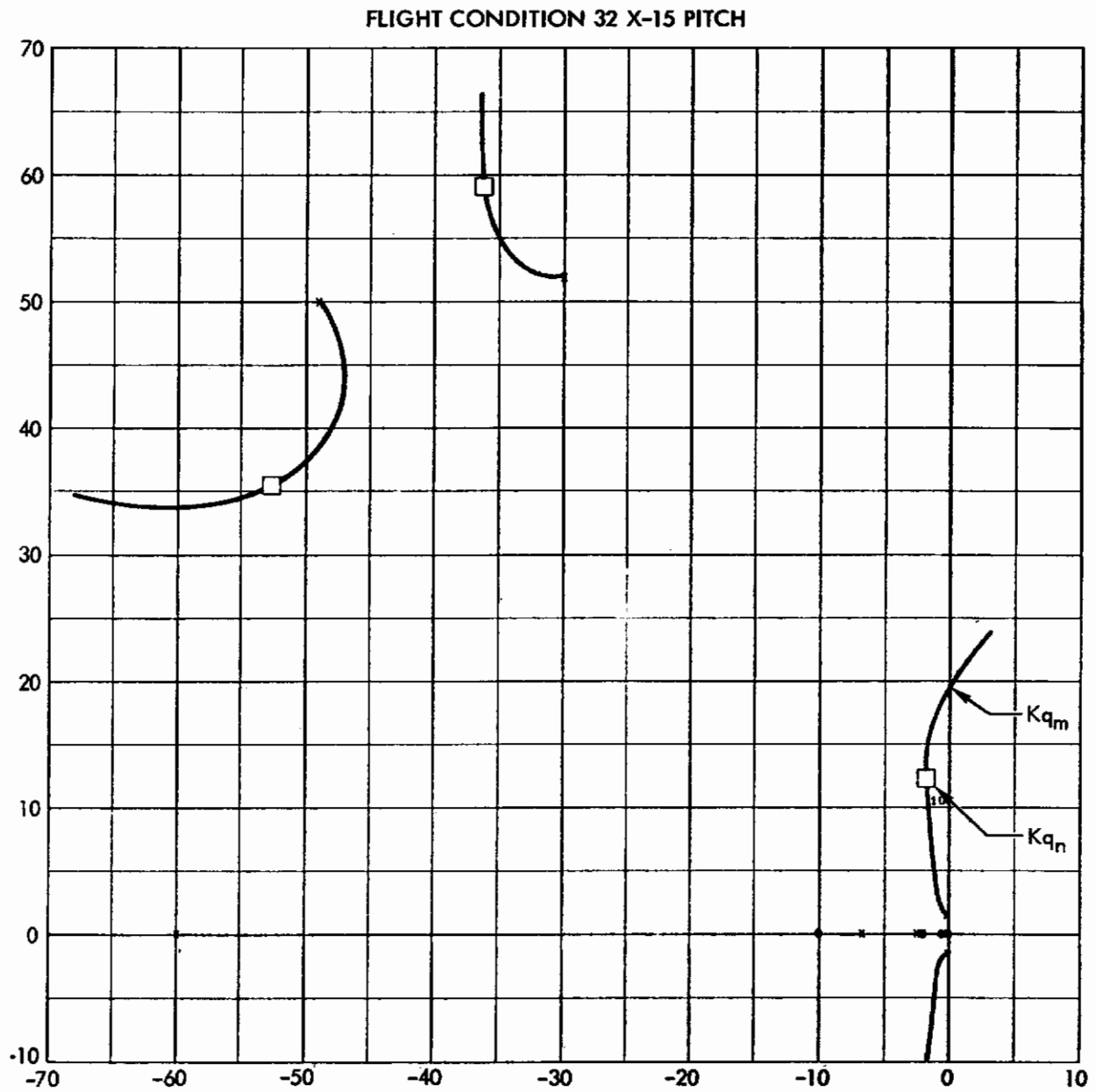


Figure 29. SAS Autopilot Root Locus, FC 32

TABLE 2.
ADAPTIVE AUTOPILOT GAIN ADJUSTMENT DATA

Flight Condition	$M_{\delta} \left(\frac{\text{deg/sec}^2}{\text{deg}} \right)$	$K_{q_m} \left(\frac{\text{deg}}{\text{deg/sec}} \right)$	$K_{q_n} \left(\frac{\text{deg}}{\text{deg/sec}} \right)$	$M_{\delta} K_{q_n}$	$\left(\text{at } K_q = K_{q_n} \right) - \frac{\sigma_A/C}{\left(\frac{1}{\text{sec}} \right)}$ (closed loop)
5	9.7589	5.13	2.565	25	1.92
13	2.2394	21.6	10.8	24	1.62
17	1.5506	31.22	15.61	24	1.63
21	20.859	2.3	1.15	24	
25	3.0919	15.632	7.816	24	
28	52.9406	1.035	0.5175	27	3.25
31	16.293	3.245	1.6225	26	
32a	0.2193	226.0	113.0	25	1.79
32b	0.2193	226.0	18.91	4.15 (K_q limited)	

$$\zeta' \omega' = \zeta_a \omega_a + K_{qn} M_\delta / 2 \quad (50)$$

Inasmuch as open-loop damping $\zeta_a \omega_a$ is usually small relative to damping provided by the control system, constant high-frequency gain provides nearly invariant damping, verifying the results obtained from the root loci.

ANALOG COMPUTER SIMULATION RESULTS

Simulation results have demonstrated the effectiveness of the parameter identification and control loop gain adjustment schemes for both pitch and lateral axes. Figures 30 and 31 illustrate a typical run for the pitch axis. The control loop was initially unstable, with the gain 10 percent above critical. The initial divergence, capture, and transient tailoff was accomplished in still air, with no pilot inputs. A two parameter model was used, with the parameters initially set to zero. The b_3^* parameter converged quickly and accurately, as is generally the case. This is fortunate, because b_3^* is used to compute the control loop gain K_q from equation (30).

Data Coverage

The X-15 raw data points available for simulation purposes were obtained from Reference 11. Figure 32 is a cross plot of mach number and altitude for the flight conditions presented therein. Seven flight conditions have been selected for study, and these seven are identified by the hexagonal markers in the figure. The seven conditions represent an even coverage of the entire flight spectrum. The derived aircraft parameters b_1 (static pitch stability) and b_3 (elevator effectiveness) are cross plotted in Figure 33. Again the seven chosen flight conditions are identified by hexagonal markers, and again an even distribution including the extremes (within the aerodynamic flight regime) is observed.

Simulation of FC 32 indicated problems associated with identifying parameters of vastly different magnitudes. Based on the original pitch axis transfer function data, the SIDAC parameters were found to have an order of magnitude difference in relative size ($b_1 = 2.274$, $b_3 = 0.2193$). Simulation and intuitive reasoning (Appendix II) based on the form of Lyapunov circle:

$$K_3 V = \frac{(b_1 - b_1^*)^2}{K_1 / K_3} + (b_3 - b_3^*)^2 \quad (51)$$

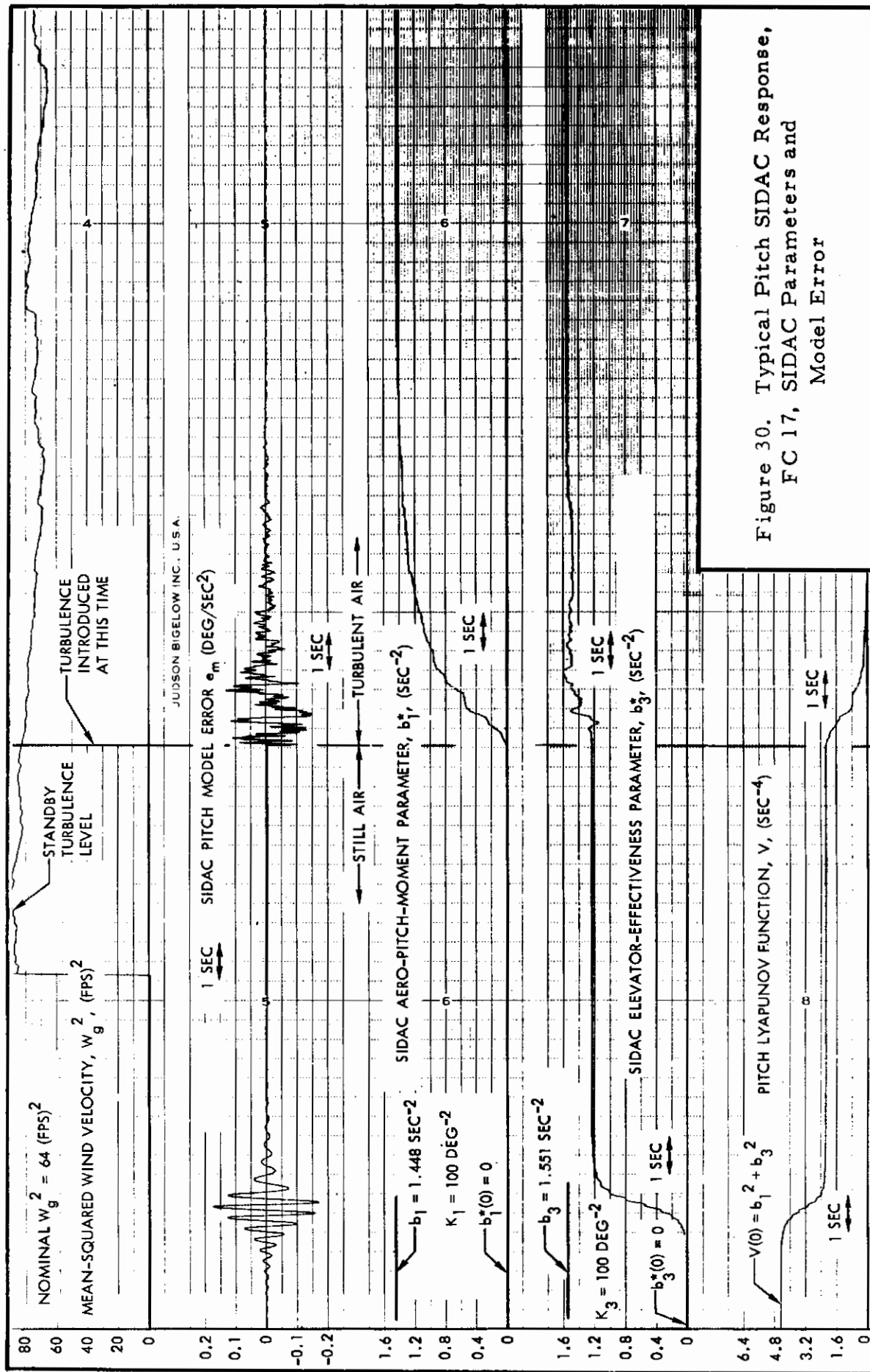


Figure 30. Typical Pitch SIDAC Response,
FC 17, SIDAC Parameters and
Model Error

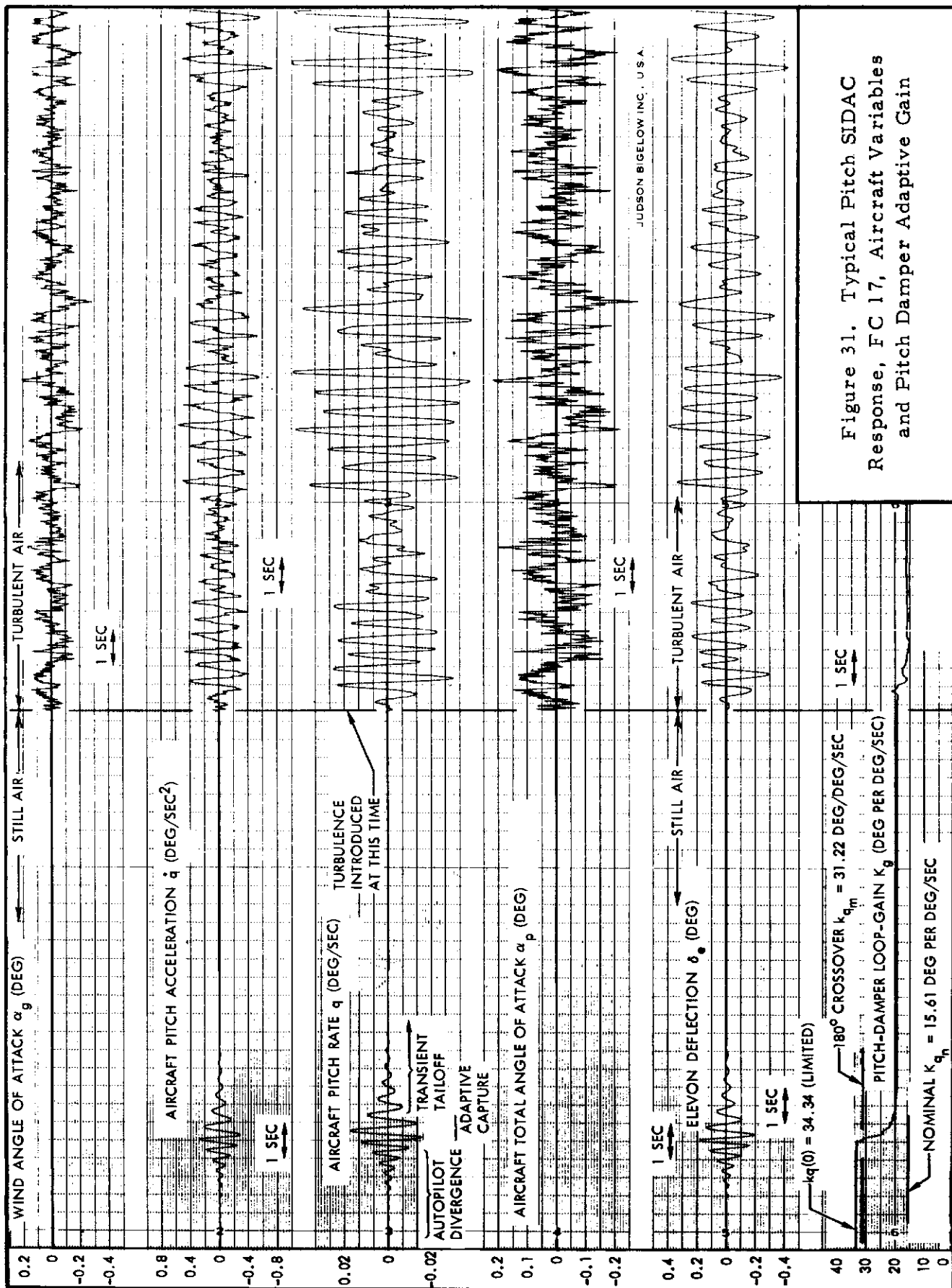


Figure 31. Typical Pitch SIDAC Response, FC 17, Aircraft Variables and Pitch Damper Adaptive Gain

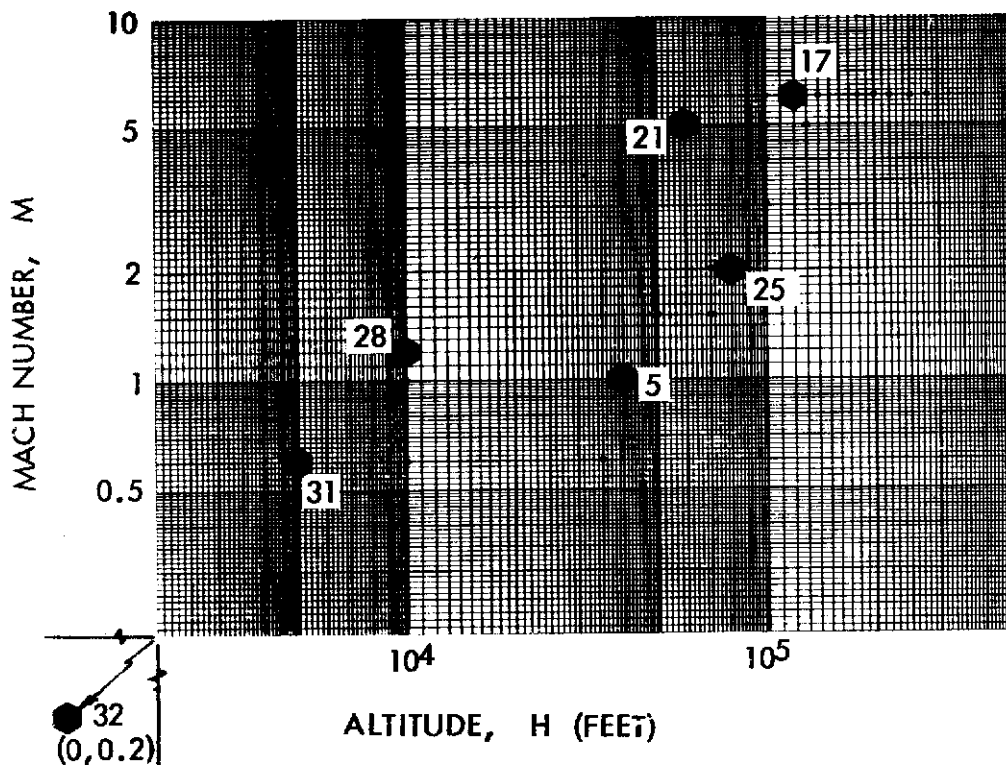


Figure 32. Typical X-15 Flight Conditions

suggested non-steep-descent parameter adjustment gains with a ratio of

$$\frac{K_1}{K_3} = \frac{(b_1^*)^2}{(b_3^*)^2} \quad (52)$$

An automatic gain ratio circuit was developed and tested. Results were excellent and gain adjustment worked well when tested at other flight conditions.

The plot of Figure 33 cast suspicion on the data of FC 32a, however, in that the parameters b_1 and b_3 were nearly equal at all other flight conditions.

The data was corrected as follows:

Original Data	Revised Data
FC32a	FC32b
$-Z_{\delta_e}$ 27.171	$-Z_{\delta_e}$ 2.7171
ω_a 1.5111	ω_a 0.5111

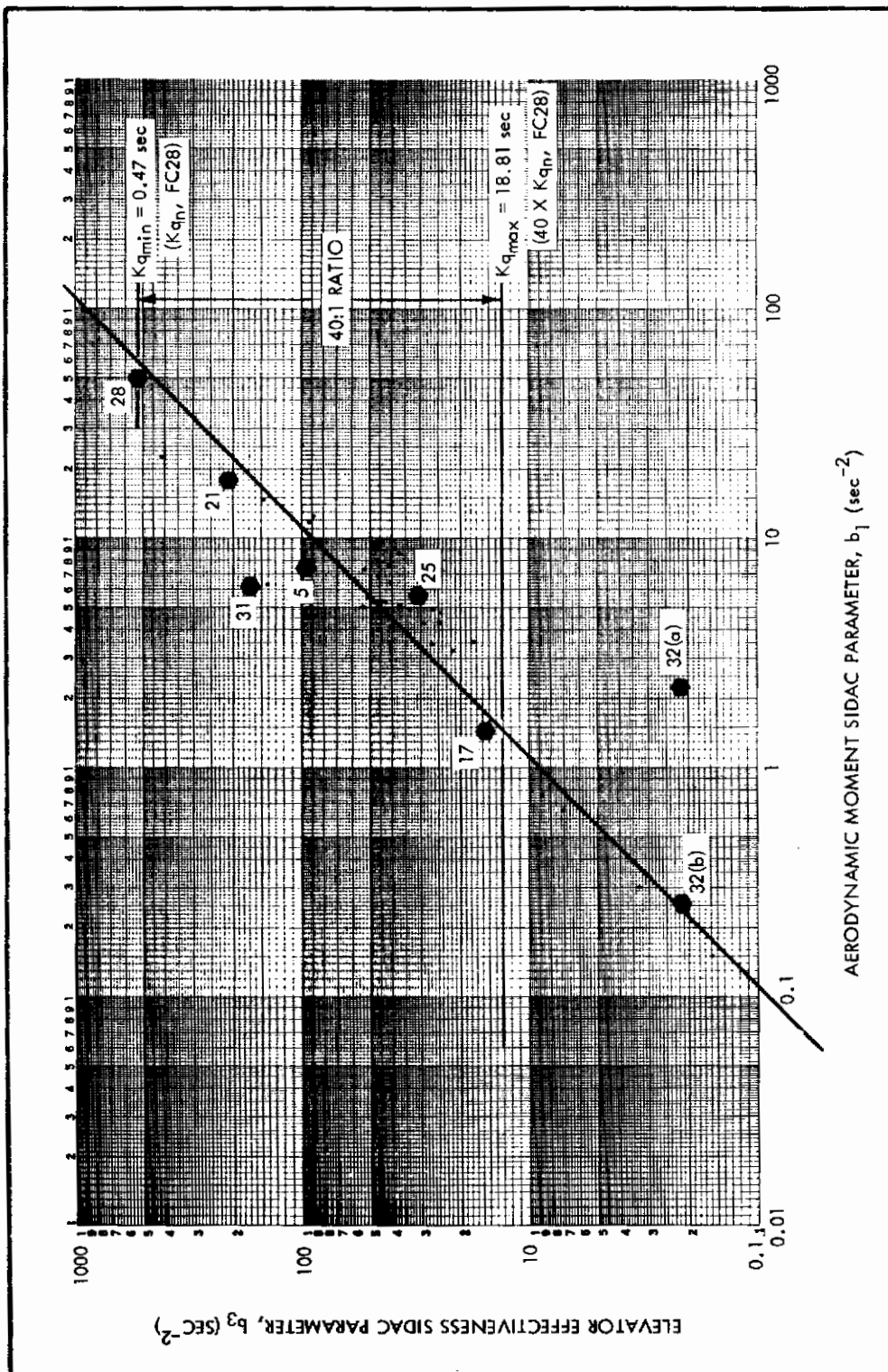


Figure 33. Typical X-15 Flight Conditions in Terms of SIDAC Parameters

With the revised data (designated FC 32b) in Figure 33, the b_1/b_3 ratio is unity, and the gain ratio adjustment is no longer required.

Except for the inconvenience of searching for the error, nothing was lost; in fact, insight into the selection of the optimum gain ratio for non-steep-descent was gained.

AGC Simulation

The need for AGC in decoupling signal level variations in identification response times was discussed in Section 3. Simulation study (as pictured in Figure 34) has been completed for each of the seven chosen flight conditions. A simplification was introduced in that AGC gain K_M was based only on elevator deflection.

Figure 35 presents the results of these studies in terms of 95 percent Lyapunov response times vs the parameter adjustment (steep descent) loop gain K . The effectiveness of AGC is evident: two of the original three flight conditions coincide, and the total spread in response time at any fixed K is only 8.5 to 1 if the FC 32a (bad data) is neglected. Ideal sensors were used.

Whereas without AGC it was impossible to pick a single value of K which would be acceptable at all flight conditions, the data of Figure 35 indicates that a value of $K = 200$ or even 500 would give excellent identification results throughout the X-15 flight spectrum.

Adaptive Loop Gain Adjustment

Loop gain adaptive adjustment based on equation (30)

$$K_q(t) = \frac{(M_{\delta e} K_{qn})_{\text{set}}}{b_3^*(t)} \cong \frac{25}{b_3^*(t)} \quad (53)$$

has been tested and proven effective at each of the seven selected flight conditions. A decision was made to limit the adaptive gain range to a 40 to 1 ratio, which established the upper limit of loop gain:

$$K_{q_{\max}} = 40 \left(\frac{25}{b_3^*} \right)_{\text{FC28}} = 18.91 \quad (54)$$

As shown in Figure 33, the 40 to 1 range makes it possible to adjust K_q to the optimum value K_{qn} at all but the landing condition FC 32 and several extremely high altitude conditions. Nevertheless, performance is

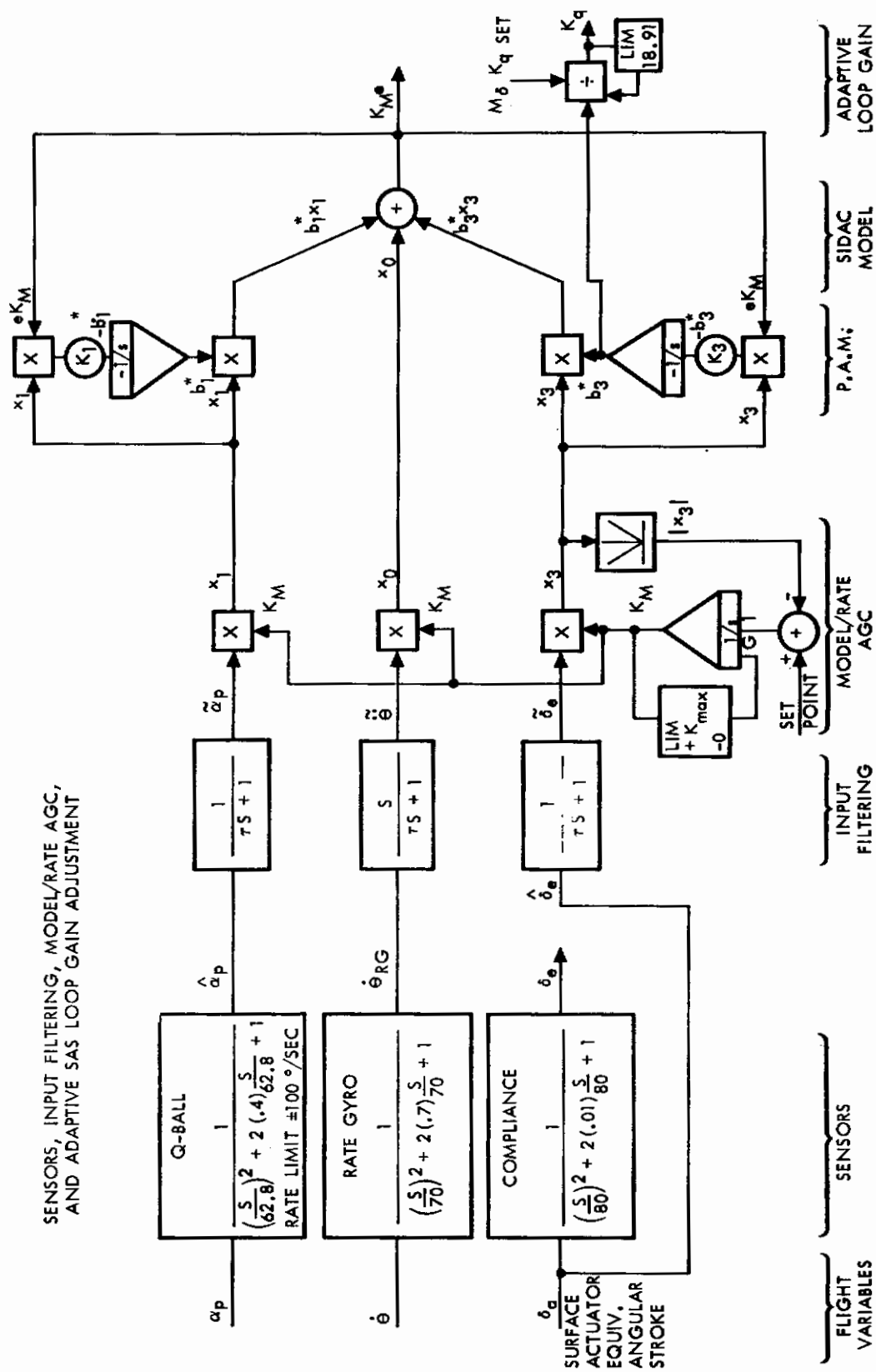


Figure 34. SIDAC Block Diagram

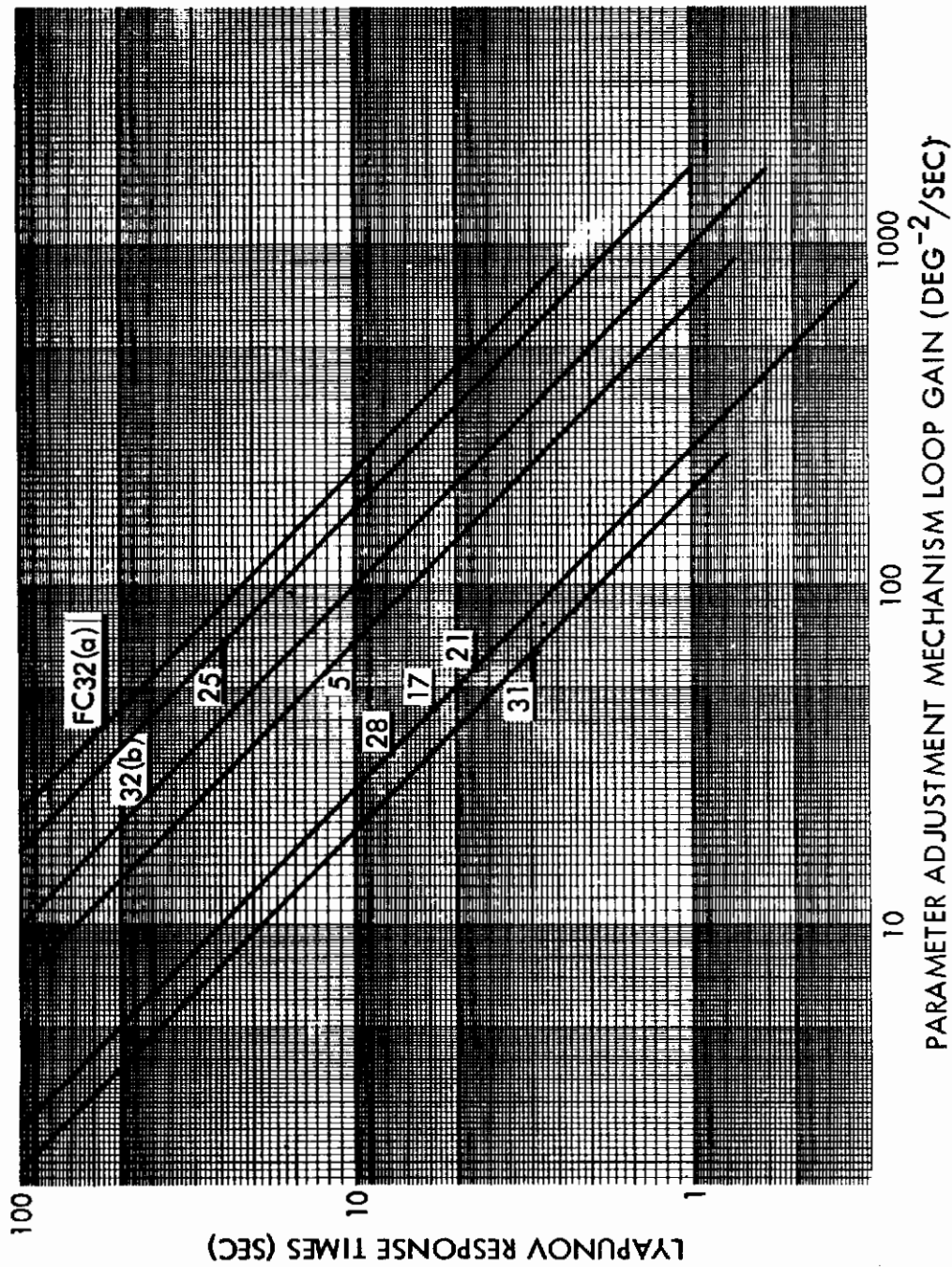


Figure 35. Pitch SIDAC Identification Times

still acceptable at landing, as can be seen in Figure 36. Reaction jet control will be required to augment the elevator aerodynamic control at the high altitude conditions.

Effects of Input Filtering

Input filtering is desirable from at least four aspects:

1. It obviates the need for an angular accelerometer since the rate gyro signal can be used to obtain the \dot{q} signal.
2. Low-pass filters will be effective in reducing the signal contamination due to sensor noise, sensor dynamics and nonlinearities, and higher order airframe dynamics such as bending and compliance.
3. High-pass filters can be used to wash out trim conditions if this proves desirable.
4. Bandpass filters can be used in special cases of severe bending or noise of concentrated bandwidth.

Only the first and second of these aspects have been investigated, as indicated by the configuration shown in Figure 34.

Figure 37 is included to show a typical run with low pass filtering, combined with derived \dot{q} information. No quantitative results are available, but no observable degradation of identification has been experienced.

Effects of Real Sensors

Sensor noise, sensor dynamics and sensor nonlinearities (e. g. , thresholds and rate or position saturations) add spurious components and modify the frequency content of sensed information.

The effect of adding a large noise component to an otherwise ideal sensor is shown in Figure 38. If the adaptive loop gain were adjusting, the flight system would become unstable for $b_3^* < \frac{25}{226} = 0.11$. This level is indicated on the b_3^* trace in Figure 38. The divergence associated with such instability would, of course, increase the signal level relative to the noise, identification would improve and loop gain would be reduced.

Figure 39 demonstrates what happens with more reasonable sensors. That is, sensor dynamics and nonlinearities as given in Figure 34 are involved but there is no sensor noise.

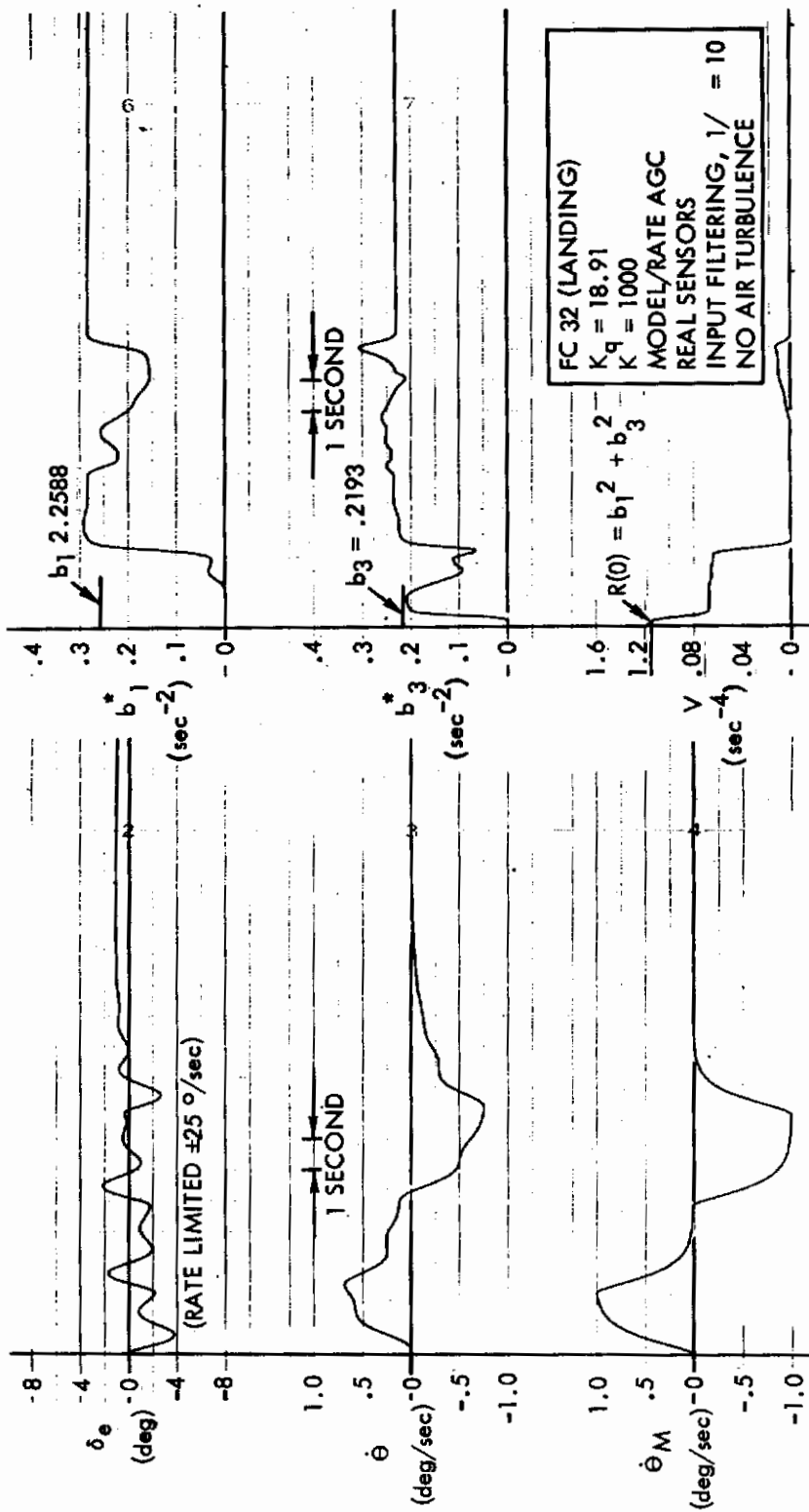


Figure 36. Identification on Pilot Inputs

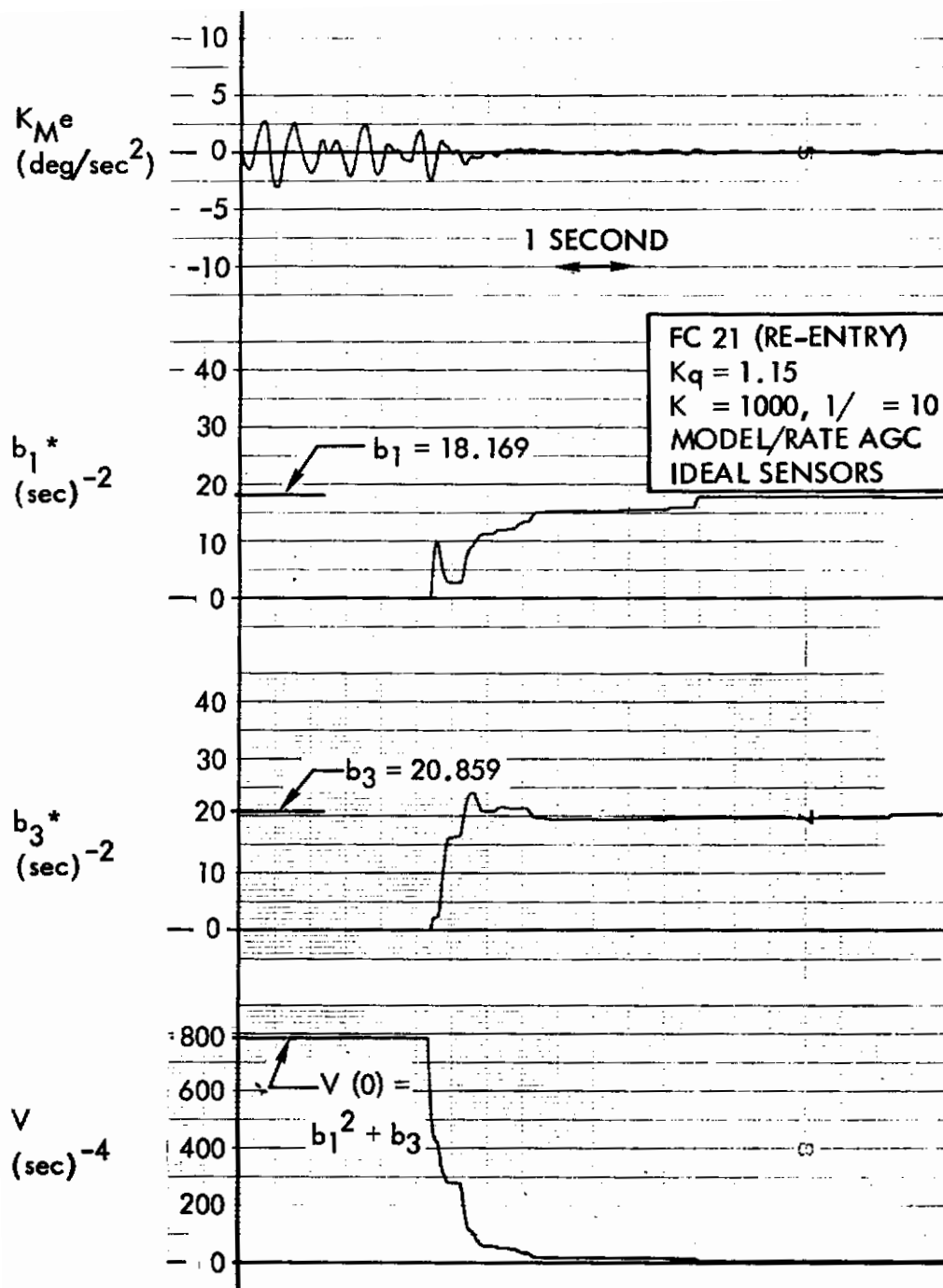


Figure 37. Effect of Input Filtering on Identification

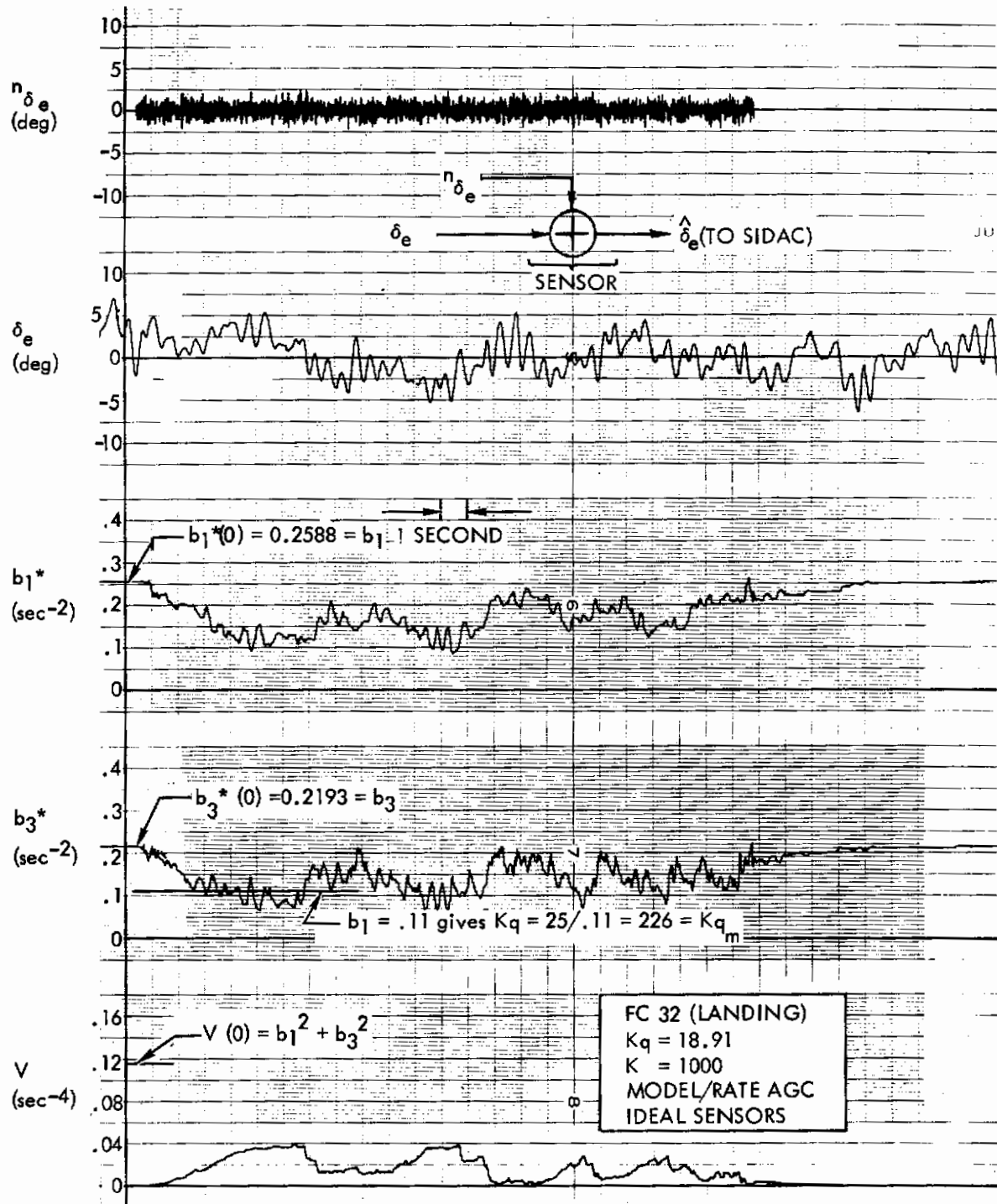


Figure 38. Effects of Sensor Noise

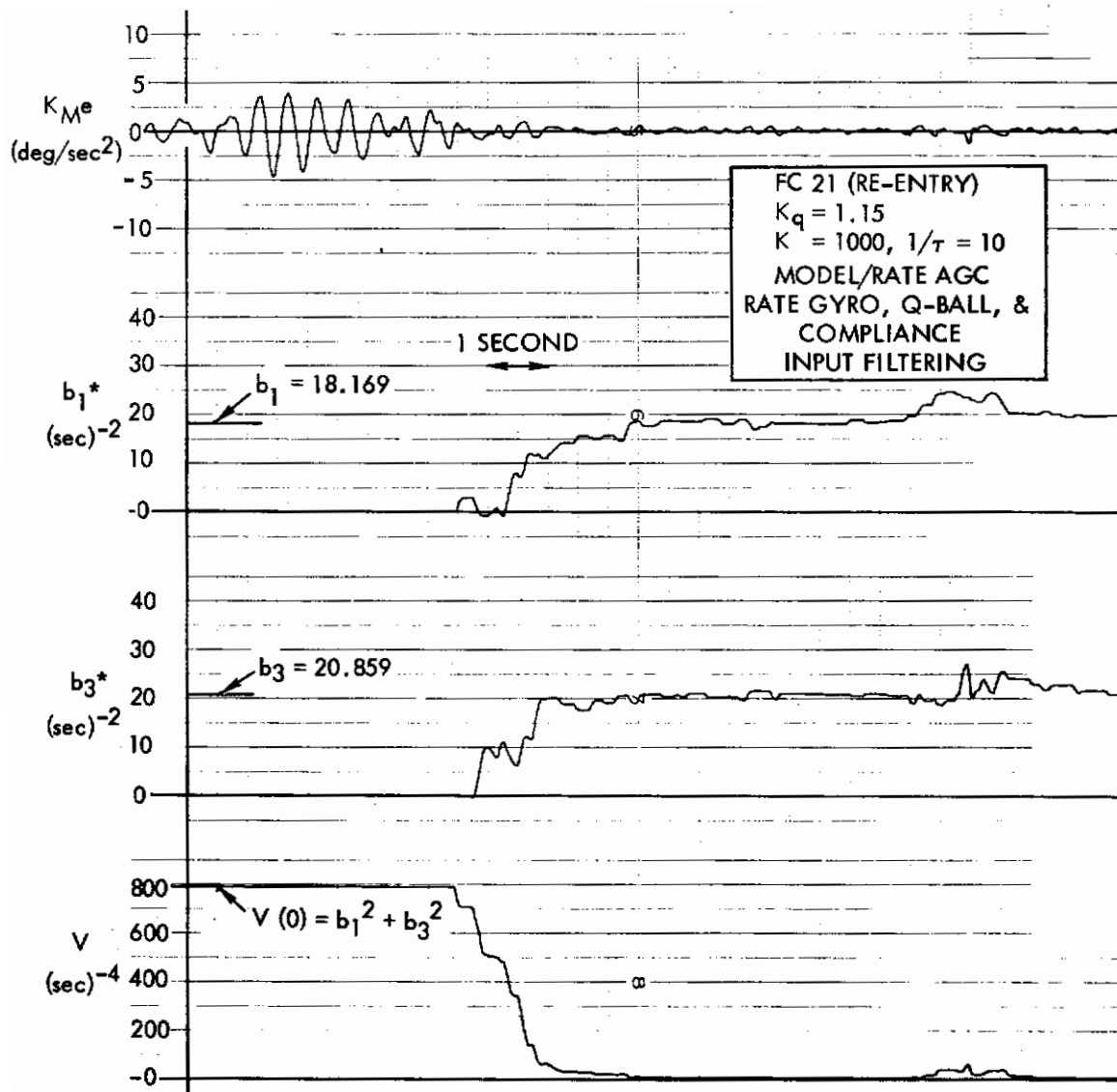


Figure 39. Effects of Real Sensors

The aircraft dynamics at FC 21 (Figure 39) have a bandwidth of 12 rps for the optimum loop gain $K_{qn} = K_{qm}/2$. The filter time constants are set at 0.1 seconds (10 rps), well below the sensor dynamics at 60 to 80 rps. The identification is smooth. At the lower-frequency FC 32b the identification is even better. The conclusion is that "typical" sensor dynamics do not seriously affect identification and that selection of the filter time constants is not critical.

Effects of Pilot Inputs

Figure 40 demonstrates that pilot inputs have no serious effects on identification. Some parameter wandering is observed, but the error deadband (i. e., the integrator clamping levels) which will help to prevent this wandering, needs further study. Figure 36 demonstrates that pilot inputs alone can be used for identification. This is true even with two-parameter identification and real sensors. Error limiting and AGC operation in the presence of pilot inputs deserve further study, particularly peak-reading for rapid reduction of AGC gain to prevent multiplier saturation.

Effects of Signal Level Variations

Figure 41 clearly indicates the ability of three basic SIDAC configurations to reduce the effect of signal level variation upon identification time. Without AGC, coupling is via the expected inverse square relation. SGN Error SIDAC (a relay operating on the sign of the SIDAC error signal replaces the parameter adjustment rate loop multipliers) is also victimized, but only to inverse first-order dependence. AGC SIDAC, however, operates independently of signal level, as indicated by the horizontal line. When the AGC gain saturates, response times revert to the inverse square law dependency.

SGN Error SIDAC Identification

For comparison purposes Figure 42 is included to show a typical SGN Error SIDAC identification response. The error signal (limited to protect the relay amplifier) and the integrator clamping signal (error deadband is required with sgn e multiplication) are shown also.

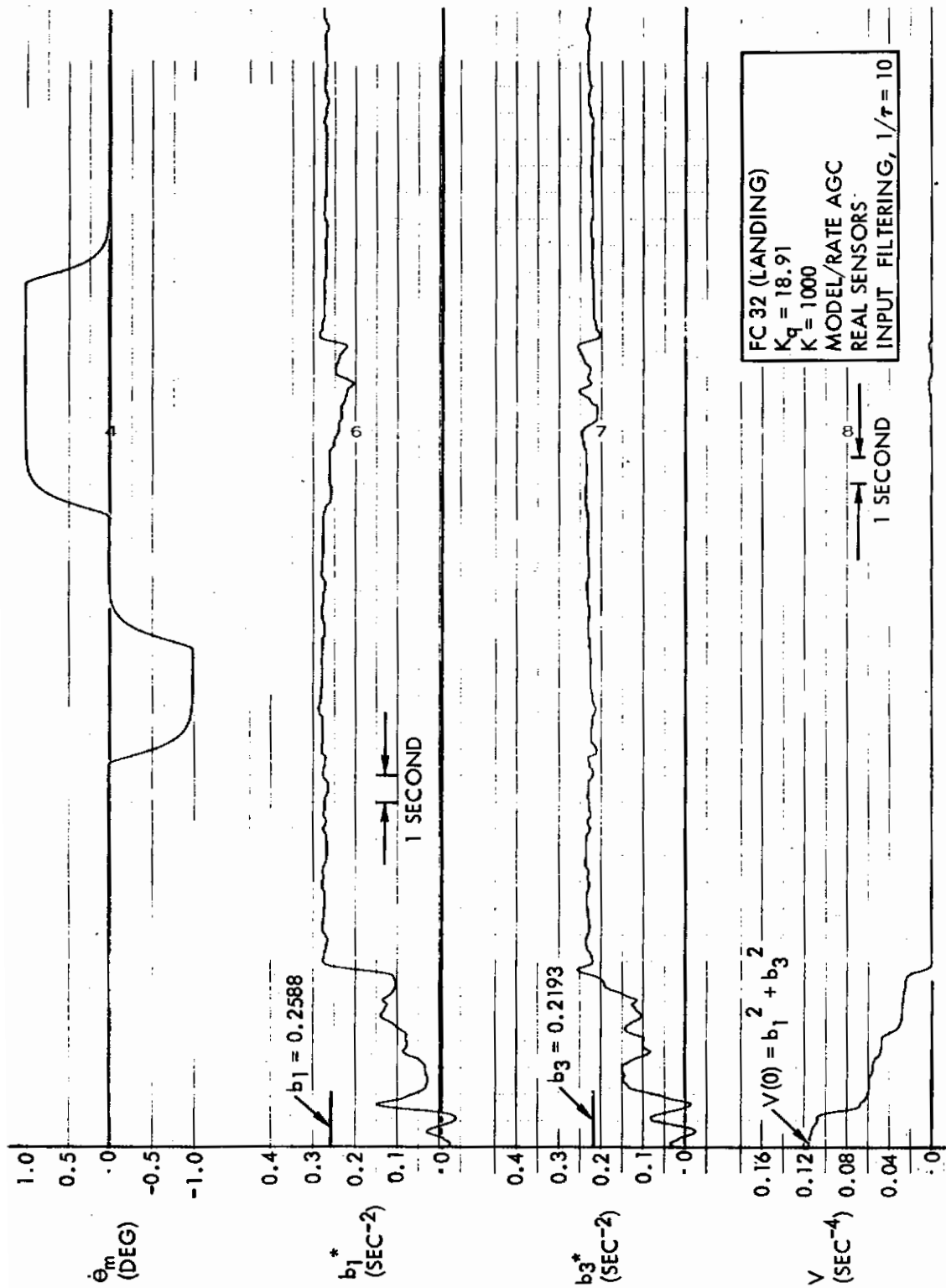


Figure 40. Effects of Pilot Inputs (Sheet 1 of 2)

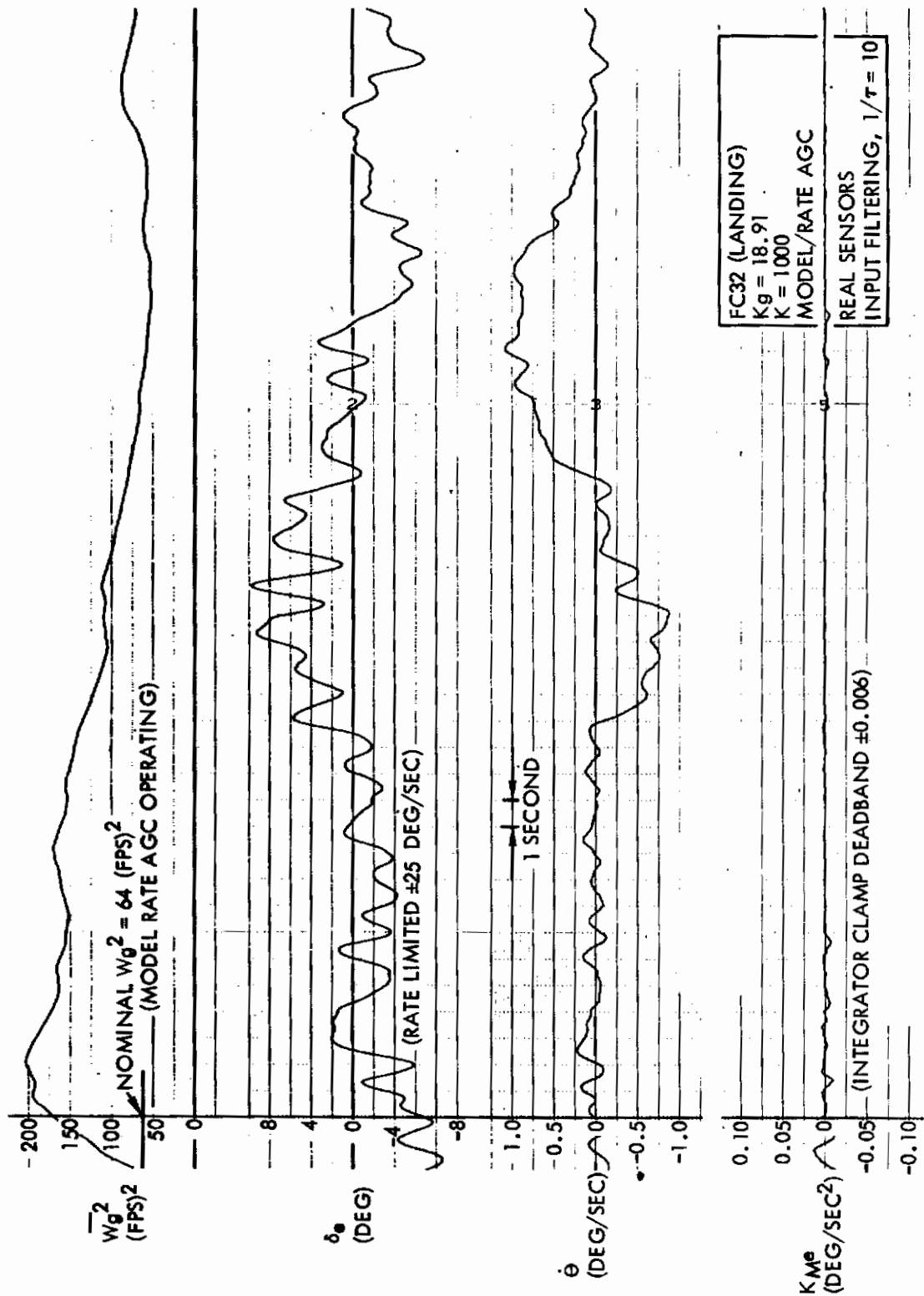


Figure 40. Effects of Pilot Inputs (Sheet 2 of 2)

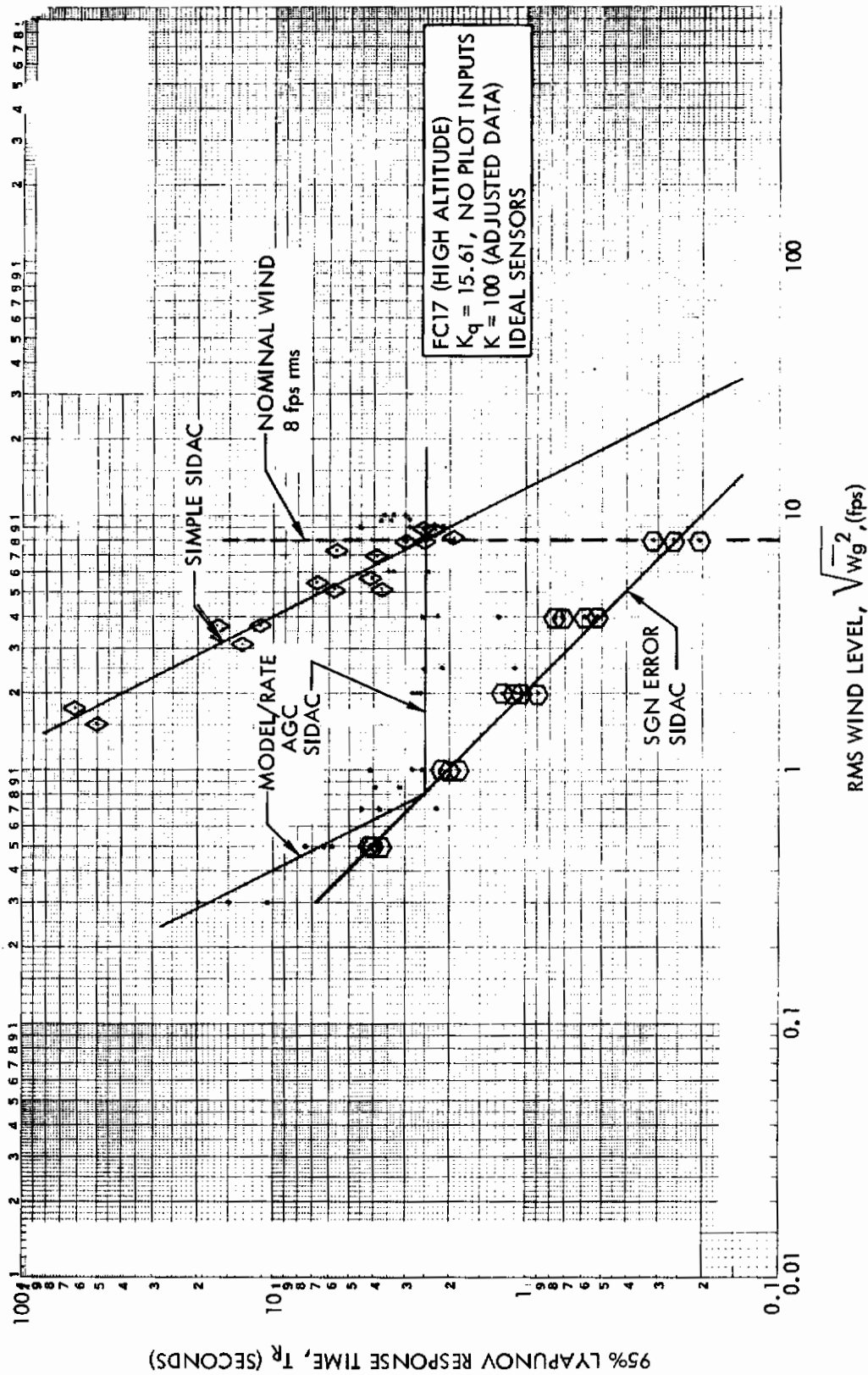


Figure 41. Typical Response Time Variation with Wind Turbulence Level for Three SIDAC Configurations

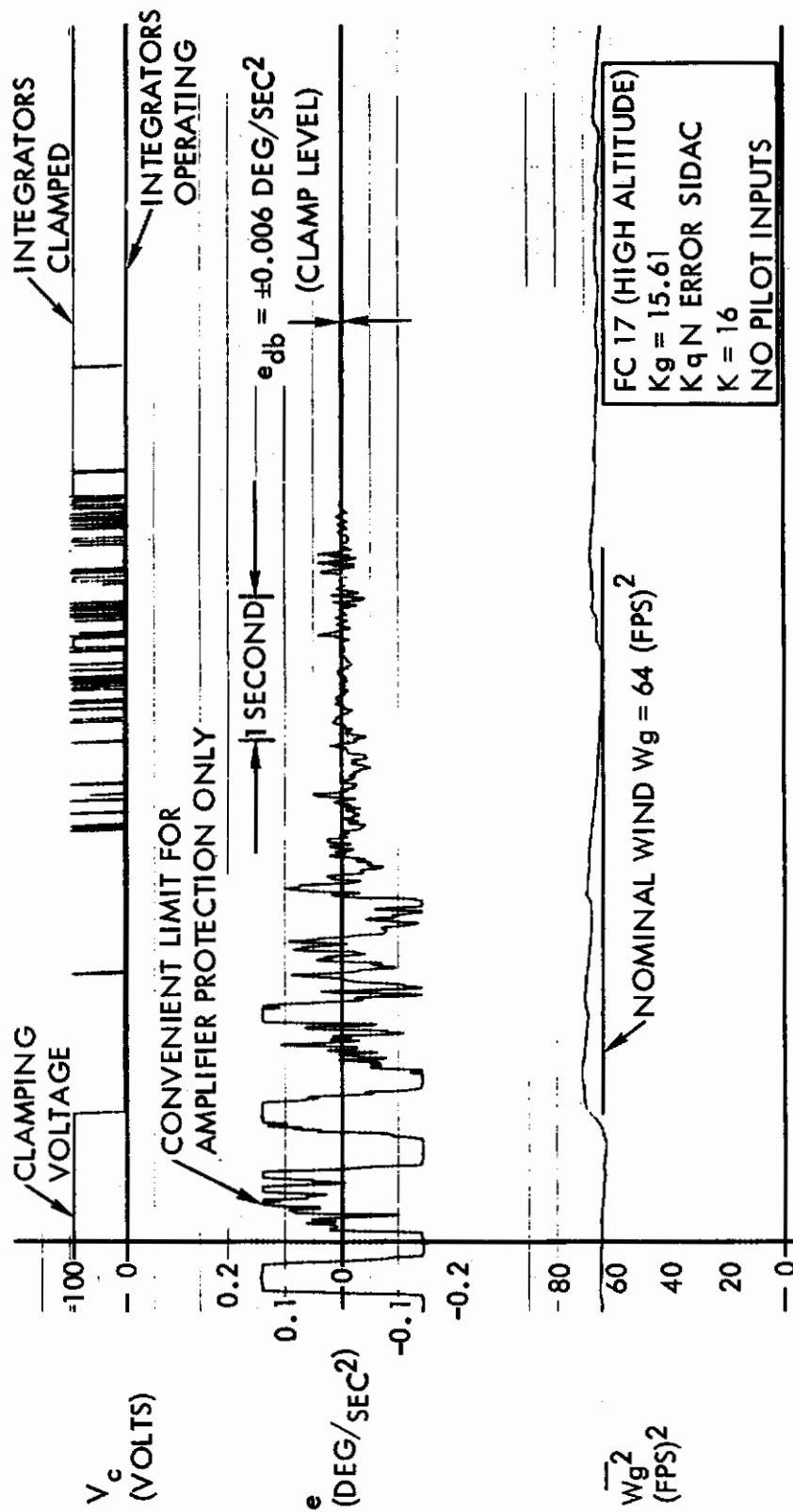


Figure 42. Typical Identification Response With SGN Error SIDAC (Sheet 1 of 2)

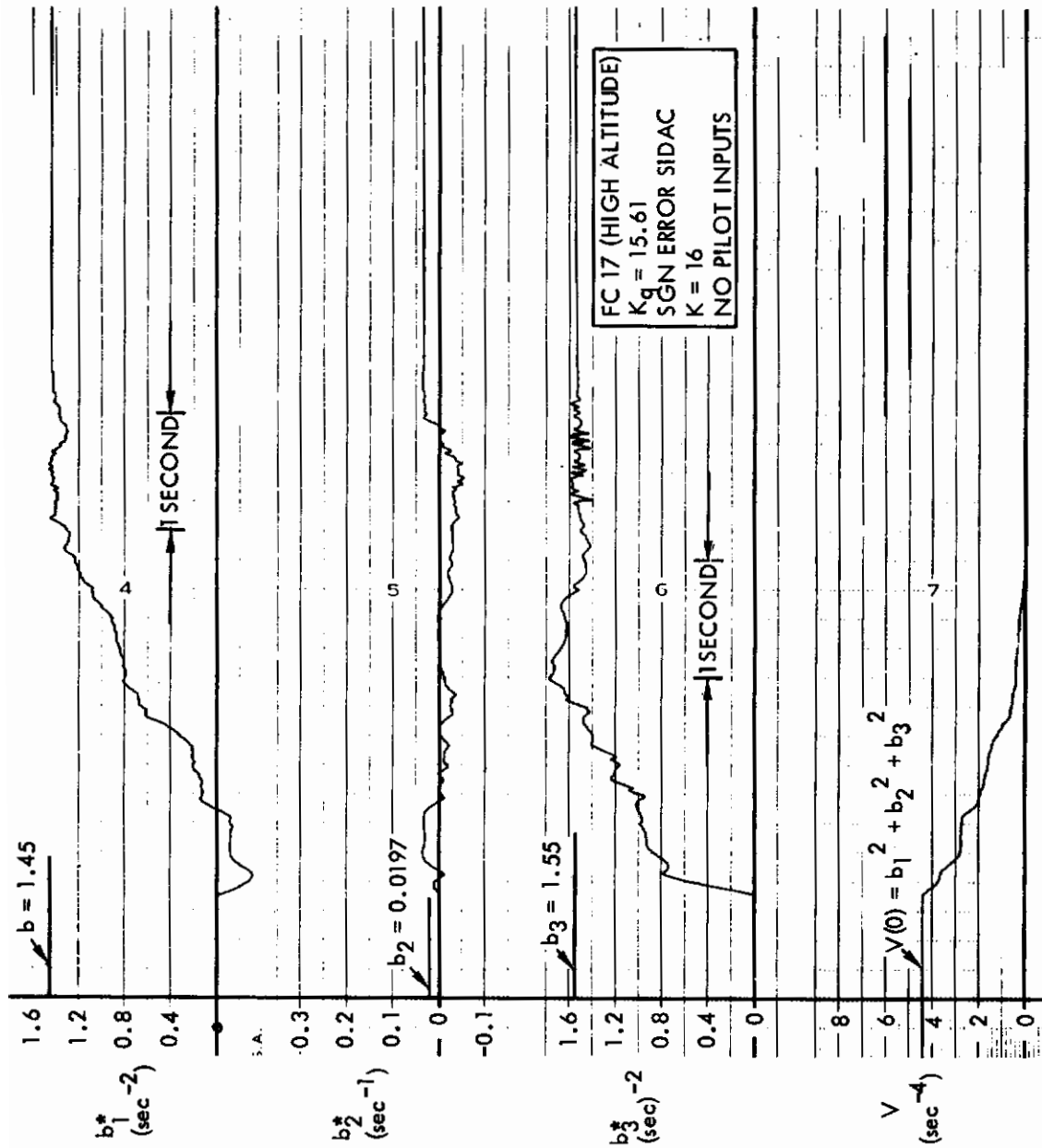


Figure 42. Typical Identification Response with SGN Error SIDAC
 (Sheet 2 of 2)

Contrails

SECTION 5

LATERAL AXES

THEORETICAL JUSTIFICATION FOR TREATING LOOPS SEPARATELY

Inasmuch as a control system for the lateral axes may involve several feedback loops, interaction between loops is an important aspect of the design problem. In this study, four separate loops are used for the roll damper, the yaw damper, lateral acceleration (turn coordination), and yaw into roll (YAR) coupling, respectively. Analytical justification is presented for treating each of these loops independently when making adaptive loop gain adjustments, provided high-gain instabilities occur at relatively high frequencies. This analysis includes the effects of steady-state angles of attack, steady-state pitch angles, cross products of inertia and location of angle of attack sensors or lateral accelerometers.

The equations of motion of the lateral axes are given by equations (II-64) of Reference 5 for stability axes, essentially as follows:

$$U_0 (\dot{\beta} + r) = g_{\psi} \sin \theta_0 + g_{\phi} \cos \theta_0 + Y_r r + U_0 Y_v \beta + Y_p p + Y_{\delta_a} \delta_a + Y_{\delta_r} \delta_r \quad (55a)$$

$$\dot{p} - \frac{I_{xz}}{I_{xx}} \dot{r} = L_r r + L_{\beta} \beta + L_p p + L_{\delta_a} \delta_a + L_{\delta_r} \delta_r \quad (55b)$$

$$\dot{r} - \frac{I_{xz}}{I_{zz}} \dot{p} = N_r r + N_{\beta} \beta + N_p p + N_{\delta_a} \delta_a + N_{\delta_r} \delta_r \quad (55c)$$

If \dot{p} is substituted from equation (55b) into equation (55c) and \dot{r} is substituted from equation (55c) into equation (55b), the result is equations (56a and (56b) (Reference 12).

$$\dot{p} = L'_r r + L'_\beta \beta + L'_p p + L'_{\delta_a} \delta_a + L'_{\delta_r} \delta_r \quad (56a)$$

$$\dot{r} = N'_r r + N'_\beta \beta + N'_p p + N'_{\delta_a} \delta_a + N'_{\delta_r} \delta_r \quad (56b)$$

where

$$L'_s = \frac{L_s + \frac{I_{xz}}{I_{xx}} N_s}{1 - \frac{I_{xz} I_{xz}}{I_{xx} I_{zz}}}, \quad N'_s = \frac{N_s + \frac{I_{xz}}{I_{zz}} L_s}{1 - \frac{I_{xz} I_{xz}}{I_{xx} I_{zz}}} \quad (57)$$

and

$s = r, \beta, p, \delta_a, \delta_r$, respectively.

Now, the Eulerian angles ϕ and ψ are related to the instantaneous angular velocities p and r by equations (58a) and (58b), which in turn are linearized forms of equations (II-38) of Reference 5, with a steady-state pitch angle θ_0 included, but with zero steady-state roll angle.

$$\dot{\psi} = r \sec \theta_0 \quad (58a)$$

$$\dot{\phi} = p + r \tan \theta_0 \quad (58b)$$

Substituting these equations into equation (55a)

$$\begin{aligned} U_0 (\dot{\beta} + r) &= g (\tan \theta_0 + \sin \theta_0) r/s + g \cos \theta_0 p/s \\ &+ Y_r r + U_0 Y_v \beta + Y_p p + Y_{\delta_a} \delta_a + Y_{\delta_r} \delta_r \end{aligned} \quad (59)$$

A lateral accelerometer responds to the sum of all external lateral forces acting upon the airframe as given by equation (59), resulting in

$$a_y + Y_r r + U_0 Y_v \beta + Y_p p + Y_{\delta_a} \delta_a + Y_{\delta_r} \delta_r \quad (60)$$

Contrails

Usually, Y_r , Y_p and Y_{δ_a} may be assumed small. Also, if the accelerometer is mounted at the center of percussion, the term Y_{δ_r} is cancelled, leaving measured acceleration approximately proportional to sideslip.

$$a_y \approx U_0 Y_v \beta \quad (61)$$

Hence, lateral acceleration and sideslip may be used more or less interchangeably for control purposes.

If equations (56a), (56b), and (59) are simulated on an analog computer, β , p , and r are obtained as integrator outputs. Inasmuch as integrators attenuate high frequencies, the high-frequency airframe dynamics are only slightly affected by integrator outputs. Equations (56a), (56b) and (60) reduce the following high-frequency approximations:

$$\dot{p} \approx L'_{\delta_a} \delta_a + L'_{\delta_r} \delta_r \quad (62a)$$

$$\dot{r} = N'_{\delta_a} \delta_a + N'_{\delta_r} \delta_r \quad (62b)$$

$$a_y \approx Y_{\delta_a} \delta_a + Y_{\delta_r} \delta_r \quad (62c)$$

If steady-state angle of attack α_0 is nonzero, the measured body axis rates \hat{p} and \hat{r} are related to the corresponding stability axis rates p and r by the following transformations:

$$\hat{r} = r \cos \alpha_0 + p \sin \alpha_0 \quad (63a)$$

$$\hat{p} = p \cos \alpha_0 - r \sin \alpha_0 \quad (63b)$$

The normal acceleration \hat{a}_y measured by an accelerometer mounted a distance l_x ahead of the center of gravity is related to the stability axis variables by

$$\hat{a}_y = a_y + l_x \dot{\hat{r}} = a_y + l_x (\dot{r} \cos \alpha_0 + \dot{p} \sin \alpha_0) \quad (63c)$$

Similarly, the sideslip measured by a sensor mounted a distance l_b ahead of the center of gravity is given by

$$\hat{\beta} = \beta + l_b \hat{r} / U_0 = \beta + l_b (r \cos \alpha_0 + p \sin \alpha_0) / U_0 \quad (63d)$$

Equations (63a), (63b), and (63c) are combined in

$$\begin{bmatrix} \hat{a}_y \\ \hat{p} \\ \hat{r} \end{bmatrix} = \begin{bmatrix} 1 & s l_x \sin \alpha_0 & s l_x \cos \alpha_0 \\ 0 & \cos \alpha_0 & -\sin \alpha_0 \\ 0 & \sin \alpha_0 & \cos \alpha_0 \end{bmatrix} \begin{bmatrix} a_y \\ p \\ r \end{bmatrix} \quad (64)$$

Four separate control loops were incorporated into the simulation of the lateral axes: a roll damper loop, yaw damper, lateral acceleration, and yaw into roll (YAR) coupling. These control loops are represented in Figure 43 and equation (65), where b_{12} , b_{23} , b_{21} , and b_{13} are the transfer functions (or gains) of the respective control loops.

$$\begin{bmatrix} \delta a \\ \delta r \end{bmatrix} = \begin{bmatrix} 0 & b_{12} & b_{13} \\ b_{21} & 0 & b_{23} \end{bmatrix} \begin{bmatrix} \hat{a}_y \\ \hat{p} \\ \hat{r} \end{bmatrix} + \begin{bmatrix} \delta a_c \\ \delta r_c \end{bmatrix} \quad (65)$$

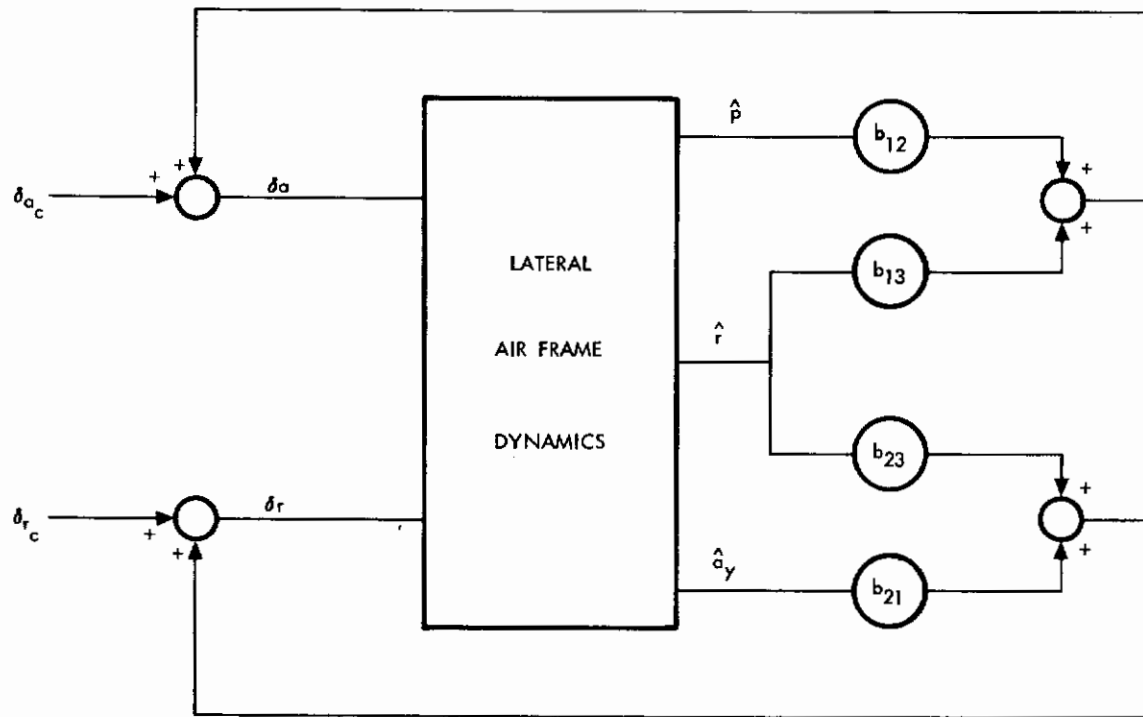


Figure 43. Basic Control System for Lateral Axes

Writing equations (62a), (62b), and (62c) in matrix form and substituting equations (65) and (64) yields

$$\begin{bmatrix} a_y \\ \dot{p} \\ \dot{r} \end{bmatrix} \approx \begin{bmatrix} Y_{\delta_a} & Y_{\delta_r} \\ L'_{\delta_a} & L'_{\delta_r} \\ N'_{\delta_a} & N'_{\delta_r} \end{bmatrix} \begin{bmatrix} 0 & b_{12} & b_{13} \\ b_{21} & 0 & b_{23} \end{bmatrix} \begin{bmatrix} 1 & s l_x \sin \alpha_0 & s l_x \cos \alpha_0 \\ 0 & \cos \alpha_0 & -\sin \alpha_0 \\ 0 & \sin \alpha_0 & \cos \alpha_0 \end{bmatrix} \begin{bmatrix} a_y \\ p \\ r \end{bmatrix} + \begin{bmatrix} \delta a_c \\ \delta r_c \end{bmatrix} \quad (66a)$$

Linear terms in p and r do not enter into high-frequency approximations, as explained previously in deriving equations (62a), (62b), and (62c). In the simulation, some lag was included in the lateral acceleration feedback loop represented by the transfer function b_{21} . Under these conditions, equation (66a) reduces to (66b) at high frequencies.

$$\begin{bmatrix} a_y \\ \dot{p} \\ \dot{r} \end{bmatrix} \approx \begin{bmatrix} Y_{\delta_a} & Y_{\delta_r} \\ L'_{\delta_a} & L'_{\delta_r} \\ N'_{\delta_a} & N'_{\delta_r} \end{bmatrix} \begin{bmatrix} \delta a_c \\ \delta r_c \end{bmatrix} \quad (66b)$$

Equation (66b) may be solved directly for the various high frequency gains of interest:

$$\lim_{s \rightarrow \infty} \frac{\dot{r}}{\delta_{r_c}} = N'_{\delta_r} \quad (67a)$$

$$\lim_{s \rightarrow \infty} \frac{\dot{p}}{\delta_{a_c}} = L'_{\delta_a} \quad (67b)$$

$$\lim_{s \rightarrow \infty} \frac{a_y}{\delta_{r_c}} = Y_{\delta_r} \quad (67c)$$

$$\lim_{s \rightarrow \infty} \frac{\dot{r}}{\delta_{a_c}} = N'_{\delta_a} \quad (67d)$$

$$\lim_{s \rightarrow \infty} \frac{p}{\delta_{r_c}} = L'_{\delta_r} \quad (67e)$$

To get the high-frequency gains in terms of measured angular rates, equations (67a) through (67e) are combined with equations (63a), (63b), and (63c). Of interest in analyzing stability of the yaw damper is

$$\lim_{s \rightarrow \infty} \frac{\dot{\hat{r}}}{\delta_{r_c}} = \lim_{s \rightarrow \infty} \frac{\dot{r} \cos \alpha_0 + \dot{p} \sin \alpha_0}{\delta_{r_c}} = N'_{\delta_r} \cos \alpha_0 + L'_{\delta_r} \sin \alpha_0 \quad (68a)$$

For the roll damper,

$$\lim_{s \rightarrow \infty} \frac{\dot{\hat{p}}}{\delta_{a_c}} = \lim_{s \rightarrow \infty} \frac{\dot{p} \cos \alpha_0 - \dot{r} \sin \alpha_0}{\delta_{a_c}} = L'_{\delta_a} \cos \alpha_0 - N'_{\delta_a} \sin \alpha_0 \quad (68b)$$

For YAR feedback,

$$\lim_{s \rightarrow \infty} \frac{\dot{\hat{r}}}{\delta_{a_c}} = \lim_{s \rightarrow \infty} \frac{\dot{r} \cos \alpha_0 + \dot{p} \sin \alpha_0}{\delta_{a_c}} = N'_{\delta_a} \cos \alpha_0 + L'_{\delta_a} \sin \alpha_0 \quad (68c)$$

For acceleration feedback, using equations (63c) and (68a),

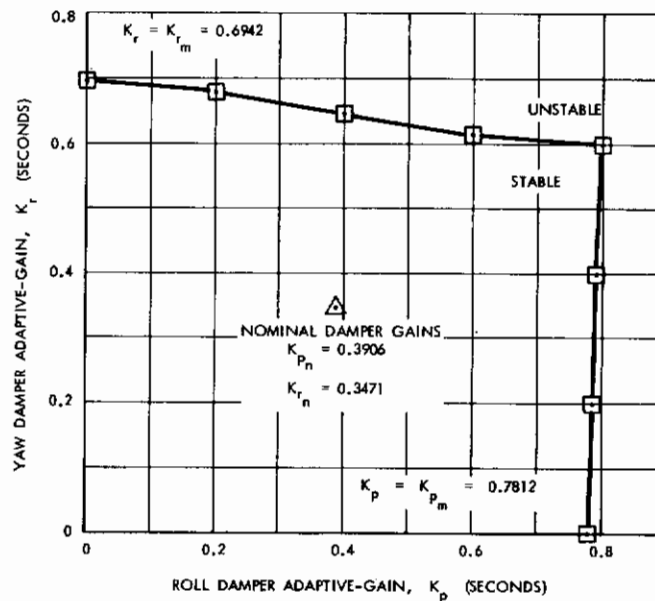
$$\lim_{s \rightarrow \infty} \frac{\hat{a}_y}{\delta_{rc}} = \lim_{s \rightarrow \infty} \frac{a_y + l_x \hat{r}}{\delta_{rc}} = Y_{\delta_r} + l_x (N'_{\delta_r} \cos \alpha_0 + L'_{\delta_r} \sin \alpha_0) \quad (68d)$$

Each high-frequency gain given by equations (68a) through (68d) is independent of the loop gains (or transfer functions b_{12} , b_{13} , b_{21} , and b_{23}). Hence, closing one loop should not seriously alter the gain at which another loop goes unstable, provided the instability occurs at a sufficiently high frequency to ensure such independence. This has been verified empirically, as illustrated in Figure 44 of this report.

It will now be shown that if the SIDAC model is fed data from the same body-mounted sensors as are used for the rest of the control system, the correct high-frequency gains will be obtained directly from the parameter identification. For the roll axis, the SIDAC model equation is defined as follows:

$$e_p = \hat{p} - L_p^* \hat{p} - L_r^* \hat{r} - L_\beta^* \hat{\beta} - L_{\delta_a}^* \delta_a - L_{\delta_r}^* \delta_r \quad (69)$$

Substituting equations (63a), (63b), and (63d) into equation (69) gives equation (70).



NOTE:
 $K_{p_o} = K_{r_o} = 0.0$
 NOTCH FILTER: $\frac{.052 s + 1}{.0185 s + 1}$

Figure 44. Roll/Yaw Damper Gain Interaction at Crossover (FC 28)

$$\begin{aligned}
 e_p = & (\dot{p} \cos \alpha_0 - \dot{r} \sin \alpha_0) - L_p^* (p \cos \alpha_0 - r \sin \alpha_0) \\
 & - L_r^* (r \cos \alpha_0 + p \sin \alpha_0) - L_\beta^* (\beta + \ell_b \cos \alpha_0 r / U_0 + \ell_b \sin \alpha_0 p / U_0) \\
 & - L_{\delta_a}^* \delta_a - L_{\delta_r}^* \delta_r
 \end{aligned} \tag{70}$$

Substituting equations (56a) and (56b) into equation (70) gives

$$\begin{aligned}
 e_p = & \beta (L_\beta^* \cos \alpha_0 - N_\beta^* \sin \alpha_0 - L_\beta^*) \\
 & + p (L_p^* \cos \alpha_0 - N_p^* \sin \alpha_0 - L_p^* \cos \alpha_0 - L_r^* \sin \alpha_0 - L_\beta^* \ell_b \sin \alpha_0 / U_0) \\
 & + r (L_r^* \cos \alpha_0 - N_r^* \sin \alpha_0 + L_p^* \sin \alpha_0 - L_r^* \cos \alpha_0 - L_\beta^* \ell_b \cos \alpha_0 / U_0) \\
 & + \delta_a (L_{\delta_a}^* \cos \alpha_0 - N_{\delta_a}^* \sin \alpha_0 - L_{\delta_a}^*) \\
 & + \delta_r (L_{\delta_r}^* \cos \alpha_0 - N_{\delta_r}^* \sin \alpha_0 - L_{\delta_r}^*)
 \end{aligned} \tag{71}$$

If the coefficients converge to their true values, then each coefficient in equation (71) must be zero in the steady state. In particular, equating the coefficient of δ_a to zero gives

$$L_{\delta_a}^* = L_{\delta_a}^* \cos \alpha_0 - N_{\delta_a}^* \sin \alpha_0 \tag{72}$$

Comparison with equation (68b) reveals that the high frequency gain for the roll axis is obtained directly.

For the yaw axis, the SIDAC model equation is defined by

$$e_r = \dot{r} - N_p^* \hat{p} - N_r^* \hat{r} - N_\beta^* \hat{\beta} - N_{\delta_a}^* \delta_a - N_{\delta_r}^* \delta_r \tag{73}$$

Substituting equations (63a), (63b), and (63d) into equation (73) gives

$$\begin{aligned}
 e_r = & \dot{r} \cos \alpha_0 + \dot{p} \sin \alpha_0 - N_p^* (p \cos \alpha_0 - r \sin \alpha_0) \\
 & - N_r^* (r \cos \alpha_0 + p \sin \alpha_0) - N_\beta^* (\beta + l_b \cos \alpha_0 r / U_0 + l_b \sin \alpha_0 p / U_0) \\
 & - N_{\delta_a}^* \delta_a - N_{\delta_r}^* \delta_r
 \end{aligned} \tag{74}$$

Substituting equation (56a) and (56b) into equation (74) gives

$$\begin{aligned}
 e_r = & \beta (N_\beta' \cos \alpha_0 + L_\beta' \sin \alpha_0 - N_\beta^*) \\
 & + p (N_p' \cos \alpha_0 + L_p' \sin \alpha_0 - N_p^* \cos \alpha_0 - N_r^* \sin \alpha_0 - N_\beta^* l_b \sin \alpha_0 / U_0) \\
 & + r (N_r' \cos \alpha_0 + L_r' \sin \alpha_0 + N_p^* \sin \alpha_0 - N_r^* \cos \alpha_0 - N_\beta^* l_b \cos \alpha_0 / U_0) \\
 & + \delta_a (N_{\delta_a}' \cos \alpha_0 + L_{\delta_a}' \sin \alpha_0 - N_{\delta_a}^*) \\
 & + \delta_r (N_{\delta_r}' \cos \alpha_0 + L_{\delta_r}' \sin \alpha_0 - N_{\delta_r}^*)
 \end{aligned} \tag{75}$$

Equating the coefficients of δ_r and δ_a to zero gives equations (76) and (77), which in turn are the high-frequency yaw and YAR gains as given by equations (68a) and (68c), respectively.

$$N_{\delta_r}^* = N_{\delta_r}' \cos \alpha_0 + L_{\delta_r}' \sin \alpha_0 \tag{76}$$

$$N_{\delta_a}^* = N_{\delta_a}' \cos \alpha_0 + L_{\delta_a}' \sin \alpha_0 \tag{77}$$

Another form for the SIDAC model is expressed in equation (78) which is of the same form as equation (60).

$$e_a = \hat{a}_y - U_0 Y_v^* \hat{\beta} - Y_p^* \hat{p} - Y_r^* \hat{r} - Y_{\delta_a}^* \delta_a - Y_{\delta_r}^* \delta_r$$

$$= a_y + l_x (\dot{r} \cos \alpha_0 + \dot{p} \sin \alpha_0) - U_0 Y_v^* \hat{\beta} - Y_p^* \hat{p} - Y_r^* \hat{r} - Y_{\delta_a}^* \delta_a - Y_{\delta_r}^* \delta_r \quad (78)$$

Substituting equations (60), (56a), (56b), (63a), (63b), and (63d) into equation (78) yields

$$\begin{aligned} e_a = & U_0 Y_v \beta + Y_p p + Y_r r + Y_{\delta_a} \delta_a + Y_{\delta_r} \delta_r \\ & + l_x \cos \alpha_0 (N'_\beta \beta + N'_p p + N'_r r + N'_{\delta_a} \delta_a + N'_{\delta_r} \delta_r) \\ & + l_x \sin \alpha_0 (L'_\beta \beta + L'_p p + L'_r r + L'_{\delta_a} \delta_a + L'_{\delta_r} \delta_r) \\ & - U_0 Y_v^* (\beta + l_b \sin \alpha_0 p / U_0 + l_b \cos \alpha_0 r / U_0) \\ & - Y_p^* (\cos \alpha_0 p - \sin \alpha_0 r) - Y_r^* (\cos \alpha_0 r + \sin \alpha_0 p) \\ & - Y_{\delta_a}^* \delta_a - Y_{\delta_r}^* \delta_r \end{aligned} \quad (79)$$

Equating the coefficient of δ_r to zero yields equation (80) which gives the high-frequency lateral acceleration gain expressed by

$$Y_{\delta_r}^* = Y_{\delta_r} + l_x (N'_{\delta_r} \cos \alpha_0 + L'_{\delta_r} \sin \alpha_0) \quad (80)$$

It has been shown that all four high-frequency loop gains of concern in the present simulation are obtainable explicitly from SIDAC parameter adjustments.

SIDAC parameter tracking models for the lateral axes which do not require measurement of sideslip may be obtained by solving for β from equation (60) and substituting into equations (56a) and (56b).

$$\beta = (a_y - Y_r r - Y_p p - Y_{\delta_a} \delta_a - Y_{\delta_r} \delta_r) / U_0 Y_v \quad (81)$$

$$\begin{aligned} \dot{p} = & L'_r r + L'_\beta (a_y - Y_r r - Y_p p - Y_{\delta_a} \delta_a - Y_{\delta_r} \delta_r) / U_0 Y_v \\ & + L'_p p + L'_{\delta_a} \delta_a + L'_{\delta_r} \delta_r \end{aligned} \quad (82)$$

$$\begin{aligned} \dot{r} = & N'_r r + N'_\beta (a_y - Y_r r - Y_p p - Y_{\delta_a} \delta_a - Y_{\delta_r} \delta_r) / U_0 Y_v \\ & + N'_p p + N'_{\delta_a} \delta_a + N'_{\delta_r} \delta_r \end{aligned} \quad (83)$$

Using equations (82) and (83) as the basis of the SIDAC models for the roll and yaw axes, respectively, leads to error equations which are independent of sideslip. For the roll axis, the form of the error is given by

$$\begin{aligned} e_{py} &= \hat{p} - L^*_p \hat{p} - L^*_r \hat{r} - L^*_y \hat{a}_y - L^*_{\delta_a} \delta_a - L^*_{\delta_r} \delta_r \\ &= (\dot{p} \cos \alpha_0 - \dot{r} \sin \alpha_0) - L^*_p (p \cos \alpha_0 - r \sin \alpha_0) \\ &\quad - L^*_r (r \cos \alpha_0 + p \sin \alpha_0) - L^*_y \left[a_y + l_x (\dot{r} \cos \alpha_0 + \dot{p} \sin \alpha_0) \right] \\ &\quad - L^*_{\delta_a} \delta_a - L^*_{\delta_r} \delta_r \end{aligned} \quad (84)$$

Substituting equations (82) and (83) into equation (84) and equating coefficients of δ_a and a_y to zero to obtain final parameter values yields equations (85a) and (85b), respectively.

$$\begin{aligned} L^*_{\delta_a} = & (L'_{\delta_a} - L'_\beta Y_{\delta_a} / U_0 Y_v) (\cos \alpha_0 - L^*_y l_x \sin \alpha_0) \\ & - (N'_{\delta_a} - N'_\beta Y_{\delta_a} / U_0 Y_v) (\sin \alpha_0 + L^*_y l_x \cos \alpha_0) \end{aligned} \quad (85a)$$

where

$$\begin{aligned} L_y^* &= L_\beta' (\cos \alpha_0 - L_y^* l_x \sin \alpha_0) / U_0 Y_v - N_\beta' (\sin \alpha_0 + L_y^* l_x \cos \alpha_0) / U_0 Y_v \\ &= (L_\beta' \cos \alpha_0 - N_\beta' \sin \alpha_0) / (U_0 Y_v + l_x (L_\beta' \sin \alpha_0 + N_\beta' \cos \alpha_0)) \end{aligned} \quad (85b)$$

For the yaw axis, the form of the error is given by

$$\begin{aligned} e_{r_y} &= \dot{r} - N_p^* \dot{p} - N_r^* \dot{r} - N_y^* \dot{a}_y - N_{\delta_a}^* \delta_a - N_{\delta_r}^* \delta_r \\ &= \dot{r} - N_p^* \dot{p} - N_r^* \dot{r} - N_y^* (a_y + l_x \dot{r}) - N_{\delta_a}^* \delta_a - N_{\delta_r}^* \delta_r \\ &= \dot{r} \cos \alpha_0 + \dot{p} \sin \alpha_0 - N_p^* (p \cos \alpha_0 - r \sin \alpha_0) \\ &\quad - N_r^* (r \cos \alpha_0 + p \sin \alpha_0) - N_y^* [a_y + l_x (\dot{r} \cos \alpha_0 + \dot{p} \sin \alpha_0)] \\ &\quad - N_{\delta_a}^* \delta_a - N_{\delta_r}^* \delta_r \end{aligned} \quad (86)$$

Substituting equations (82) and (83) into equation (86) and equating coefficients of δ_a , δ_r , and a_y to zero yields equations (87a), (87b) and (87c), respectively.

$$\begin{aligned} N_{\delta_a}^* &= \left[(N_{\delta_a}' - N_\beta' Y_{\delta_a} / U_0 Y_v) \cos \alpha_0 + (L_{\delta_a}' - L_\beta' Y_{\delta_a} / U_0 Y_v) \sin \alpha_0 \right] \\ &\quad (1 - N_y^* l_x) \end{aligned} \quad (87a)$$

$$\begin{aligned} N_{\delta_r}^* &= \left[(N_{\delta_r}' - N_\beta' Y_{\delta_r} / U_0 Y_v) \cos \alpha_0 + (L_{\delta_r}' - L_\beta' Y_{\delta_r} / U_0 Y_v) \sin \alpha_0 \right] \\ &\quad (1 - N_y^* l_x) \end{aligned} \quad (87b)$$

$$N_y^* = (N_\beta' \cos \alpha_0 + L_\beta' \sin \alpha_0) (1 - N_x^* l_x) / U_0 Y_v$$

$$= 1 / \left[l_x + U_0 Y_v / (N_\beta' \cos \alpha_0 + L_\beta' \sin \alpha_0) \right] \quad (87c)$$

If Y_{δ_a} , Y_{δ_r} and l_x are all small enough to be negligible, equations (85a), (87a), and (87b) reduce to equations (72), (77) and (76), respectively.

However, finite values for Y_{δ_a} , Y_{δ_r} , and l_x may lead to significant errors in parameter adjustments and, hence, in control loop gain settings. This was not true when sideslip was sensed as shown in equations (69) and (73). Hence, it is clear that some price must be paid for elimination of sideslip data. If loop gain errors are excessive for a particular airframe, it may be necessary to cancel the \hat{r} component of the accelerometer output (i.e., if l_x is not negligible) or to correct model parameter settings prior to computing control loop gains (i.e., if Y_{δ_a} or Y_{δ_r} is not negligible).

It may be concluded from the foregoing results that if sideslip is sensed and used by the SIDAC computer for parameter adjustment, the high frequency gains for the control loops will be obtained correctly without modification, provided the same sensors are used for both identification and control. However, if the SIDAC computer utilizes only inertial data (acceleration and angular rates), corrections may be required to compensate for accelerometer locations other than the center of gravity as well as the fact that the stability derivatives Y_{δ_a} and Y_{δ_r} may not be negligible.

ANALOG COMPUTER SIMULATION RESULTS

The X-15 lateral axes were simulated, together with a modified Honeywell stability augmentation system (SAS) (Reference 3). Block diagrams for the roll and yaw systems appear in Figures 45 and 46, respectively. Figure 47 shows typical responses for the roll axis with the adaptive gain adjustment mechanism operating, and Figure 48 shows the corresponding results for the yaw axes. The high-frequency gains $N_{\delta_r}^*$ and $L_{\delta_a}^*$ converge rapidly and smoothly. A large number of additional runs were made with the adaptive gain adjustment mechanism inoperative to test parameter identification capability at several flight conditions, and the results are summarized in Figures 49 and 50. The results for flight condition 32 were rather poor, and were not included in the figures. Although the difficulties could definitely be traced to the simulation equipment, particularly noise and bias in the time division multipliers, it is not certain whether or not a weakness in the basic mechanization is indicated. Simulation with improved multipliers (quarter square) or digital simulation should provide further answers.

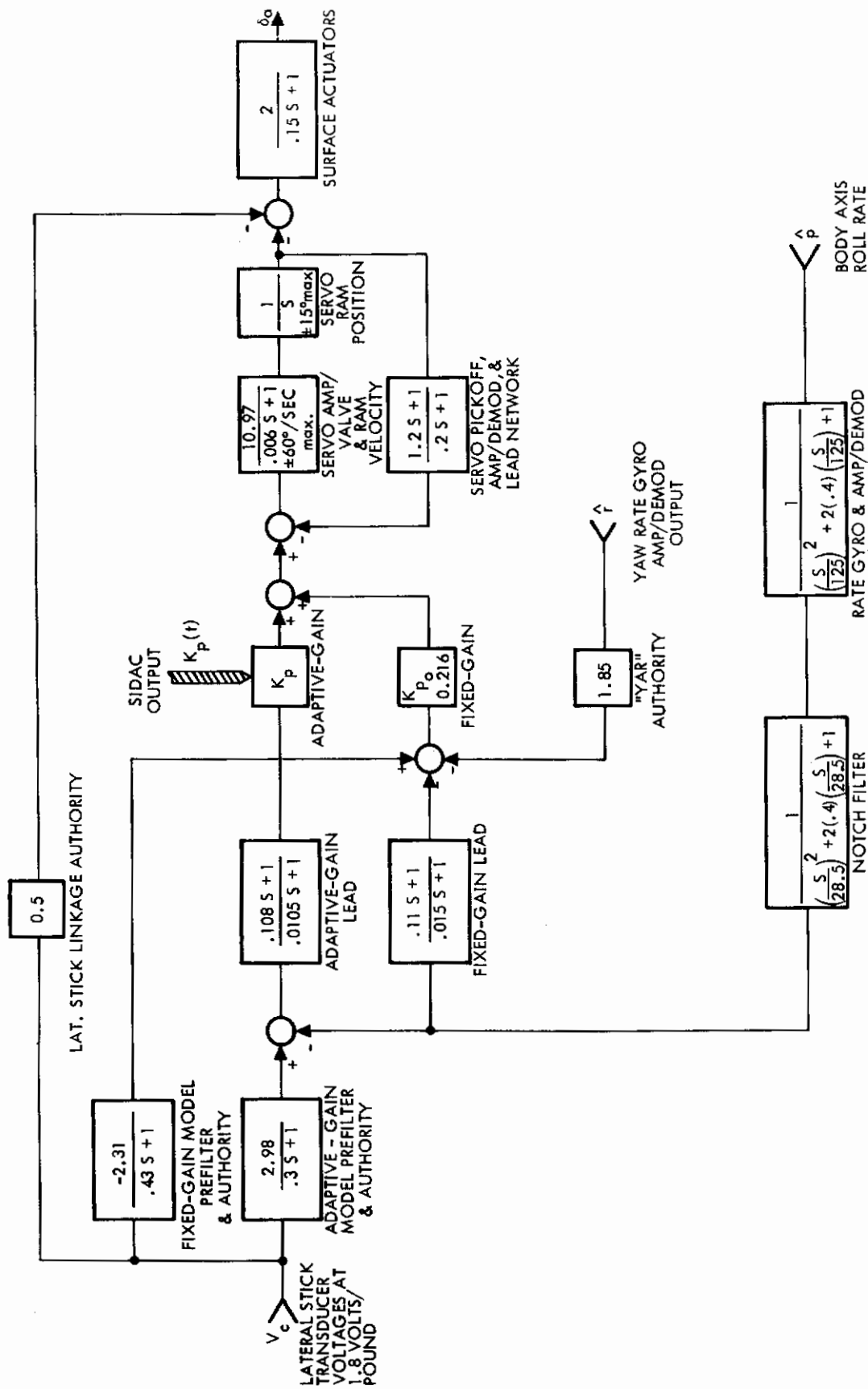


Figure 45. Roll Stability Augmentation System

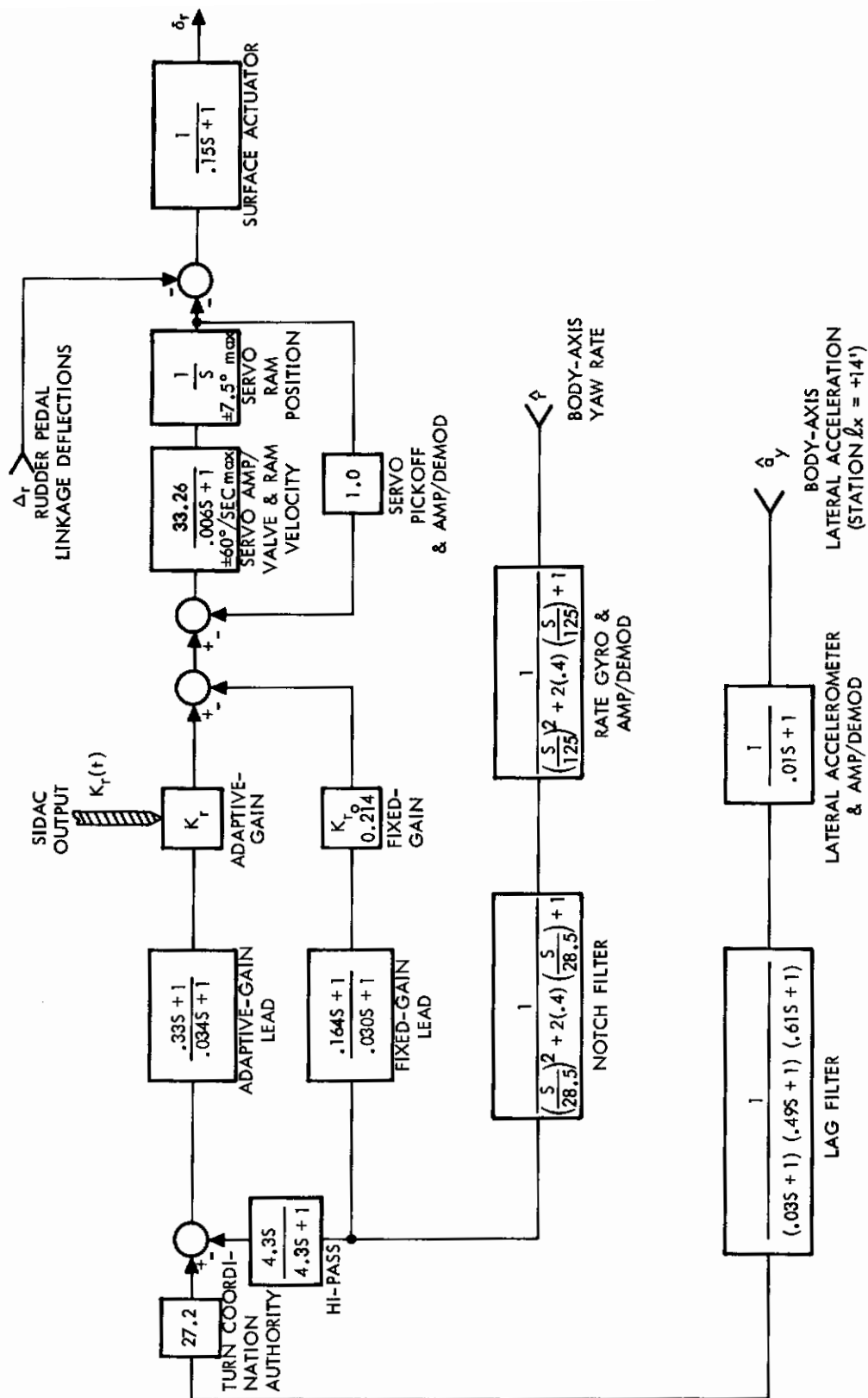


Figure 46. Yaw Stability Augmentation System

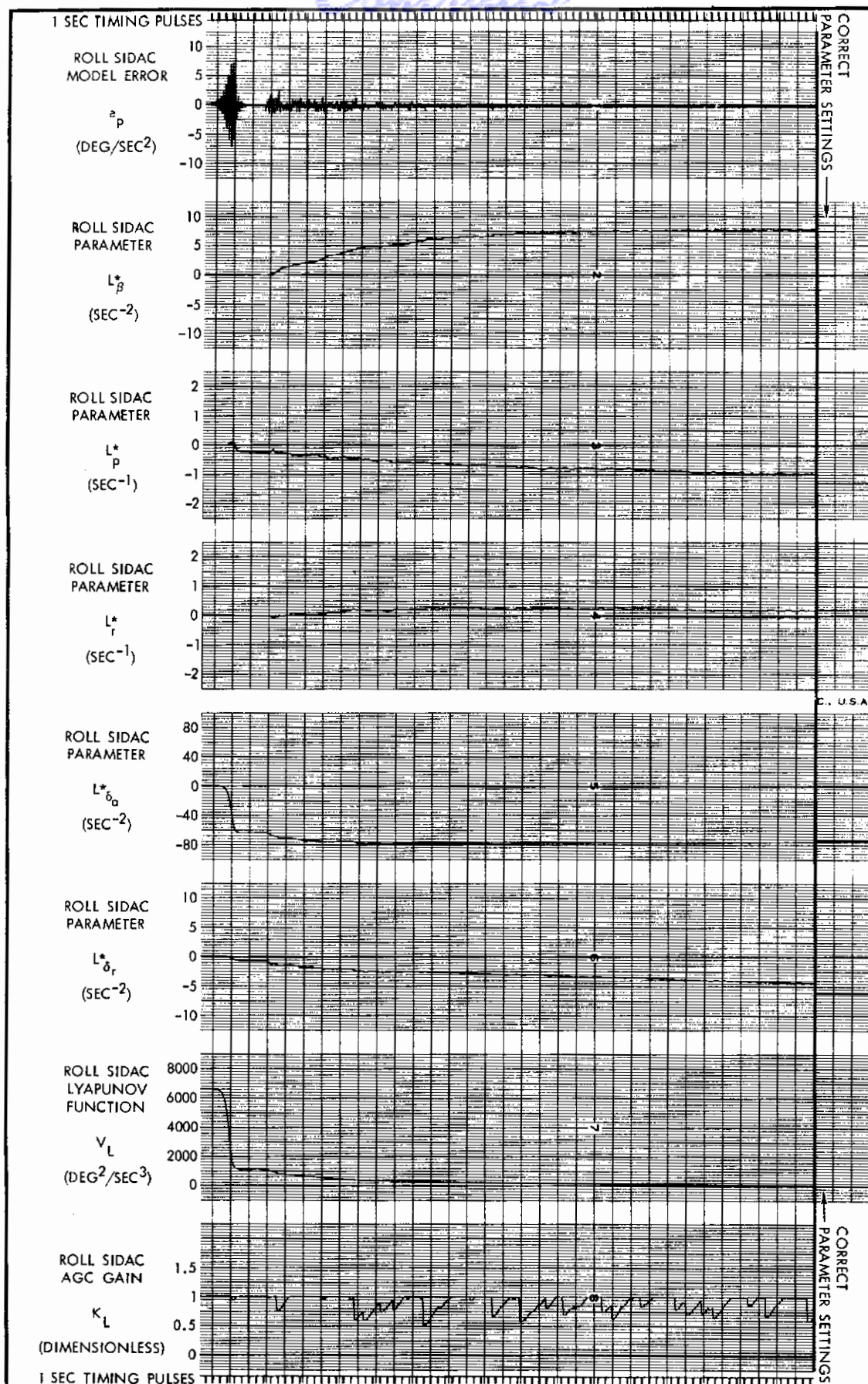


Figure 47. Typical Roll SIDAC Response FC 21 (Sheet 1 of 3)

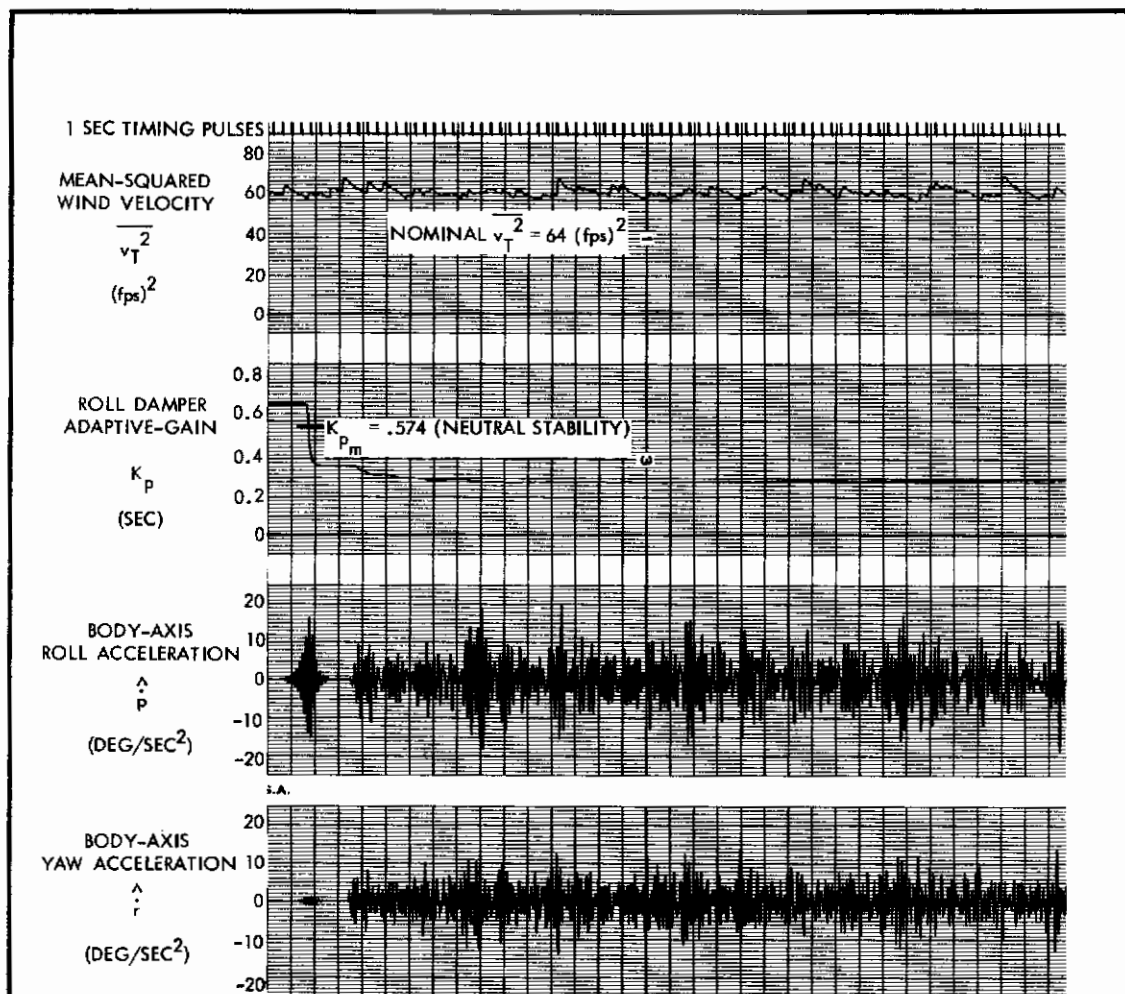


Figure 47. Typical Roll SIDAC Response FC 21 (Sheet 2 of 3)

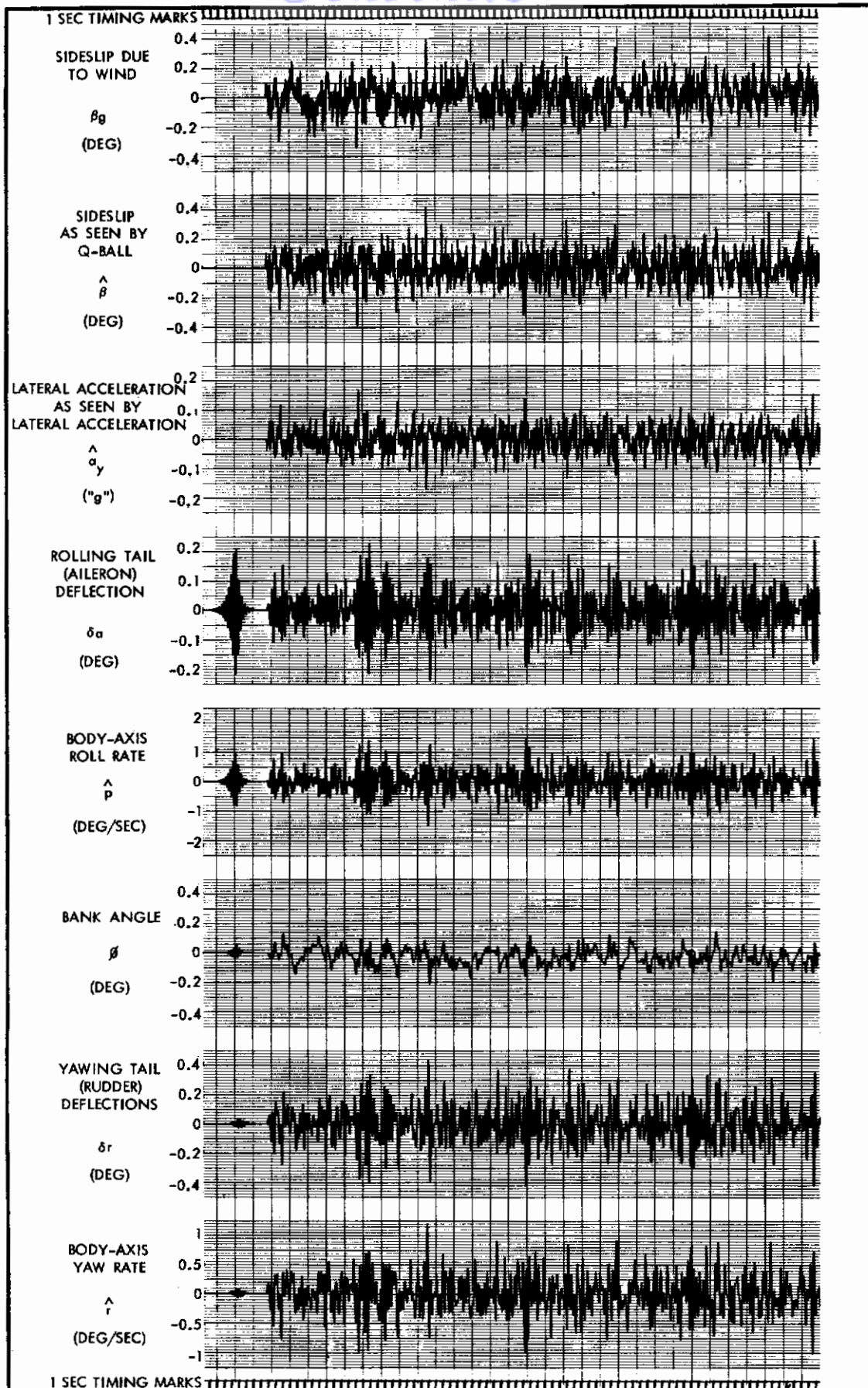


Figure 47. Typical Roll SIDAC Response FC 21 (Sheet 3 of 3)

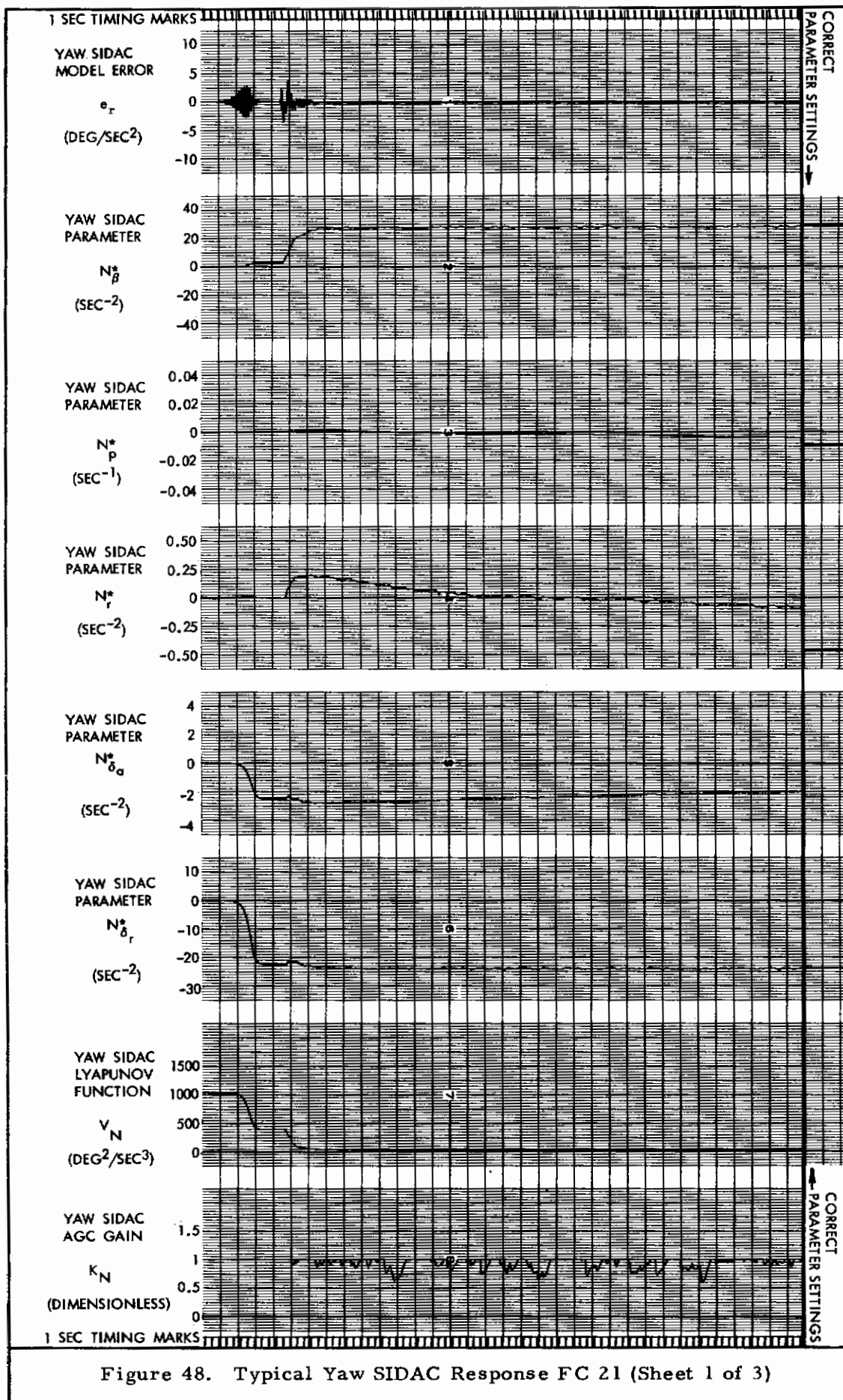
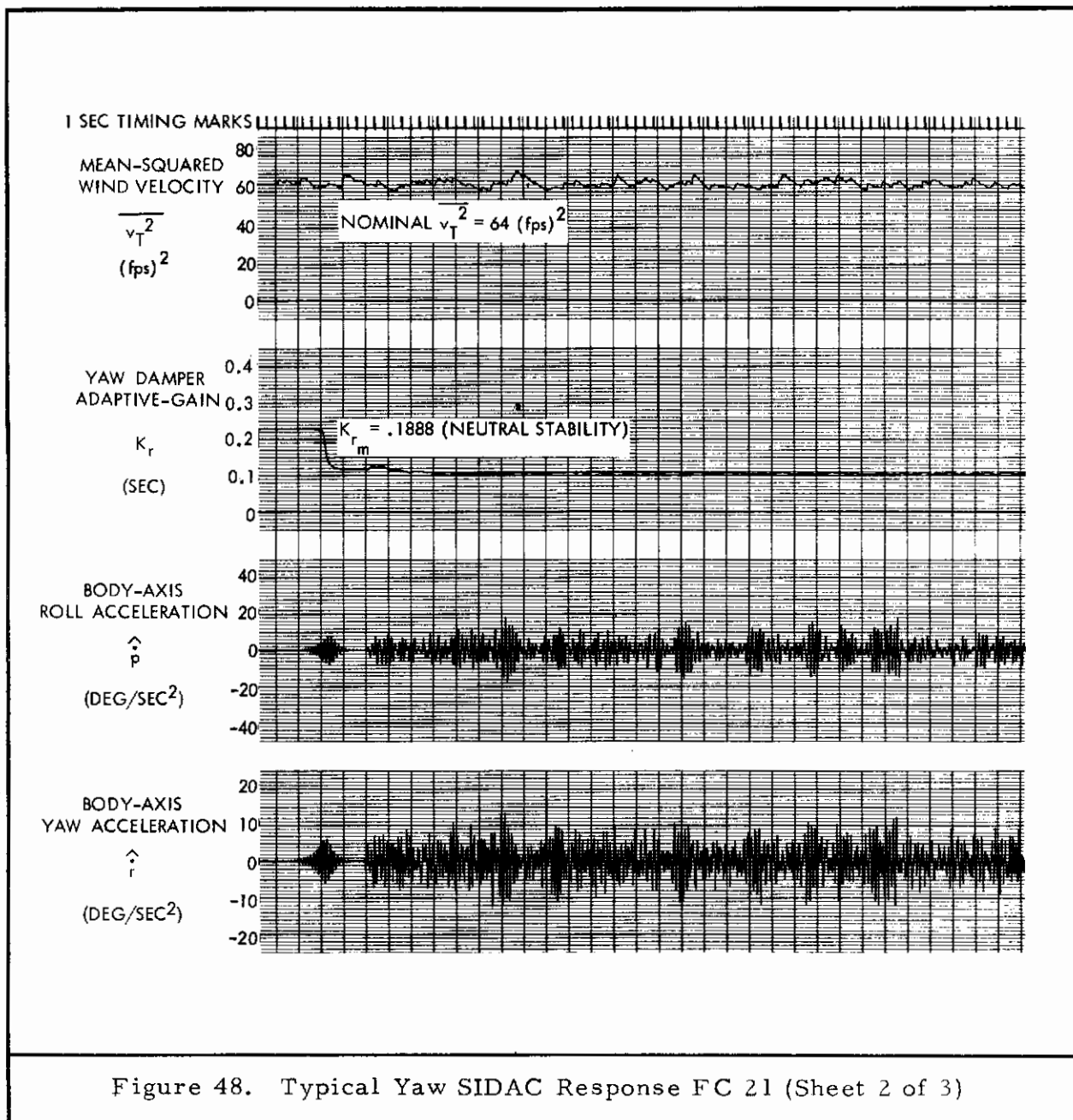


Figure 48. Typical Yaw SIDAC Response FC 21 (Sheet 1 of 3)



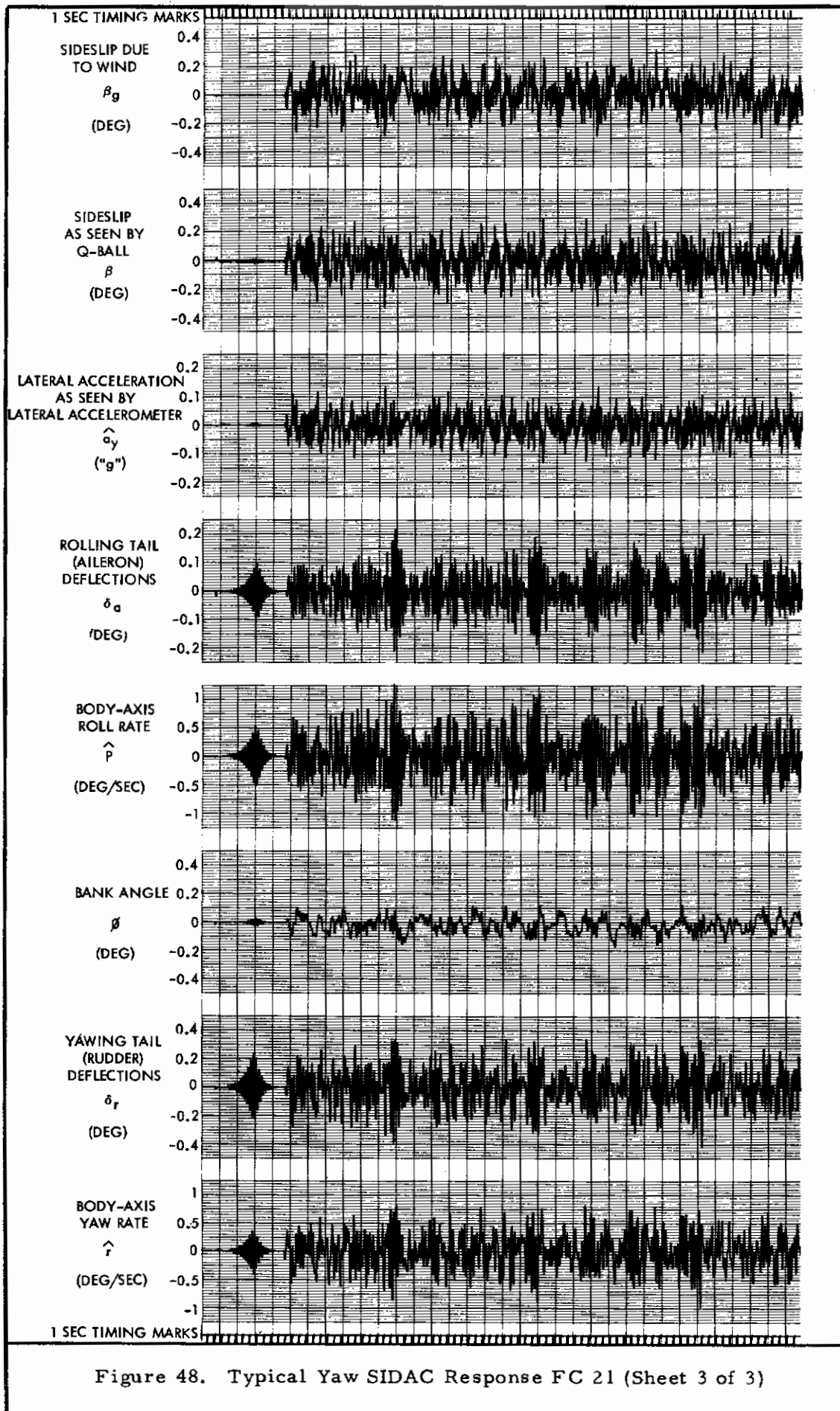


Figure 48. Typical Yaw SIDAC Response FC 21 (Sheet 3 of 3)

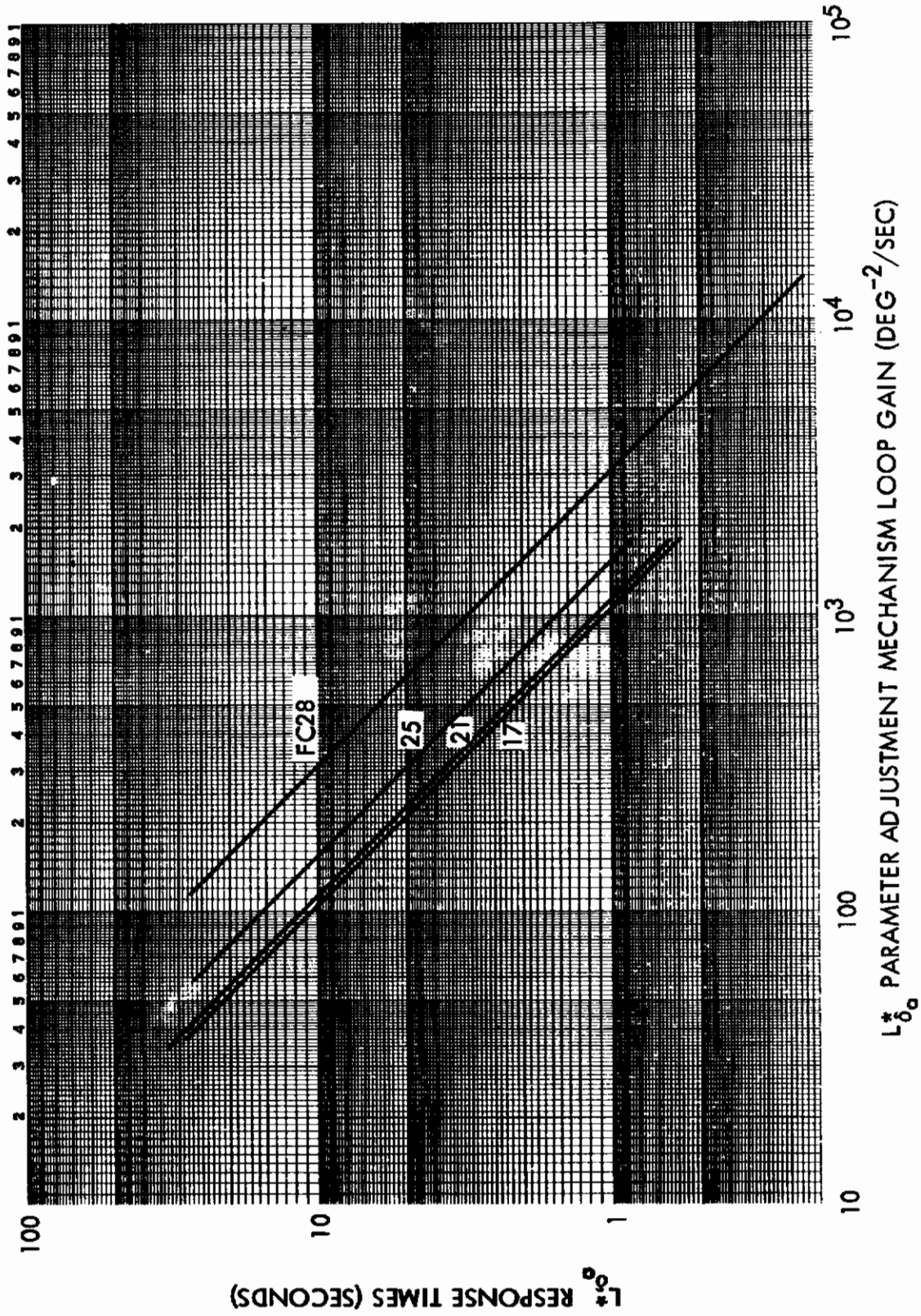


Figure 49. Roll SIDAC Identification Times

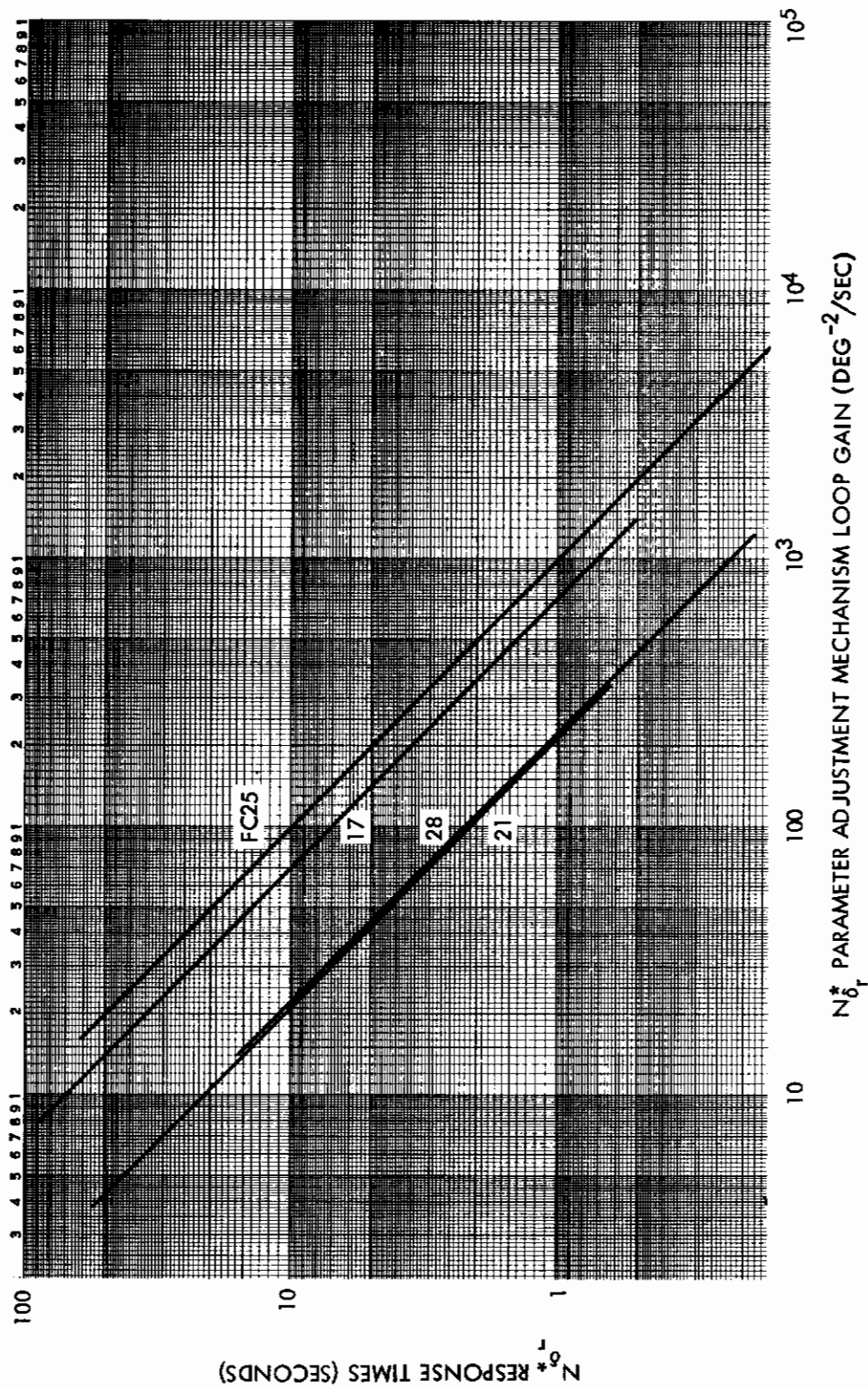


Figure 50. Yaw SIDAC Identification Times.

Contrails

SECTION 6

DIGITAL IMPLEMENTATION REQUIREMENTS

COMPUTER REQUIREMENTS

Simplified programs were written for a two parameter pitch axis identification. These programs contain all basic functions of the complete program, and expansion to a three-axis program entails only repetition of the coding for the basic functions. It is estimated that the length and computation time of the complete program would be approximately four times the length and computation time of the simplified version.

The basic SIDAC pitch axis equations required for a two parameter identification using simple rectangular integration are as follows:

$$x_0 = K_M \ddot{\theta} \quad (88a)$$

$$x_1 = K_M \alpha_p \quad (88b)$$

$$x_3 = K_M \delta e \quad (88c)$$

$$e = x_0 + b_1 x_1 + b_3 x_3 \quad (89)$$

$$b_{1k+1}^* = b_{1k}^* - K_1 T e_k x_{1k} \quad (90a)$$

$$b_{3k+1}^* = b_{3k}^* - K_3 T e_k x_{3k} \quad (90b)$$

$$K_q = K_p / b_3^* \quad (91)$$

$$AGC = K_1 x_1^2 + K_3 x_3^2 \quad (92)$$

$$AGC = SP (K_M \text{ Adjustment}) \quad (93)$$

These equations, together with various limiting operations and other minor functions are outlined in detail in the flow chart of Figure 51.

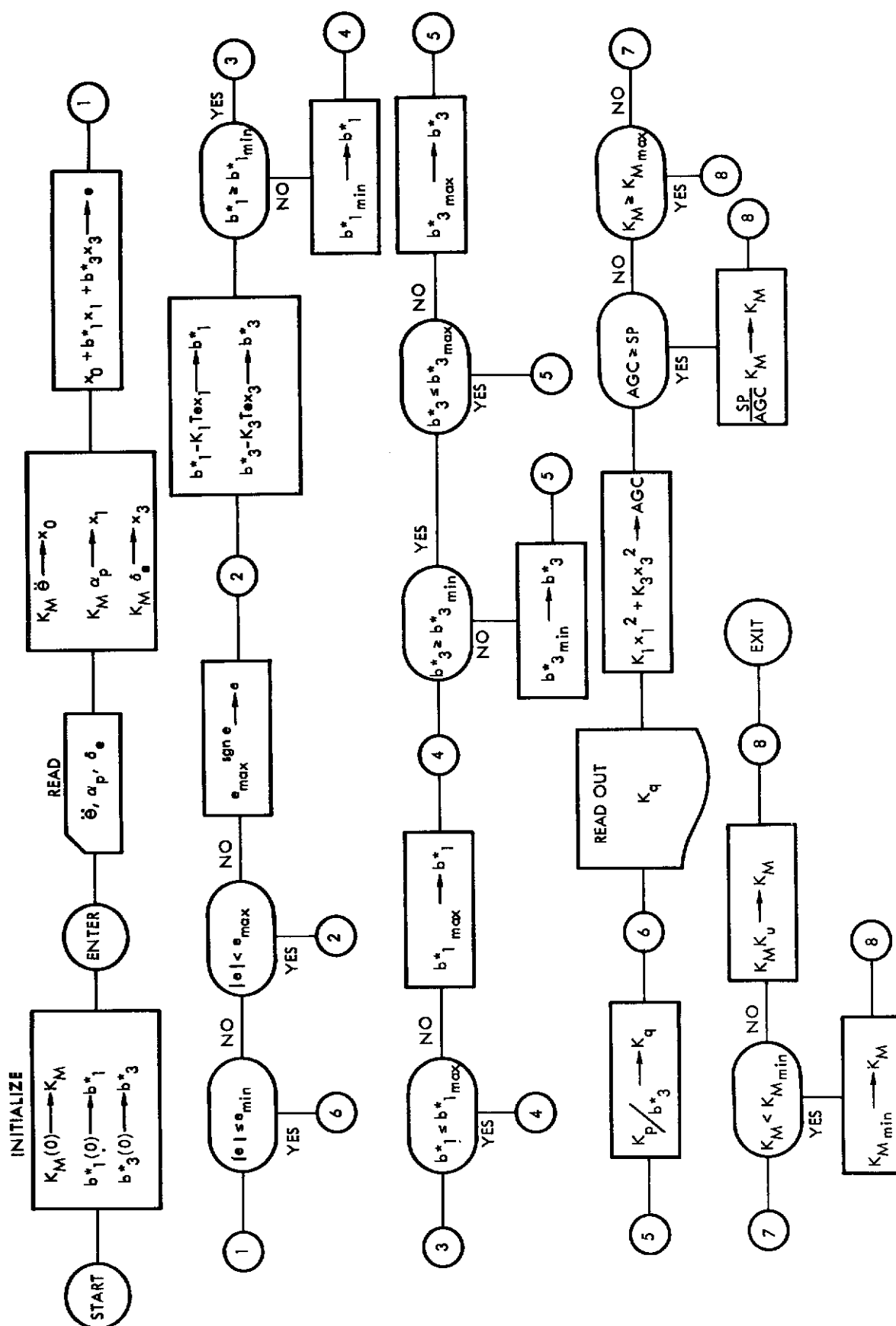


Figure 51. Pitch Axis Flow Chart

A preliminary estimate of computing requirements was made by writing a program for a hypothetical single address machine. A total of 150 instructions was required to mechanize SIDAC for the pitch axis. These instructions were subdivided as follows:

- 15 multiplications
- 3 divisions
- 5 additions and subtractions
- 30 load
- 26 store
- 13 jumps
- 10 tests
- 10 shift left and shift right
- 38 miscellaneous

Assuming the number of programming instructions for the lateral axes to be approximately three times the number for the pitch axis, the total number of instructions for a complete program would be about 600 for single address machines or 390 for two address machines. Approximately 12 inputs and three outputs, in addition to discrete lines, are required.

The preliminary estimate of computing requirements was verified by programming two commercially available airborne computers using mnemonic coding.

A total of 152 instructions was required to program a two-address machine for the pitch axis. These instructions were subdivided as follows:

- 37 test
- 22 subtractions
- 18 jump
- 15 multiplications
- 13 additions
- 12 load
- 11 store
- 11 shift left and shift right
- 7 input and output
- 3 copy
- 2 division
- 1 halt

152 Total instructions

Estimated computation time is 1.323 milliseconds per iteration.

A small (35 pounds) single-address machine was programmed for comparison, requiring 898 microseconds to execute 217 instructions.

Use of a digital differential analyzer (DDA) was not considered feasible because of slewing (rate limiting) problems. These slewing problems arise because the integrator outputs of the DDA can change by, at most, one increment during each iteration.

In order to scale a real-time sine wave

$$x(t) = a \sin 2\pi f t, \quad (94)$$

the rate limits require satisfaction of the following equation:

$$n \geq \frac{dx}{dt} \max = a 2\pi f \quad (95)$$

where

n : number of iterations per second

a : number of increments to represent peak amplitude

f : frequency of sine wave

For example, if the maximum frequency to be considered is assumed to be 3 cps, an iteration rate of 250 per second gives

$$a \leq \frac{n}{2\pi f} = \frac{250}{2\pi \times 3} = 13.2 \quad (96)$$

Hence, quantization error would be approximately 8 percent of maximum amplitude, even with optimum scaling.

STABILITY ANALYSIS

At the present time, it is planned to implement the final form of SIDAC digitally, even though all simulation work to date has been performed on an analog basis. A digital implementation will provide greater resolution and freedom from component noise, bias, and multiplier errors than is obtainable from analog equipment. However, a digital implementation requires sampling of measured data which is generally destabilizing.

For comparison, consider a continuous system and the corresponding Lyapunov function

$$V \triangleq \sum (b_j^* - b_j)^2 \quad (97)$$

where b_j is the j 'th parameter (assumed constant) and b_j^* is the present estimate of the j 'th parameter. Differentiating equation (97) with respect to time gives

$$\dot{V} = 2 \sum (b_j^* - b_j) \dot{b}_j^*. \quad (98)$$

Equation (98) is subject to the control law (all integrator gains equal)

$$\dot{b}_j^* = -\frac{K}{2} e(t) x_j. \quad (99)$$

Also,

$$e(t) = \sum (b_j^* - b_j) x_j \quad (100)$$

Substituting equation (99) into equation (98), and (100) into the result gives

$$\dot{V} = -K e(t) \sum (b_j^* - b_j) x_j = -K e^2(t). \quad (101)$$

Hence, \dot{V} is always negative, and the adjustment is stable.

For the discrete case, equation (97) becomes

$$V_k \triangleq \sum (b_{j_k}^* - b_j)^2 \quad (102)$$

where V_k is the value of V at the k 'th instant, and $b_{j_k}^*$ is the value of the j 'th parameter at the k 'th instant. Taking the first difference of (102) with respect to k gives

$$\begin{aligned} V_{k+1} - V_k &= \sum \left[(b_{j(k+1)}^* - b_j)^2 - (b_{j_k}^* - b_j)^2 \right] \\ &= \sum (b_{j(k+1)}^* - b_{j_k}^*) (b_{j(k+1)}^* + b_{j_k}^* - 2b_j). \end{aligned} \quad (103)$$

If this first difference is always negative, the adjustment will always be stable. Several cases will not be considered.

Case I: Rectangular Integration, Input Delayed by One Sample (Figure 52)

If equation (99) is evaluated by rectangular integration based on past input,

$$b_{j(k+1)}^* = b_{j_k}^* - \frac{KT}{2} e_k x_{j_k} \quad (104)$$

Substituting equation (104) into equation (103) gives

$$\begin{aligned} V_{k+1} - V_k &= \sum \left(-\frac{KT}{2} e_k x_{j_k} \right) \left(2b_{j_k}^* - 2b_j - \frac{KT}{2} e_k x_{j_k} \right) \\ &= -\frac{KT}{2} e_k \left[2 \sum (b_{j_k}^* - b_j) x_{j_k} - \frac{KT}{2} e_k \sum x_{j_k}^2 \right]. \end{aligned} \quad (105)$$

Substituting the digital equivalent of equation (100) into equation (105) gives

$$V_{k+1} - V_k = -KT e_k^2 \left[1 - \frac{KT}{4} \sum x_{j_k}^2 \right] \quad (106)$$

If the second term in brackets in equation (106) is zero, the sampled-data system will always be stable, just as the continuous system is always stable as revealed by equation (101). However, because the second term in brackets in equation (106) is always negative, the sampled-data system is always less stable than a continuous system could be. The sampled-data system is of course always stable for small gains or inputs such that

$$\frac{KT}{4} \sum x_{j_k}^2 < 1. \quad (107)$$

The next two cases to be considered are not physically realizable because they require present (rather than past) values of the integrator input. In a feedback arrangement, this means that while present values of the output are required to compute present values of the inputs, the converse is true, and present values of the input are required to compute present values of the output. While no direct solution to this quandary is readily available, it may be partially circumvented by using input prediction. However, before the effects of input prediction are considered, the non-realizable cases will be considered as an aid to further understanding the problem.

Case II: Rectangular Integration With No Input Delay (Figure 53)

If equation (99) were evaluated by rectangular integration based upon present input,

$$b_{j(k+1)}^* = b_{j_k}^* - \frac{KT}{2} e_{k+1} x_{j(k+1)} \quad (108)$$

Substituting equation (108) into equation (103),

$$\begin{aligned} V_{k+1} - V_k &= \Sigma \left(-\frac{KT}{2} e_{k+1} x_{j(k+1)} \right) (2b_{j(k+1)}^* - 2b_j + \frac{KT}{2} e_{k+1} x_{j(k+1)}) \\ &= -\frac{KT}{2} e_{k+1} \left[2 \Sigma (b_{j(k+1)}^* - b_j) x_{j(k+1)} \right. \\ &\quad \left. + \frac{KT}{2} e_{k+1} \Sigma x_{j(k+1)}^2 \right] \end{aligned} \quad (109)$$

Substituting equation (100) into equation (109),

$$V_{k+1} - V_k = -KT e_{k+1}^2 \left[1 + \frac{KT}{4} \Sigma x_{j(k+1)}^2 \right] \quad (110)$$

If this approach could be implemented, the parameter adjustment loops would always be stable, and would also be more heavily damped than the equivalent continuous system.

Case III: Trapezoidal Integration (Figure 54)

If equation (99) were evaluated by trapezoidal integration,

$$b_{j(k+1)}^* = b_{j_k}^* - \frac{KT}{4} (e_{k+1} x_{j(k+1)} + e_k x_{j_k}) \quad (111)$$

Substituting equation (111) into equation (103),

$$V_{k+1} - V_k = -\frac{KT}{4} \Sigma (e_{k+1} x_{j(k+1)} + e_k x_{j_k}) (b_{j(k+1)}^* - b_j + b_{j_k}^* - b_j)$$

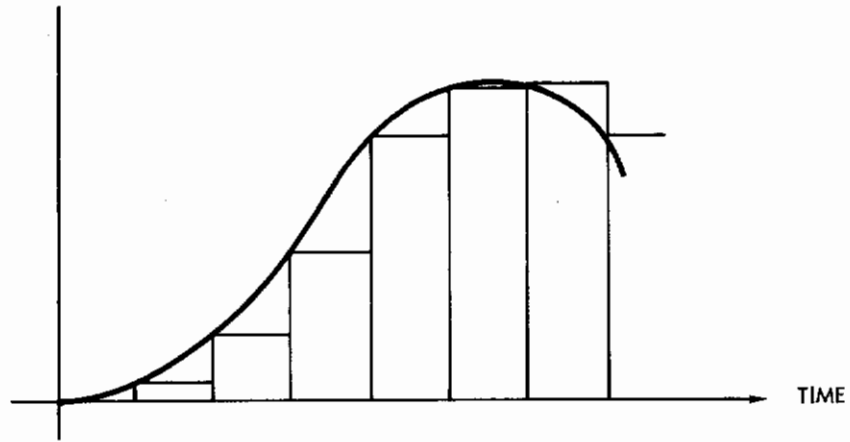


Figure 52. Rectangular Integration Based On Past Input

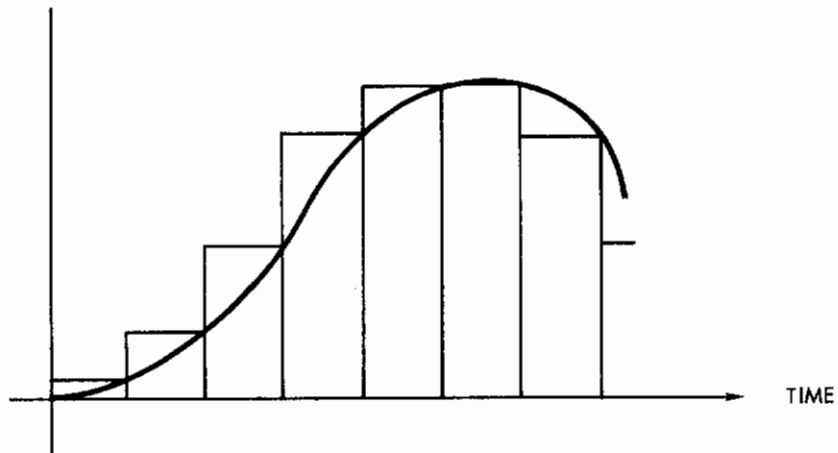


Figure 53. Rectangular Integration Based On Present Input

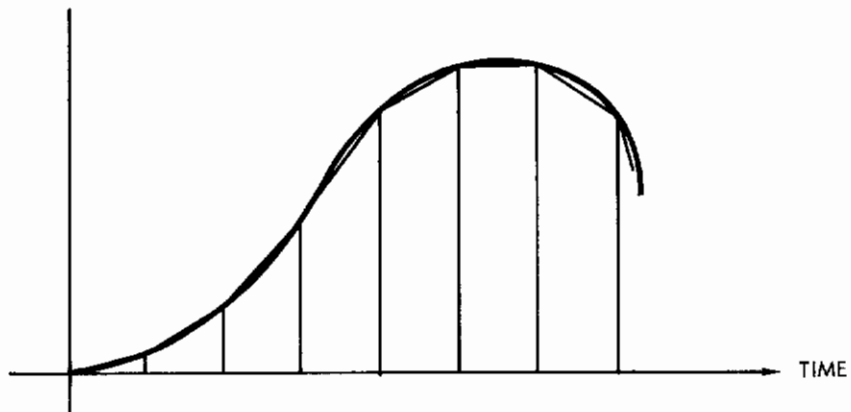


Figure 54. Trapezoidal Integration

$$\begin{aligned}
 &= -\frac{KT}{4} \left[e_{k+1}^2 + e_k^2 + e_{k+1} \sum x_{j(k+1)} (b_{j_k}^* - b_j) \right. \\
 &\quad \left. + e_k \sum x_{j_k} (b_{j(k+1)}^* - b_j) \right] \\
 &= -\frac{KT}{4} \left[e_{k+1}^2 + e_k^2 + e_{k+1} \sum x_{j(k+1)} \left[b_{j(k+1)}^* \right. \right. \\
 &\quad \left. \left. - b_j + \frac{KT}{4} (e_{k+1} x_{j(k+1)} + e_k x_{j_k}) \right] \right. \\
 &\quad \left. + e_k \sum x_{j_k} \left[b_{j_k}^* - b_j - \frac{KT}{4} (e_{k+1} x_{j(k+1)} + e_k x_{j_k}) \right] \right] \\
 &= -\frac{KT}{4} \left[2e_{k+1}^2 + 2e_k^2 + \frac{KT}{4} e_{k+1}^2 \sum x_{j(k+1)}^2 \right. \\
 &\quad \left. - \frac{KT}{4} e_k^2 \sum x_{j_k}^2 \right] \\
 &= -\frac{KT}{2} \left[e_{k+1}^2 + e_k^2 + \frac{KT}{8} (e_{k+1}^2 \sum x_{j(k+1)}^2 \right. \\
 &\quad \left. - e_k^2 \sum x_{j_k}^2) \right] \tag{112}
 \end{aligned}$$

While Case III is more stable, as indicated by equation (112), than Case I (106), it is apparently more lightly damped than Case II (110). This is entirely in agreement with results obtainable from linear sampled-data theory for these approximations.

Of the three cases discussed so far, only Case I may be realized physically, and it was the least stable of all. To realize the other two cases on an approximate basis, linear input prediction may be used. For example, suppose one denotes the input to an integrator by u , and the output by v , as illustrated in Figure 55. For a linear first order predictor, it is assumed that the past, present and predicted future values of the input may be connected by a straight line, as indicated in Figure 56. The slope along the straight line is constant, yielding

$$u_{k+1} - u_k \approx u_k - u_{k-1} \tag{113}$$

or

$$u_{k+1} \approx 2u_k - u_{k-1} \tag{114}$$

This basic input prediction algorithm may now be combined with Cases II and III to yield realizable computational schemes as follows:

Case IV: Rectangular Integration with Input Prediction

Referring to Figures 53 and 55, the integrator output for rectangular integration is

$$v_{k+1} = v_k - KT u_{k+1}. \quad (115)$$

Substituting equation (114) into equation (115)

$$v_{k+1} \approx v_k - KT(2u_k - u_{k-1}) \quad (116)$$

which is realizable because only past inputs are required. If equation (99) is evaluated using equation (116) then

$$b_{j(k+1)}^* = b_{jk}^* - \frac{KT}{2} (2e_k x_{jk} - e_{k-1} x_{j(k-1)}). \quad (117)$$

Substituting equation (117) into equation (103) gives

$$\begin{aligned} V_{k+1} - V_k &= -\frac{KT}{2} \sum (2e_k x_{jk} - e_{k-1} x_{j(k-1)}) (2b_{jk}^* - 2b_j) \\ &\quad - \frac{KT}{2} \left[2e_k x_{jk} - e_{k-1} x_{j(k-1)} \right] \\ &= -\frac{KT}{2} \left[4e_k^2 - 2e_k - 1 \sum (b_{jk}^* - b_j) x_{j(k-1)} \right. \\ &\quad \left. - \frac{KT}{2} (4e_k^2 \sum x_{jk}^2 + e_{k-1}^2 \sum x_{j(k-1)}^2 \right. \\ &\quad \left. - 4e_k e_{k-1} \sum x_{jk} x_{j(k-1)}) \right] \end{aligned} \quad (118)$$

Indexing equation (117) gives

$$b_{jk}^* = b_{j(k-1)}^* - \frac{KT}{2} (2e_k - 1 x_{j(k-1)} - e_{k-2} x_{j(k-2)}) \quad (119)$$

from which,

$$\begin{aligned}
 \sum (b_{j_k}^* - b_j) x_{j(k-1)} &= \sum \left[b_{j(k-1)}^* - b_j \right. \\
 &\quad \left. - \frac{KT}{2} (2e_{k-1} x_{j(k-1)} \right. \\
 &\quad \left. - e_{k-2} x_{j(k-2)}) \right] x_{j(k-1)} \\
 &= e_{k-1} - KT e_{k-1} \sum x_{j(k-1)}^2 + \frac{KT}{2} e_{k-2} \\
 &\quad \sum x_{j(k-1)} x_{j(k-2)}. \tag{120}
 \end{aligned}$$

Substituting equation (120) into equation (118)

$$\begin{aligned}
 V_{k+1} - V_k &= - \frac{KT}{2} \left[4e_k^2 - 2e_{k-1}^2 - \frac{KT}{2} (-4e_{k-1}^2 \sum x_{j(k-1)}^2 \right. \\
 &\quad \left. + 2e_{k-1} e_{k-2} \sum x_{j(k-1)} x_{j(k-2)} \right. \\
 &\quad \left. + 4e_k^2 \sum x_{j_k}^2 + e_{k-1}^2 \sum x_{j(k-1)}^2 \right. \\
 &\quad \left. - 4e_k e_{k-1} \sum x_{j_k} x_{j(k-1)}) \right] \\
 &= -KT \left[2e_k^2 - e_{k-1}^2 \right] \\
 &\quad + \left(\frac{KT}{2} \right)^2 \left[4e_k^2 \sum x_{j_k}^2 - 4e_{k-1}^2 \sum x_{j(k-1)}^2 \right. \\
 &\quad \left. + e_{k-1}^2 \sum x_{j(k-1)}^2 \right. \\
 &\quad \left. + 2e_{k-1} e_{k-2} \sum x_{j(k-1)} x_{j(k-2)} \right. \\
 &\quad \left. - 4e_k e_{k-1} \sum x_{j_k} x_{j(k-1)} \right]. \tag{121}
 \end{aligned}$$

If the sampling rate is high and the gain K low, e_k will approximate e_{k-1} and x_{j_k} will approximate $x_{j(k-1)}$. Under these conditions, equation (121) may be written

$$V_{k+1} - V_k \approx -KT e_k^2 \left[1 + \frac{KT}{4} \sum x_{j_k}^2 \right] \quad (122)$$

which is essentially the same as equation (110), as might have been expected. Thus, under these conditions, the digital system is slightly better damped than the continuous system. However, as gain increases, the adjustment rate will increase, and e_k will no longer approximate e_{k-1} . For example, suppose the sign of the error alternates with each successive sample. Then,

$$e_k \approx -e_{k-1} \quad (123)$$

and equation (121) becomes approximately

$$V_{k+1} - V_k \approx -KT e_k^2 \left[1 - 3 \frac{KT}{4} \sum x_{j_k}^2 \right] \quad (124)$$

This is somewhat worse than Case I, as indicated by equation (106). Thus, Case III is the best method discussed so far at low gain and high sampling rate, but may tend to go unstable in such a manner that the error alternates in sign for high gain. This phenomenon is also common in linear systems, wherein it is recognized that the prediction scheme introduces an extraneous pole at the origin which may result in an extraneous mode at half the sampling frequency. This is illustrated by the root locus for a single-loop system in Figure 57, where the root leaving the unit circle along the negative real axis gives rise to the oscillation at half the sampling frequency. Here, the numerical integration algorithm is of the form of equation (116).

Taking the z -transform of equation (116),

$$z[V(z)] = V(z) - KT [2U(z) - z^{-1}U(z)]. \quad (125)$$

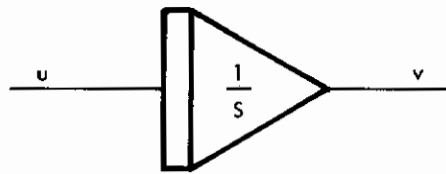


Figure 55. Integrator

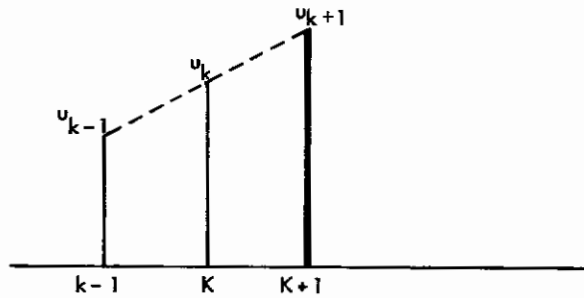


Figure 56. Linear Input Prediction

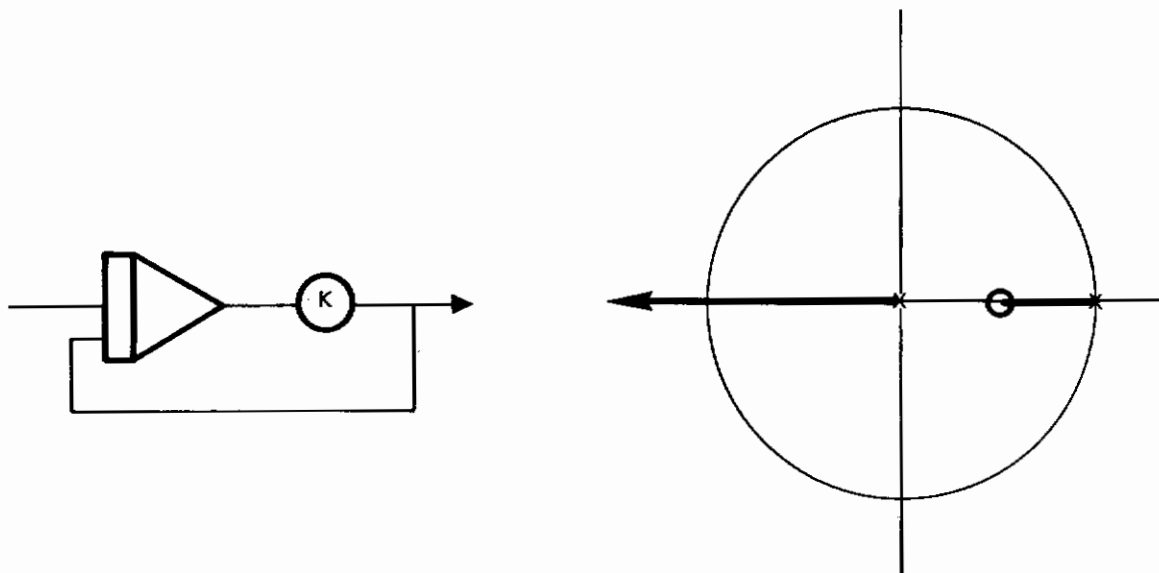


Figure 57. Root Locus for Rectangular Integration with Input Prediction

Rearranging gives

$$\frac{V(z)}{U(z)} = -2KT \frac{(z - 1/2)}{z(z - 1)}. \quad (126)$$

The pole at + 1 performs the integration, whereas the extraneous pole at the origin creates the instability. This does not mean that input prediction is destabilizing, because without it, the zero in equation (126) would also disappear, and instability could still occur.

By way of summary, it may be said that rectangular integration with input prediction (Case IV) is superior to rectangular integration without input prediction (Case I) at high sampling rates and moderate gain, but is not necessarily so when gains are so high as to cause the system to approach instability.

Case V: Trapezoidal Integration with Input Prediction

Let

$$u_{k+i} = e_k + i x_j(k+i)$$

then, equation (114) becomes for $i = -1, 0, +1$

$$e_{k+1} x_j(k+1) \approx 2e_k x_{j_k} - e_{k-1} x_j(k-1). \quad (127)$$

Substituting equation (127) into equation (111)

$$b_{j(k+1)}^* = b_{j_k}^* - \frac{KT}{4} (3e_k x_{j_k} - e_{k-1} x_j(k-1)) \quad (128)$$

which, unlike equation (111), is physically realizable because only past values of data are used. Substituting equation (128) into equation (103) gives

$$\begin{aligned}
 V_{k+1} - V_k &= -\frac{KT}{4} \sum (3e_k x_{jk} - e_{k-1} x_{j(k-1)}) (2b_{jk}^* \\
 &\quad - 2b_j - \frac{KT}{4} \left[3e_k x_{jk} - e_{k-1} x_{j(k-1)} \right]) \\
 &= -\frac{KT}{4} \left[6e_k^2 - 2e_{k-1} \sum (b_{jk}^* - b_j) x_{j(k-1)} \right. \\
 &\quad \left. - \frac{KT}{4} (9e_k^2 \sum x_{jk}^2 - 6e_k e_{k-1} \sum x_{jk} x_{j(k-1)} \right. \\
 &\quad \left. + e_{k-1}^2 \sum x_{j(k-1)}^2) \right]. \tag{129}
 \end{aligned}$$

However, replacing k by $k-1$ in equation (128)

$$\begin{aligned}
 \sum (b_{jk}^* - b_j) x_{j(k-1)} &= \sum \left[b_{j(k-1)}^* - b_j - \frac{KT}{4} (3e_{k-1} x_{j(k-1)} \right. \\
 &\quad \left. - e_{k-2} x_{j(k-2)}) \right] x_{j(k-1)} \\
 &= e_{k-1} - \frac{KT}{4} \sum (3e_{k-1} x_{j(k-1)} \\
 &\quad - e_{k-2} x_{j(k-2)}) x_{j(k-1)}. \tag{130}
 \end{aligned}$$

Substituting equation (130) into equation (129)

$$\begin{aligned}
 V_{k+1} - V_k &= -\frac{KT}{4} \left[6e_k^2 - 2e_{k-1}^2 + \frac{KT}{2} (3e_{k-1}^2 \sum x_{j(k-1)}^2 \right. \\
 &\quad \left. - e_{k-1} e_{k-2} \sum x_{j(k-1)} x_{j(k-2)}) \right. \\
 &\quad \left. - \frac{KT}{4} (9e_k^2 \sum x_{jk}^2 - 6e_k e_{k-1} \sum x_{jk} x_{j(k-1)} \right. \\
 &\quad \left. + e_{k-1}^2 \sum x_{j(k-1)}^2) \right] = -\frac{KT}{2} \left[3e_k^2 - e_{k-1}^2 \right]
 \end{aligned}$$

$$\begin{aligned}
 & + \left(\frac{KT}{4}\right)^2 \left[9e_k^2 \sum x_{jk}^2 - 5e_{k-1}^2 \sum x_{j(k-1)}^2 \right. \\
 & \quad \left. - 6e_k e_{k-1} \sum x_{jk} x_{j(k-1)} \right. \\
 & \quad \left. + 2e_{k-1} e_{k-2} \sum x_{j(k-1)} x_{j(k-2)} \right] \quad (131)
 \end{aligned}$$

At high sampling rate and low gain, this reduces approximately to

$$V_{k+1} - V_k \approx -KT e_k^2 \quad (132)$$

such that the system is about as well damped as a linear system, and more lightly damped than Case IV. If instability occurs at half the sampling frequency, equation (123) applies again, and the high-gain approximation is

$$V_{k+1} - V_k \approx -KT e_k^2 \left(1 - \frac{KT}{2} \sum x_{jk}^2\right) \quad (133)$$

which is slightly better than equation (124) for Case IV, and worse than equation (106) for Case I. Thus, while Case V is inferior to Case IV at low gains, this is not necessarily so at high gains.

Summary Of Cases I Through V

Cases II and III are not physically realizable, and were included for comparison only. Hence, as far as implementation is concerned, only Cases I, IV, and V need be considered. Case V uses the most complex algorithm, and from the point of view of stability, is inferior to Case I at high gain and to Case IV at low gain. Case I seems to be at least as good as Case IV at high gain, so it would seem to be the logical choice; provided the damping of parameter adjustments is adequate at lower gains.

Case I, which is simple rectangular integration without prediction, uses the simplest algorithm, appears to be about as good as the other cases in overall quality and introduces no extraneous response modes.

REFERENCES

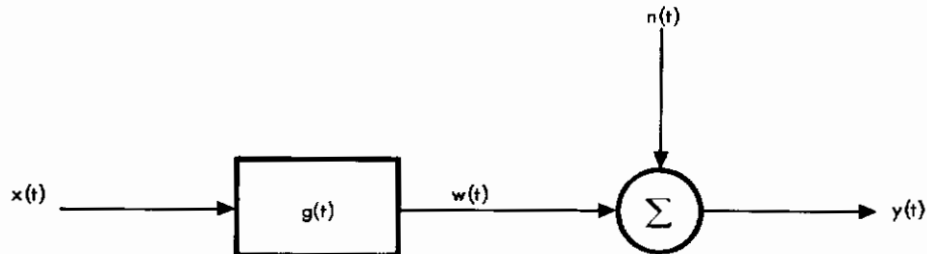
1. SID 63-1139, Accession No. 26457, Proposal for Study of an Advanced Adaptive Control Technique, 17 September 1963, NAA.
2. P. C. Gregory, ed. Proceedings of the Self-Adaptive Flight Control Systems Symposium, WADC TR-59-49, ASTIA Document No. AD 209389, (March 1959).
3. J. Lindahl, W. McGuire, M. Reed. Advanced Flight Vehicle Self-Adaptive Control System, Part VII, Documentary Report WADD-TDR-60-651, Part VII, Air Force Flight Dynamics Laboratory, RTD, Air Force Systems Command, Wright-Patterson Air Force Base, Ohio (December 1963).
4. J. C. Lindenlaub and G. R. Cooper, "Noise Limitations of System Identification Techniques," IEEE Trans. on Automatic Control, Vol. AC-8 (January 1963), pp. 43-48.
5. Bureau of Aeronautics Flight Control and Fire Control System Manuals, Vol. II, Dynamics of the Airframe, AE-61-4 II, Northrop Corporation, Norair Division, Hawthorne, California, September 1952.
6. T. F. Potts, G. N. Ornstein, A. B. Clymer. The Automatic Determination of Human and Other System Parameters, presented at the Western Joint Computer Conference (May 1961).
7. B. J. Miller. "A General Method of Computing System Parameters with an Application to Adaptive Control," AIEE Winter General Meeting, New York, New York. (January 28-February 2, 1962).
8. P. Shipley. "A Unified Approach to Synthesis of Linear Systems," IEEE Trans. on Automatic Control, Vol. AC-8, Number 2, April 1963, pp. 114-120.
9. J. T. Tou. Modern Control Theory, McGraw-Hill Book Company, New York, New York. (1964).
10. Isaac M. Horowitz. "Linear-Adaptive Flight Control Design for Re-Entry Vehicles," IEEE Trans. on Automatic Control, Vol. AC-9, Number 1, January 1964, pp. 90-97.

11. WADD TR-60-651, Part I, "Advanced Flight Vehicle Self-Adaptive Flight Control System—Study Phase," MH Aero Report 2373-TR1.
12. WADD-TR-60-651, Part III, Advanced Flight Vehicle Self-Adaptive Flight Control System—Support Equipment Study, MH Aero Report 2378-TR8.
13. State Space Techniques for Control Systems—Workshop, Papers Presented at the 1962 Joint Automatic Control Conference, Published by AIEE, New York.

APPENDIX I

OPTIMUM CORRELATION TIME

In Reference 4, the problem of identifying by correlation using contaminated data is considered in terms of the following configuration.



Using relatively mild assumptions, it is shown that the optimum (shortest possible) identification time without prior knowledge of vehicle dynamics is

$$T_I = \frac{2W_G K_G}{\gamma \sigma^2} \quad (I-1)$$

where

T_I = optimum identification time

K_G = system low-frequency power gain

W_G = system bandwidth

γ = signal/noise ratio = $\overline{w^2}/\overline{n^2}$

σ^2 = variance of impulse response estimate

EXAMPLE:

$$W_G = 5 \text{ rad/sec}$$

$$K_G = 1.0$$

$$\gamma = 1.0$$

$$\sigma^2 = 0.01$$

$$T_I = \frac{2 \times 5 \times 1}{1 \times 0.01} = 1000 \text{ sec}$$

Contrails

APPENDIX II

A COMPARATIVE TREATMENT OF CERTAIN TECHNIQUES FOR PARAMETER IDENTIFICATION BASED ON THE STATE SPACE APPROACH

Rather close relationships exist among various approaches to parameter identification. These relationships, in turn, are analogous to similar relationships which exist among techniques for solving linear algebraic equations. The objective of this communication is to clarify some of these relationships through a unified treatment based upon the state space approach (Reference 13). A knowledge of this subject is of importance in understanding the S&ID approach to adaptive control, particularly if interaction among parameter adjustments is serious.

BASIC STATE VARIABLE CONCEPTS

In an analog computer circuit, the total input to each integrator is a function of the various integrator outputs, of inputs from external sources, and of time. Thus, if there are M integrator outputs x_i ($i = 1, 2, \dots, M$), and N inputs from external sources u_i ($i = 1, 2, \dots, N$), the total input to the i 'th integrator is

$$\dot{x}_i = f_i(x_1, x_2, \dots, x_M; u_1, u_2, \dots, u_N, t) \quad (\text{II-1a})$$

The entire system may be represented by a set of equations in the form of equation (II-1a), one for each integrator. These equations may be combined into a single matrix equation as in equation (II-1b).

$$\begin{bmatrix} \dot{x}_1 \\ \dot{x}_2 \\ \vdots \\ \dot{x}_M \end{bmatrix} = \begin{bmatrix} f_1(x_1, x_2, \dots, x_M; u_1, u_2, \dots, u_N, t) \\ f_2(x_1, x_2, \dots, x_M; u_1, u_2, \dots, u_N, t) \\ \vdots \\ f_M(x_1, x_2, \dots, x_M; u_1, u_2, \dots, u_N, t) \end{bmatrix} \quad (\text{II-1b})$$

This is commonly written in a more compact form as (see Figure 58).

$$\dot{\underline{x}} = \underline{f}(\underline{x}, \underline{u}, t) \quad (\text{II-2a})$$

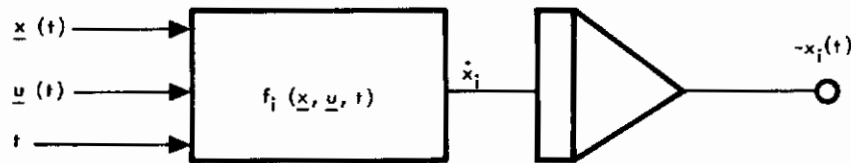


Figure 58. Analog Counterpart of Equation (II-2a)

Where a bar under a letter denotes a column matrix:

$$\underline{x} \triangleq \begin{bmatrix} x_1 \\ x_2 \\ \vdots \\ x_M \end{bmatrix}, \quad \underline{u} \triangleq \begin{bmatrix} u_1 \\ u_2 \\ \vdots \\ u_N \end{bmatrix}, \quad \underline{f} \triangleq \begin{bmatrix} f_1 \\ f_2 \\ \vdots \\ f_M \end{bmatrix} \quad (\text{II-2b})$$

The elements x_i of \underline{x} are commonly referred to as state variables, and together are sufficient to describe the state of the system. The state of the system at any time, t , may be determined from the state at some previous time, t_0 , provided all N elements of the input matrix \underline{u} are known for all time between t and t_0 , simply by allowing the analog computer to operate normally.

The elements x_i of the matrix \underline{x} in equation (II-2b) are commonly associated with components of a vector in M -dimensional space. Hence, \underline{x} is commonly referred to as the state vector, the components x_i as state variables, and \underline{u} as the control vector.

If $\underline{f}(\underline{x}, \underline{u}, t)$ is linear in \underline{x} and \underline{u} and time invariant, (II-2a) may be written in the form

$$\dot{\underline{x}} + \underline{A}\underline{x} = \underline{B}\underline{u} \quad (\text{II-3})$$

where \underline{A} is a square M by M matrix, and \underline{B} is an M by N matrix, both \underline{A} and \underline{B} having constant elements.

To illustrate how ordinary differential equations may be converted into the form of equation (II-3), consider a single linear second order differential equation with constant coefficients.

$$\ddot{y} + a \dot{y} + b y = r(t) \quad (\text{II-4a})$$

This may be programmed for an analog computer as shown in Figure 59.

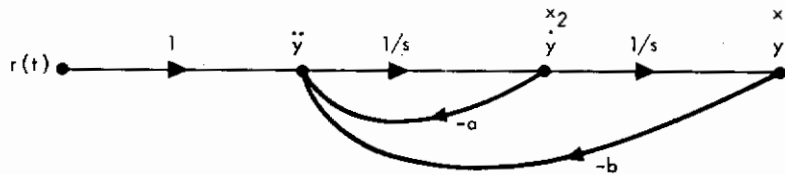


Figure 59. Analog Counterpart of Equation (II-4a)

Defining x_1 to be y and x_2 to be \dot{y} , equation (II-4a) reduces to

$$\dot{x}_1 = x_2 \quad (\text{II-4b})$$

$$\dot{x}_2 = -a x_2 - b x_1 + r \quad (\text{II-4c})$$

or in matrix form,

$$\begin{bmatrix} \dot{x}_1 \\ \dot{x}_2 \end{bmatrix} = \begin{bmatrix} 0 & 1 \\ -b & -a \end{bmatrix} \begin{bmatrix} x_1 \\ x_2 \end{bmatrix} + \begin{bmatrix} 0 \\ r \end{bmatrix} \quad (\text{II-4d})$$

This is of the form of equation (II-3) where $\begin{bmatrix} 0 & 1 \\ -b & -a \end{bmatrix}$ corresponds to $-A$.

Taking the Laplace Transform of equation (II-3) yields (note that taking the Laplace Transform equation of (II-3) corresponds to transforming each first-order scalar equation represented by equation (II-3), then recombining in matrix form),

$$s \underline{X} - \underline{x}(0) + A \underline{X} = B \underline{U} \quad (\text{II-5a})$$

or

$$(s I + A) \underline{X} = \underline{x}(0) + B \underline{U} \quad (\text{II-5b})$$

where I is the unit matrix.

Applying Cramer's rule to solve for the transfer function between any two points of the system, it is seen that the roots of the denominator are the roots of

$$\left| s I + A \right| = 0 \quad (\text{II-6})$$

where $\left| s I + A \right|$ denotes the determinant of the matrix $(s I + A)$. It is well known from elementary differential equation theory that the system described by equation (II-3) is stable only if none of these roots has positive real parts.

Now, the eigenvalues of a matrix A are defined to be the roots of the characteristic equation

$$\left| \lambda I - A \right| = 0. \quad (\text{II-7})$$

Comparison of equation (II-6) with equation (II-7) reveals that the eigenvalues of A are the negatives of the roots of equation (II-6), and the system described by equation (II-3) is stable only if none of the eigenvalues of the matrix A has negative real parts.

Now, consider a scalar function

$$V = \tilde{x} A x \quad (\text{II-8})$$

where \tilde{x} denotes the transpose of x . The function V and the matrix A are both defined to be positive definite, negative definite, nonpositive, or nonnegative if V is respectively positive, negative, nonpositive, or nonnegative whenever at least one component of x is nonzero. It may be shown that if A is a real symmetric matrix, all eigenvalues of A are real, and also respectively positive, negative, nonpositive, or nonnegative. That is, if all eigenvalues of A have the same sign, this sign agrees with the sign of V , such that for stable systems, V (and hence A) must be nonnegative. If, in addition, none of the eigenvalues of A is zero, A is positive definite.

A real matrix A is symmetric and nonnegative if (and only if) there exists a real matrix B such that

$$A = \tilde{B} B \quad (\text{II-9})$$

The matrix A is positive definite if B , and thus A , is nonsingular (having a nonzero determinant). To verify that $\tilde{B} B$ is nonnegative, equation (II-9) may be substituted into equation (II-8) to obtain (using the rule $\tilde{A} B = \tilde{B} A$ for transposing matrix products),

$$V = \tilde{x} \tilde{B} B x = \tilde{B} x B x \quad (\text{II-10})$$

Now, define

$$\underline{y} \triangleq B \underline{x} \quad (\text{II-11})$$

Then,

$$V = \tilde{\underline{y}} \underline{y} = \sum y_i^2 \geq 0 \quad (\text{II-12})$$

which shows that $\tilde{B} B$ is nonnegative. Similarly, $- \tilde{B} B$ is nonpositive. Premultiplying equation (II-11) by B^{-1} ,

$$\underline{x} = B^{-1} \underline{y} \quad (\text{II-13})$$

provided B is not singular (in which case it could not be inverted). It follows that if B is nonsingular, \underline{x} will have nonzero components only if \underline{y} has also. Hence, if \underline{x} is nonzero, so is V in equation (II-12), and $\tilde{B} B$ is positive definite as stated earlier. The rule $\tilde{A}B = \tilde{B} A$ for transposing matrix products used in equation (II-10) may be derived quite easily from the definition of matrix multiplication. Thus, if

$$C = AB \quad (\text{II-14})$$

then the definition of matrix multiplication is

$$c_{ij} = \sum a_{ik} b_{kj} \quad (\text{II-15})$$

Interchanging i and j ,

$$c_{ij} = \sum b_{ki} a_{jk} \quad (\text{II-16})$$

which corresponds to the matrix equation

$$\tilde{C} = \tilde{B} A \quad (\text{II-17})$$

Combining equations (14) and (17),

$$\tilde{A}B = \tilde{B} A \quad (\text{II-18})$$

Now, consider the homogeneous (no input) version of equation (II-3)

$$\dot{\underline{x}} + A \underline{x} = \underline{0} \quad (\text{II-19})$$

and the Lyapunov function

$$V = \tilde{\underline{x}} \underline{x} = \sum x_i^2 \geq 0 \quad (\text{II-20a})$$

which is a special case of equation (II-8) with A equal to the unit matrix. Inasmuch as the system represented by equation (II-3) is linear, stability may be analyzed without considering inputs. Hence, equation (II-3) represents a stable system if and only if equation (II-19) does also. An autonomous (homogeneous and time invariant) system is said to be stable in the sense of Lyapunov if there exists a positive definite function V of the state vector \underline{x} such that \dot{V} is nonpositive. That is, $\dot{V} \leq 0$ (V never increases at any time). Differentiating equation (II-20a) and substituting equation (II-19).

$$\dot{V} = 2 \sum x_i \dot{x}_i = 2 \underline{\tilde{x}} \dot{\underline{x}} = -2 \underline{\tilde{x}} A \underline{x} \quad (\text{II-20b})$$

That is, Lyapunov stability requires that A be nonnegative, which is the same requirement as was derived earlier for stability in the conventional sense (no negative eigenvalues). Some of these results could be extended to cases where A is not symmetric. However, such cases are not of interest in the following discussion.

SOLUTION OF LINEAR ALGEBRAIC EQUATIONS

Certain aspects of the problem of solving sets of linear algebraic equations will now be discussed as a preliminary to consideration of the parameter identification problem. Consider a set of linear algebraic equations expressed in matrix form as

$$A \underline{x} = \underline{b} \quad (\text{II-21})$$

As a first step in setting up the solution for the vector \underline{x} , an error quantity \underline{e} is defined in terms of an estimate \underline{X} for the actual solution vector \underline{x} .

$$\underline{e} \triangleq A \underline{X} - \underline{b} \quad (\text{II-22})$$

or

$$e_i = \sum_j A_{ij} X_j - b_i \quad (\text{II-23})$$

A positive definite Lyapunov function in \underline{e} is then

$$V = \underline{\tilde{e}} \underline{e} = \sum_i e_i^2 \geq 0. \quad (\text{II-24})$$

Differentiating V with respect to time by the chain rule,

$$\dot{V} = \sum_i \frac{\partial V}{\partial X_i} \dot{X}_i = \frac{\partial V}{\partial \underline{X}} \dot{\underline{X}} \quad (\text{II-25})$$

where $\frac{\partial \tilde{V}}{\partial \underline{X}}$ denotes the row vector $(\frac{\partial V}{\partial X_1}, \frac{\partial V}{\partial X_2}, \dots, \frac{\partial V}{\partial X_N})$, and N is the order of the matrix A.

It is apparent from equation (II-25) that $\dot{\tilde{V}}$ is negative definite in $\partial V / \partial \underline{X}$ if $\dot{\underline{X}}$ is of the form

$$\dot{\underline{X}} = - \tilde{B} B \frac{\partial V}{\partial \underline{X}} \quad (\text{II-26})$$

A special case of this is

$$\dot{\underline{X}} = -K \frac{\partial V}{\partial \underline{X}} \quad (\text{II-27})$$

where K is some positive constant. The rule for adjusting \underline{X} expressed by equation (II-27) is commonly referred to as steepest descent, inasmuch as the velocity $\dot{\underline{X}}$ of the \underline{X} vector points in a direction opposite the gradient $\partial V / \partial \underline{X}$ in hyperspace. It is not necessarily better than other possible versions of equation (II-26), but is commonly used because of its simplicity and its simple geometric interpretation. From equations (II-24) and (II-23),

$$\frac{\partial V}{\partial X_k} = 2 \sum_i e_i \frac{\partial e_i}{\partial X_k} = 2 \sum_i e_i A_{ik} = 2 \sum_i A_{ik} e_i. \quad (\text{II-28})$$

Or in vector notation,

$$\partial V / \partial \underline{X} = 2 \tilde{A} \underline{e} = 2 \tilde{A} (A \underline{X} - \underline{b}) = 2 [\tilde{A} A \underline{X} - \tilde{A} \underline{b}] \quad (\text{II-29})$$

Substituting equation (II-29) into equation (II-26),

$$\dot{\underline{X}} = -2 \tilde{B} B [\tilde{A} A \underline{X} - \tilde{A} \underline{b}] \quad (\text{II-30})$$

or for steepest descent,

$$\dot{\underline{X}} = -2 K [\tilde{A} A \underline{X} - \tilde{A} \underline{b}] \quad (\text{II-31})$$

This represents a linear set of first-order differential equations, and is readily implemented with an analog computer. It was derived in such a manner as to be stable in the sense of Lyapunov. Inasmuch as $\tilde{A} A$ is nonnegative definite, it is also apparent from equation (II-31) that stability

exists, and because $\tilde{A} A$ is symmetric, all eigenvalues are real. This means that the time history of each parameter will be a sum of real exponentials, so there is never any tendency toward oscillation. When a solution is reached, all components of $\underline{\dot{X}}$ become zero, and from equation (II-31),

$$\tilde{A} A \underline{X} = \tilde{A} \underline{b} \quad (\text{II-32})$$

multiplying equation (II-21) by \tilde{A} ,

$$\tilde{A} A \underline{x} = \tilde{A} \underline{b} \quad (\text{II-33})$$

subtracting equation (II-32)

$$\tilde{A} A (\underline{x} - \underline{X}) = \underline{0} . \quad (\text{II-34})$$

If A is nonsingular, equation (II-34) may be premultiplied by \tilde{A}^{-1} , then by A^{-1} to obtain

$$\underline{x} = \underline{X} \quad (\text{II-35})$$

and the adjustment always converges to the true solution if such a solution exists and is unique.

Comparison of equation (II-33) with equation (II-21) reveals that a set of linear algebraic equations may be reduced to a form with a symmetric positive definite matrix simply by multiplying by the transpose of the original matrix. This is sometimes used to facilitate numerical computation, by taking advantage of various simplified schemes available for solving sets of equations involving symmetric positive definite matrices.

SIDAC PARAMETER IDENTIFICATION

The foregoing concepts may now be applied to the problem of computing parameter values in dynamical systems from measured input/output data. If the dynamics of a system may be expressed in terms of a set of linear differential equations wherein some of the variables are physically accessible for measurement; then, if those variables which are not measurable are eliminated algebraically, a smaller set of equations is obtained in terms of the measurable variables only. Each of these equations is then of the form (Reference 6)

$$x_0 + \sum_{i=1}^M b_i x_i = 0 \quad (\text{II-36})$$

where the x_i 's are the variables in the reduced set of equations, and the b_i 's are the associated coefficients.

The problem now is to measure the variables as a function of time, and somehow deduce the values of the coefficients therefrom. To do this, an error may be defined as

$$e = x_0 + \sum_{i=1}^M b_i^* x_i \quad (\text{II-37})$$

where the b_i^* coefficients are estimates of the actual b_i coefficients. This error may be obtained from a physical or mathematical model as shown in Figure 60.

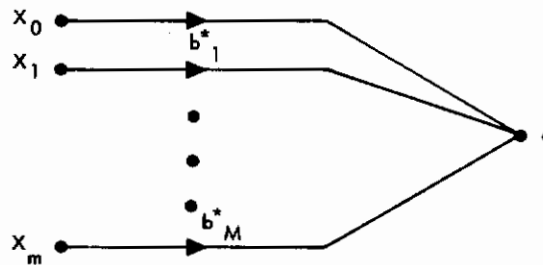


Figure 60. Model Equivalent to Equation (II-37)

Subtracting equation (II-36) from equation (II-37),

$$e = \sum_{i=1}^M (b_i^* - b_i) x_i = (\underline{b}^* - \underline{b}) \underline{x} \quad (\text{II-38})$$

where \underline{x} is a vector containing all of the x_i 's except x_0 .

Now, define a Lyapunov function (Reference 7) which is positive definite in terms of the parameter adjustment errors.

$$V \triangleq (\underline{b}^* - \underline{b}) (\tilde{B} B)^{-1} (\underline{b}^* - \underline{b}) \geq 0 \quad (\text{II-39})$$

where B is any nonsingular matrix. A special case of equation (II-39) is when $\tilde{B} B$ is the unit matrix, in which Case V is the sum of the squares of the parameter adjustment errors.

$$V = (\underline{b}^* - \underline{b}) (\underline{b}^* - \underline{b}) = \sum_{i=1}^M (b_i^* - b_i)^2 \quad (\text{II-40})$$

Differentiating equation (II-39) with respect to time,

$$\begin{aligned}
 \dot{V} &= (\underline{b}^* - \underline{b}) (\tilde{B} B)^{-1} (\dot{\underline{b}}^* - \dot{\underline{b}}) + (\dot{\underline{b}}^* - \dot{\underline{b}}) (\tilde{B} B)^{-1} (\underline{b}^* - \underline{b}) \\
 &= 2 (\underline{b}^* - \underline{b}) (\tilde{B} B)^{-1} (\dot{\underline{b}}^* - \dot{\underline{b}}) \\
 &= 2 (\underline{b}^* - \underline{b}) (\tilde{B} B)^{-1} \dot{\underline{b}}^* - 2 (\dot{\underline{b}}^* - \dot{\underline{b}}) (\tilde{B} B)^{-1} \underline{b}
 \end{aligned} \tag{II-41}$$

The term containing $\dot{\underline{b}}$ represents tracking error due to changes in the actual system parameters, and is, therefore, not directly associated with stability of the adjustment loop. This term disappears if the system parameters are held constant. Then,

$$\dot{V} = 2 (\underline{b}^* - \underline{b}) (\tilde{B} B)^{-1} \dot{\underline{b}}^* \tag{II-42}$$

Now, choose $\dot{\underline{A}}$ as follows:

$$\dot{\underline{b}}^* = - (\tilde{B} B) e \frac{\partial e}{\partial \underline{b}^*} = - (\tilde{B} B) e \underline{x} \tag{II-43}$$

Substituting equation (II-43) into equation (II-42) and applying equation (II-38),

$$\dot{V} = - 2 e (\underline{b}^* - \underline{b}) \underline{x} = - 2 e^2 \tag{II-44}$$

Thus, V is always negative as long as an error exists. It follows that parameters will continue to adjust until the error becomes zero. Hopefully, this means that the parameters will all be adjusted to their correct values. However, this is not true for certain input combinations. The general conditions for which e is zero are easily obtained from equation (II-37).

If any input is a linear algebraic combination of the other inputs except as expressed by equation (II-36), it is not possible to solve for all coefficients individually. Such an input might be obtained through a feedback loop. For this reason, if one is identifying parameters in a closed loop system, it is important to check for independence of inputs.

Just as equation (II-30) reduced to equation (II-31) as a special case (steepest descent) in the solution of linear algebraic equations, equation (II-43) is sometimes reduced to

$$\dot{\underline{b}}^* = - K e \frac{\partial e}{\partial \underline{b}^*} \tag{II-45}$$

or

$$\dot{b}_{*i}^* = - K e \frac{\partial e}{\partial b_{*i}^*} \tag{II-46}$$

This formulation requires that all integrator gains be equal, whereas, equation (II-43) permits a different gain for each integrator, and cross-coupling among integrators, as long as the matrix ($\tilde{B} B$) describing the manner in which the integrator inputs are generated is positive definite and symmetric. The symmetry of the matrix implies that if the i 'th and j 'th integrators are cross-coupled by feeding some fraction of the i 'th input into the j 'th integrator, an equal fraction of the j 'th input must be fed into the i 'th integrator.

One way to choose the matrix $\tilde{B} B$ is to set up a simulation of the system and proceed empirically. Initially, steepest descent may be used, then individual integrator gains may be varied to improve convergence time. Finally, if any two parameters appear to be interacting seriously, cross-coupling between these parameters may be used.

It is informative to note that, although equation (II-45) was derived as a special case of equation (II-43), equation (II-43) may be derived from equation (II-45). Suppose a fictitious set of parameters \underline{a}^* is defined in terms of the physical parameters \underline{b}^* by the transformation

$$\underline{a}^* = B \underline{b}^* \quad (\text{II-47})$$

Then,

$$a^*_j = \sum_{i=1}^M B_{ji} b^*_i \quad (\text{II-48})$$

Differentiating e by the chain rule,

$$\frac{\partial e}{\partial b^*_i} = \sum_{j=1}^M \frac{\partial e}{\partial a^*_j} \frac{\partial a^*_j}{\partial b^*_i} = \sum_{j=1}^M \frac{\partial e}{\partial a^*_j} B_{ji} \quad (\text{II-49})$$

or

$$\frac{\partial e}{\partial \underline{b}^*} = \tilde{B} \frac{\partial e}{\partial \underline{a}^*} \quad (\text{II-50})$$

Differentiating equation (II-47) with respect to time,

$$\dot{\underline{a}}^* = B \dot{\underline{b}}^* \quad (\text{II-51})$$

Substituting equations (II-50) and (II-51) into equation (II-45),

$$B^{-1} \dot{\underline{a}}^* = -K e \tilde{B} \frac{\partial e}{\partial \underline{a}^*} \quad (\text{II-52})$$

$$\dot{\underline{a}}^* = -K B \tilde{B} e \frac{\partial e}{\partial \underline{a}^*} = -K B \tilde{B} e \frac{\partial e}{\partial \underline{a}^*} \quad (\text{II-53})$$

If K is equal to unity, equation (II-53) is identical in form to equation (II-43). Thus, any adjustment scheme of the form equation (II-43) may be construed to be steepest descent in a transformed set of coordinates, where the transformation is expressed by equation (II-47), provided B is not singular. Similarly, cross-coupling and scaling of integrator gains corresponds to transforming coordinates as indicated in equation (II-47). Inasmuch as this transformation is general enough to permit both rotation and change of scale, a rather flexible means is provided for changing the shape of a poorly conditioned Lyapunov function. Suppose, for example, two parameters b_1^* and b_2^* are being adjusted, and that mean-squared error E , as a function of these parameters, appears as shown in Figure 61.

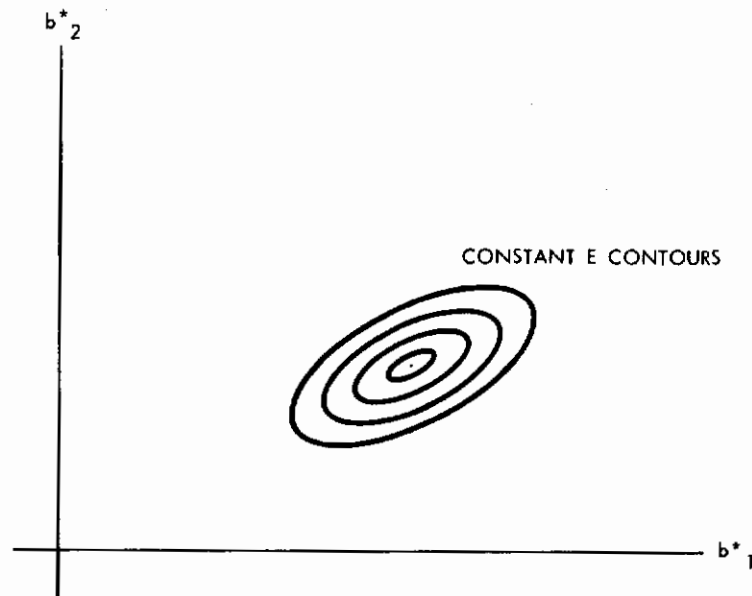


Figure 61. Contours of Constant Mean-Squared Error

Using steepest descent, there will be a definite tendency for the two parameter adjustments to oppose each other. After rotation (accomplished by cross-coupling integrators), Figure 62 is obtained

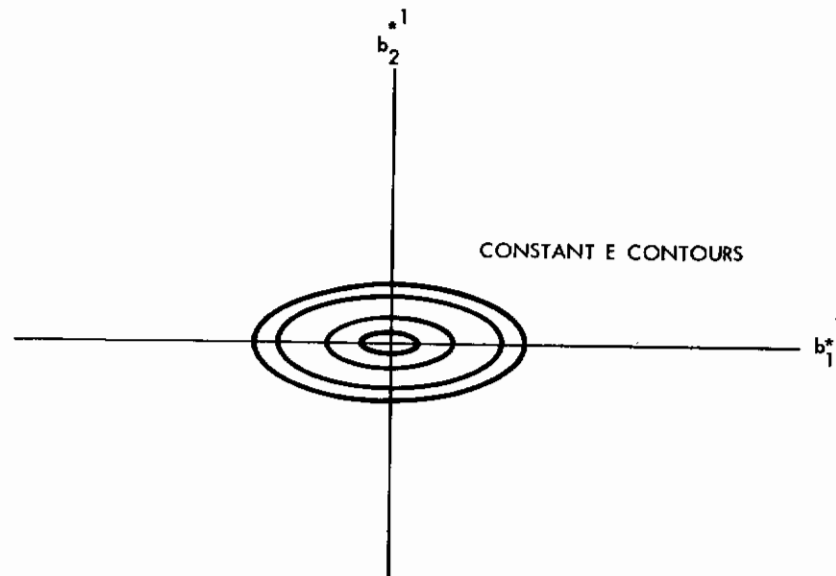


Figure 62. Rotated and Translated E Contours

Then, after scaling changes (accomplished by changing integrator gains), Figure 63 is obtained

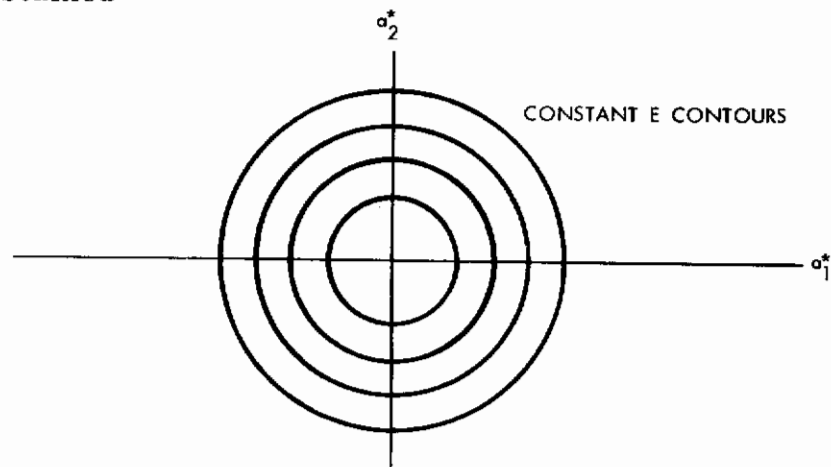


Figure 63. E Contours After Scaling

Thus, it is possible to transform elongated ellipses or ellipsoids into circles or spheres, thereby enhancing convergence properties. This can be very important in cases when steepest descent does not converge as rapidly as required in a given situation.

It is interesting to compare the foregoing results with those obtained by least-squares minimization. For this purpose, the mean-squared error E may be defined in terms of equation (II-37) as

$$E = \overline{e^2} = \left(x_0 + \sum_{i=1}^M b_i^*(0) x_i(t) \right)^2$$

$$= \lim_{T \rightarrow \infty} \frac{1}{T} \int_{-T}^0 \left[x_0(t) + \sum_{i=1}^M b_i^*(0) x_i(t) \right]^2 dt \quad (\text{II-54})$$

Of course, alternate definitions could be used, such as that obtained by passing e^2 through a low pass filter. The important aspect of the definition given by equation (II-54) is that the present value of b_i^* is used in the computation, even though b_i^* changes with time. Thus, E is not the quantity which would be obtained by computing $e^2(t)$ as a function of time from equation (II-37), and then integrating. Although this point may appear rather trivial, it is of basic importance in the following discussion.

Now, if data is averaged over a sufficiently long period of time, E becomes independent of short-term variations in the x_i 's and

$$\dot{E} = \frac{d}{dt} \overline{e^2} = \sum_{i=1}^M \frac{\partial E}{\partial b_i^*} \dot{b}_i^* = \frac{\partial E}{\partial \underline{b}^*} \dot{\underline{b}}^* \quad (\text{II-55})$$

Now, the reason for the rather obscure definition of E becomes apparent. If \dot{E} had been computed simply by averaging the output of the model illustrated in Figure 60, E must have been identically zero, inasmuch as instantaneous changes in the b_i^* parameters could not have produced immediate changes in the averaged output. Hence, no useful information could have been derived from equation (II-55).

From equation (II-55), \dot{E} is always negative, provided

$$\dot{\underline{b}}^* = - \tilde{B} B \partial E / \partial \underline{b}^* = - \tilde{B} B \overline{\partial e^2 / \partial \underline{b}^*} = - 2 \tilde{B} B \overline{e \partial e / \partial \underline{b}^*} \quad (\text{II-56})$$

However, from equation (II-37)

$$\partial e / \partial b_i^* = x_i \quad (\text{II-57})$$

or

$$\partial e / \partial \underline{b}^* = \underline{x} \quad (\text{II-58})$$

Substituting equation (II-58) into equation (II-56) and applying equation (II-37),

$$\dot{\underline{b}}^* = -2 \tilde{B} B \overline{\underline{e} \underline{x}} = -2 \tilde{B} B \overline{\underline{x} \underline{e}} = -2 \tilde{B} B \underline{x} \underline{x}_0 + \underline{x} \tilde{\underline{x}} \underline{b}^* \quad (\text{II-59})$$

or, remembering that \underline{b}^* is treated as a constant with respect to the averaging process,

$$\begin{bmatrix} \dot{b}_1^* \\ \dot{b}_2^* \\ . \\ . \\ . \\ \dot{b}_M^* \end{bmatrix} = -2 \tilde{B} B \left\{ \begin{bmatrix} \overline{x_1 x_1} & \overline{x_1 x_2} & \dots & \overline{x_1 x_M} \\ \overline{x_2 x_1} & \overline{x_2 x_2} & \dots & \overline{x_2 x_M} \\ . & . & . & . \\ . & . & . & . \\ . & . & . & . \\ \overline{x_M x_1} & \overline{x_M x_2} & \dots & \overline{x_M x_M} \end{bmatrix} \begin{bmatrix} b_1^* \\ b_2^* \\ . \\ . \\ . \\ b_M^* \end{bmatrix} + \begin{bmatrix} \overline{x_1 x_0} \\ \overline{x_2 x_0} \\ . \\ . \\ . \\ \overline{x_M x_0} \end{bmatrix} \right\} \quad (\text{II-60})$$

It is easily shown that the sum or average of several nonnegative matrices is also nonnegative. Thus, for example, if

$$\begin{aligned} \tilde{\underline{x}} \underline{A} \underline{x} \geq 0, \quad \tilde{\underline{x}} \underline{B} \underline{x} \geq 0, \quad \tilde{\underline{x}} \underline{C} \underline{x} \geq 0, \quad \text{then} \\ \tilde{\underline{x}} \underline{A} \underline{x} + \tilde{\underline{x}} \underline{B} \underline{x} + \tilde{\underline{x}} \underline{C} \underline{x} = \tilde{\underline{x}} \left[\underline{A} \underline{x} + \underline{B} \underline{x} + \underline{C} \underline{x} \right] = \tilde{\underline{x}} \left[\underline{A} + \underline{B} + \underline{C} \right] \underline{x} \geq 0 \end{aligned} \quad (\text{II-61})$$

The matrix in equation (II-60) is of the form $\underline{x} \tilde{\underline{x}}$, and is therefore symmetric and nonnegative, showing that the parameter adjustment scheme represented by equation (II-56) is indeed stable.

Although the matrix $\underline{x} \tilde{\underline{x}}$ is always singular, the averaged matrix $\overline{\underline{x} \tilde{\underline{x}}}$ is not in general so, inasmuch as the sum or average of several singular matrices is not in general singular. Thus, unless measured data is degenerate in the sense that the x_i 's are linearly related to each other, the matrix in equation (II-60) is normally positive definite, and the parameter adjustments converge exponentially.

Comparing equation (II-59) with equation (II-43), it is seen that the parameter adjustments are stable either with or without averaging. However, the solution converges exponentially with averaging, whereas little may be said about the nature of convergence without averaging. Thus, when averaging is not used, the adjustments may be very lightly damped, and

may oscillate for a substantial period of time unless careful design procedures are used. On the other hand, doubling the adjustment rates of all parameters in equation (II-60) would not change the nature of the solution, but would simply cut the time scale in half. Thus, it would theoretically be possible to converge to the solution in an arbitrarily short period of time, simply by raising the integrator gains high enough, provided the complexity of implementing equation (II-60) could be tolerated. Of course, the benefits of such a rapid solution may not normally be realized, due primarily to the extensive averaging time required to make equation (II-55) valid.

So far, the analysis has been based either upon very great averaging time, or upon no averaging at all. Inasmuch as averaging time must be limited in any practical application, it is of interest to consider the case of finite averaging time. If equation (II-43) had been based upon quantities averaged over a finite period of time, a form identical to equation (II-60) would have been obtained, except that each quantity would be averaged for a finite time only. Thus,

$$\dot{\underline{b}}^* = - (\tilde{\underline{B}} \underline{B}) \overline{\underline{e} \underline{x}} \quad (\text{II-62})$$

where the averaging is now performed over a finite interval of time. Substituting equation (II-62) into equation (II-42)

$$\dot{\underline{V}} = - 2 (\underline{b}^* - \underline{b}) \overline{\underline{e} \underline{x}} \quad (\text{II-63})$$

Inasmuch as the averaging was performed in such a way that \underline{b}^* and \underline{b} could be treated as constants with respect to the averaging process,

$$\dot{\underline{V}} = - 2 \overline{(\underline{b}^* - \underline{b}) \underline{x}} = - 2 \overline{\underline{e}^2} \leq 0. \quad (\text{II-64})$$

Hence, the adjustment is stable for finite averaging time.

The adjustment specified by equation (II-63) is always stable, but inasmuch as finite averages are not entirely constant, the solution will not be exactly exponential. One way to obtain exponential convergence with finite averaging would be to stop taking data during the parameter adjustments, so that even finite averages would be constant.

As the parameters approach their final values, their derivatives approach zero, and \underline{b}^* becomes a null vector. Equations (II-60) and (II-63) then become conventional sets of correlation equations which may be solved explicitly for the \underline{b} vector, much the same as equation (II-31) degenerated into equation (II-32) in the case of solving linear simultaneous equations. Thus, one might say that the reason equations (II-60) and (II-63) may be made to converge in an arbitrarily short period of time is that the data

contained in the correlation functions at each instant of time are sufficient to obtain an immediate solution explicitly, whereas no such statement may be made regarding the smaller amount of stored data required to implement equation (II-43).

Contrails

APPENDIX III

NOISE ANALYSIS

Sensor noise results in two types of errors in parameter estimates: bias and variance. Bias is an error in the average value of an estimate, and variance is a measure of the amount by which the estimate fluctuates about the average. The analytical results derived in this Appendix verify qualitatively the results obtained from simulations reported in Section 4. In general, sensor noise tends to drive the parameters toward zero, but at the same time increases the variance. As in Appendix II, the state space approach is used.

The state of a system consists of a minimum set of state variables which contains sufficient information to describe the present and future outputs. Consider a linear time invariant system written in the form

$$\dot{\underline{x}} + \underline{K}\underline{x} = \underline{A}\underline{u} \quad (\text{III-1})$$

where M by 1 matrix \underline{x} describes the state of the system; \underline{K} and \underline{A} are M by M and M by N matrices; and \underline{u} is the N by 1 matrix, representing N control inputs from external sources.

A matrix \underline{K} and the associated quadratic form $\tilde{\underline{x}} \underline{K} \underline{x}$ are said to be positive definite if the quadratic form is real and is >0 for all real $(x_1, x_2, \dots, x_M) \neq (0, 0, \dots, 0)$. A symmetric matrix \underline{K} is positive definite if (and only if) there exists a real matrix \underline{B} such that

$$\underline{K} = \tilde{\underline{B}} \underline{B} \quad (\text{III-2})$$

where $\tilde{\underline{B}}$ is the transpose of \underline{B} .

BIASING ERRORS

If the dynamics of a system are expressed by a set of linear differential equations in terms of measurable variables, the error output $e(t)$ of the SIDAC model of Figure 64 becomes

$$e(t) = \sum_{j=1}^3 b_j^* x_j + x_0 \quad (\text{III-3})$$

where b_j^* coefficients are the estimated values of the actual b_j coefficients. If the estimated values are exact equation (III-3) becomes

$$0 = \sum_{j=1}^3 b_j x_j + x_0 \quad (\text{III-4})$$

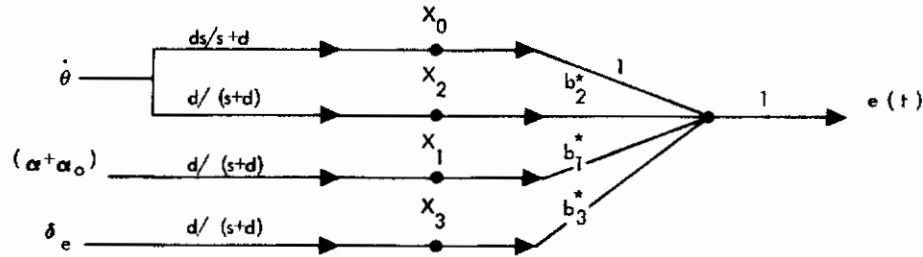


Figure 64. SIDAC Model (Pitch Axis)

By choosing $\dot{\underline{b}}^*$ as

$$\dot{\underline{b}}^* = -K e(t) \underline{x} \quad (\text{III-5})$$

with $\dot{\underline{b}}^* = \begin{bmatrix} \dot{b}_1^* \\ \dot{b}_2^* \\ \dot{b}_3^* \end{bmatrix}$ and $\underline{x} = \begin{bmatrix} x_1 \\ x_2 \\ x_3 \end{bmatrix}$ where K is a symmetric positive definite

matrix, then there exists a real nonsingular matrix B such that $K = \tilde{B} B$.

$$\dot{\underline{b}}^* = -\tilde{B} B e(t) \underline{x} \quad (\text{III-6})$$

$$= -\tilde{B} B \left[\sum_{j=1}^3 b_j^* x_j + x_0 \right] \underline{x} \quad (\text{III-7})$$

The bias of SIDAC is primarily due to sensor noise. With the presence of the sensor noise n , equation (III-7) yields, after adjustment, $E[\dot{\underline{b}}^*] = 0$, where $E[\dot{\underline{b}}^*]$ is the expected value of $\dot{\underline{b}}^*$.

$$E[\dot{\underline{b}}^*] = -\tilde{B} B E \left[\sum_{j=1}^3 b_j^* (x_j + n_j) + (x_0 + n_0) \right] \left[\underline{x} + \underline{n} \right] \quad (\text{III-8})$$

$$= -\tilde{B} B E \left[\tilde{b}^*(\underline{x} + \underline{n}) + x_0 + n_0 \right] \left[\underline{x} + \underline{n} \right] = 0 \quad (\text{III-9})$$

It follows that

$$\begin{aligned} E \left[\tilde{b}^*(\underline{x} + \underline{n}) + x_o + n_o \right] \left[\underline{x} + \underline{n} \right] \\ = E \left[x_o \underline{x} + \tilde{b}^*(\underline{x} + \underline{n}) (\underline{x} + \underline{n}) + x_o \underline{n} + n_o \underline{x} + n_o \underline{n} \right] = 0. \end{aligned} \quad (\text{III-10})$$

Assume the noise from each sensor is uncorrelated with the signal and with all other noise sources. If the \underline{b}^* parameters are slowly varying with respect to \underline{x} and \underline{n} ,

$$E \left[\underline{x}_o \underline{x} \right] + E(\underline{\tilde{x}\tilde{x}}) \underline{b}^* E(\underline{\tilde{n}\tilde{n}}) \underline{b}^* = 0. \quad (\text{III-11})$$

After transposing,

$$\overline{x_o \tilde{x}} + \tilde{b}^*(\underline{\tilde{x}\tilde{x}}) + \tilde{b}^* \underline{\tilde{n}\tilde{n}} = 0. \quad (\text{III-12})$$

The notation $x_o \underline{\tilde{x}}$ is used instead of $E \left[x_o \underline{\tilde{x}} \right]$ and so on.

Let

$$X = \underline{\tilde{x}\tilde{x}} = \begin{bmatrix} \overline{x_1 x_1} & \overline{x_1 x_2} & \overline{x_1 x_3} \\ \overline{x_2 x_1} & \overline{x_2 x_2} & \overline{x_2 x_3} \\ \overline{x_3 x_1} & \overline{x_3 x_2} & \overline{x_3 x_3} \end{bmatrix} = \tilde{X} \quad (\text{III-13})$$

since $\overline{x_i x_j} = \overline{x_j x_i}$.

Similarly denote N as

$$N = \underline{\tilde{n}\tilde{n}} = \begin{bmatrix} \overline{n_1^2} & 0 & 0 \\ 0 & \overline{n_2^2} & 0 \\ 0 & 0 & \overline{n_3^2} \end{bmatrix} = \tilde{N} \quad (\text{III-14})$$

Using equations (III-13) and (III-14), equation (III-11) becomes

$$(X + N) \underline{b}^* + \overline{x_o \underline{x}} = 0 \quad (\text{III-15})$$

$$\underline{b}^* = - (X + N)^{-1} \overline{x_o \underline{x}} \quad (\text{III-16})$$

If no noise is present, equation (III-15) becomes

$$X \underline{b} + \overline{x_o \underline{x}} = 0. \quad (\text{III-17})$$

Subtracting equation (III-17) from equation (III-15)

$$X(\underline{b}^* - \underline{b}) + N \underline{b}^* = 0. \quad (\text{III-18})$$

Hence, it follows from equations (III-18) and (III-16) that

$$\underline{b}^* - \underline{b} = -X^{-1} N \underline{b}^* = X^{-1} N (X + N)^{-1} \overline{x_o \underline{x}}. \quad (\text{III-19})$$

For low noise case, $(X + N) \approx X$. Therefore, equation (III-19) can be approximated as

$$\underline{b}^* - \underline{b} = X^{-1} N X^{-1} \overline{x_o \underline{x}}. \quad (\text{III-20})$$

Since

$$N^{-1} = \begin{bmatrix} \frac{1}{n_1^2} & 0 & 0 \\ 0 & \frac{1}{n_2^2} & 0 \\ 0 & 0 & \frac{1}{n_3^2} \end{bmatrix}^{-1} = \begin{bmatrix} \frac{1}{n_1^2} & 0 & 0 \\ 0 & \frac{1}{n_2^2} & 0 \\ 0 & 0 & \frac{1}{n_3^2} \end{bmatrix} \quad (\text{III-21})$$

$$N^{-1} X = \begin{bmatrix} \frac{1}{n_1^2} & 0 & 0 \\ 0 & \frac{1}{n_2^2} & 0 \\ 0 & 0 & \frac{1}{n_3^2} \end{bmatrix} \begin{bmatrix} \overline{x_1 x_1} & \overline{x_1 x_2} & \overline{x_1 x_3} \\ \overline{x_1 x_2} & \overline{x_2 x_2} & \overline{x_3 x_3} \\ \overline{x_1 x_3} & \overline{x_2 x_3} & \overline{x_3 x_3} \end{bmatrix}$$

$$= \begin{bmatrix} \frac{\overline{x_1 x_1}}{\overline{n_1^2}} & \frac{\overline{x_1 x_2}}{\overline{n_1^2}} & \frac{\overline{x_1 x_3}}{\overline{n_1^2}} \\ \frac{\overline{x_1 x_2}}{\overline{n_2^2}} & \frac{\overline{x_2 x_2}}{\overline{n_2^2}} & \frac{\overline{x_2 x_3}}{\overline{n_2^2}} \\ \frac{\overline{x_1 x_3}}{\overline{n_3^2}} & \frac{\overline{x_2 x_3}}{\overline{n_3^2}} & \frac{\overline{x_3 x_3}}{\overline{n_3^2}} \end{bmatrix} = \underline{\underline{\gamma}}$$

which is the signal to noise ratio matrix $\underline{\underline{\gamma}}$.

$$\underline{\underline{X}}^{-1} \underline{\underline{N}} = (\underline{\underline{N}}^{-1} \underline{\underline{X}})^{-1} = \underline{\underline{\gamma}}^{-1} \quad (\text{III-22})$$

Combining equations (III-20) and (III-22) yields

$$\underline{\underline{b}}^* - \underline{\underline{b}} = \underline{\underline{\gamma}}^{-1} \underline{\underline{X}}^{-1} \underline{\underline{x_0 \underline{\underline{x}}}} \quad (\text{III-23})$$

On the other hand, $(\underline{\underline{X}} + \underline{\underline{N}})^{-1} \approx \underline{\underline{N}}^{-1}$ for high noise case and equation (III-16) becomes

$$\underline{\underline{b}}^* \approx -\underline{\underline{N}}^{-1} \underline{\underline{x_0 \underline{\underline{x}}}} \quad (\text{III-24})$$

From equation (III-24), it is observed that high noise has the tendency to drive all $\underline{\underline{b}}^*$ parameters toward zero.

If only the j th parameter is varied, and the remaining parameters are kept constant, then equation (III-4) can be rewritten as

$$\underline{\underline{x_0}} + \underline{\underline{\tilde{b}}^* \underline{\underline{x}}} + (\underline{\underline{b}}_j - \underline{\underline{b}}_j^*) \underline{\underline{x}}_j = 0 \quad (\text{III-25})$$

The above equation is post-multiplied by the matrix $\underline{\underline{\tilde{x}}}$ and is averaged to obtain equation (III-26)

$$\underline{\underline{x_0 \underline{\underline{\tilde{x}}}}} + \underline{\underline{\tilde{b}}^* \underline{\underline{x \underline{\underline{\tilde{x}}}}}} = -(\underline{\underline{b}}_j - \underline{\underline{b}}_j^*) \underline{\underline{x_j \underline{\underline{\tilde{x}}}}} \quad (\text{III-26})$$

From equations (III-26) and (III-12)

$$(\underline{\underline{b}}_j - \underline{\underline{b}}_j^*) \underline{\underline{x_j \underline{\underline{\tilde{x}}}}} = \underline{\underline{\tilde{b}}^* \underline{\underline{n \underline{\underline{\tilde{n}}}}}} \quad (\text{III-27})$$

or

$$(b_j - b_j^*) \overline{x_j^2} = b_j^* \overline{n_j^2} \quad (\text{III-28})$$

From equation (III-19)

$$\underline{b}^* - \underline{b} = -X^{-1} N \underline{b}^* = -\underline{\gamma}^{-1} \underline{b}^*. \quad (\text{III-29})$$

Then,

$$(\underline{I} + \underline{\gamma}^{-1}) \underline{b}^* = \underline{b} \quad (\text{III-30})$$

where \underline{I} is the identity matrix

or

$$\underline{b}^* = \underline{\gamma} (\underline{I} + \underline{\gamma})^{-1} \underline{b} \quad (\text{III-31})$$

Denote signal to noise ratio by $\gamma = \frac{\overline{x_j^2}}{\overline{n_j^2}}$, which is a special case of the matrix $\underline{\gamma}$,

$$\frac{b_j^* - b_j}{b_j^*} = -\frac{1}{\gamma} \quad (\text{III-32})$$

and

$$\frac{b_j^*}{b_j} = \frac{\gamma}{1 + \gamma} \quad (\text{III-33})$$

Consider the noise-free case. As γ approaches infinity

$$\lim_{\gamma \rightarrow \infty} b_j^* = \lim_{\gamma \rightarrow \infty} \left(\frac{\gamma}{1 + \gamma} \right) b_j = b_j \quad (\text{III-34})$$

It is worth noting specifically that if the noise level increases, γ will decrease and vanish at the limit.

$$\lim_{\gamma \rightarrow 0} b_j^* = 0 \quad (\text{III-35})$$

Referring to Figure 64, the large noise drives all b^* parameters toward zero in order to minimize the mean-squared value of the error $e(t)$.

VARIANCE OF BIASING ERRORS

The variance of biasing errors is a measure of the intensity of the varying a-c component. It is the mean-squared value of the errors about the mean.

The variance of b^* parameters of SIDAC is defined as

$$\sigma_{b^*}^2 = \Sigma (b_j^* - \bar{b}_j^*)^2 = \overline{\tilde{b}^* \tilde{b}^*} - \bar{\tilde{b}^*} \bar{\tilde{b}^*} \quad (\text{III-36})$$

Transposing equation (III-20) gives

$$\tilde{b}^* = \tilde{b} + \tilde{x}_0 \tilde{x}^{-1} \tilde{N} \tilde{X}^{-1} \quad (\text{III-37})$$

Therefore,

$$\begin{aligned} \tilde{b}^* \tilde{b}^* &= (\tilde{b} + \tilde{x}_0 \tilde{x}^{-1} \tilde{N} \tilde{X}^{-1}) (\tilde{b} + \tilde{x}^{-1} \tilde{N} \tilde{X}^{-1} \tilde{x}_0 \tilde{x}) \\ &= \tilde{b} \tilde{b} + \tilde{b} \tilde{x}^{-1} \tilde{N} \tilde{X}^{-1} \tilde{x}_0 \tilde{x} + (\tilde{b} \tilde{x}^{-1} \tilde{N} \tilde{X}^{-1} \tilde{x}_0 \tilde{x}) \\ &\quad + \tilde{x}_0 \tilde{x}^{-1} \tilde{N} \tilde{X}^{-1} \tilde{x}^{-1} \tilde{N} \tilde{X}^{-1} \tilde{x}_0 \tilde{x} \end{aligned} \quad (\text{III-38})$$

$$\begin{aligned} \overline{\tilde{b}^* \tilde{b}^*} &= \overline{\tilde{b} \tilde{b}} + \overline{\tilde{b} \tilde{x}^{-1} \tilde{N} \tilde{X}^{-1} \tilde{x}_0 \tilde{x}} + \overline{\tilde{b} \tilde{x}^{-1} \tilde{N} \tilde{X}^{-1} \tilde{x}_0 \tilde{x}} \\ &\quad + \overline{\tilde{x}_0 \tilde{x}^{-1} \tilde{N} \tilde{X}^{-1} \tilde{x}^{-1} \tilde{N} \tilde{X}^{-1} \tilde{x}_0 \tilde{x}} \end{aligned} \quad (\text{III-39})$$

The second term of equation (III-36) yields

$$\begin{aligned} \bar{\tilde{b}^*} \bar{\tilde{b}^*} &= \overline{(\tilde{b} + \tilde{x}^{-1} \tilde{N} \tilde{X}^{-1} \tilde{x}_0 \tilde{x})} \overline{(\tilde{b} + \tilde{x}^{-1} \tilde{N} \tilde{X}^{-1} \tilde{x}_0 \tilde{x})} \\ &= \overline{\tilde{b} \tilde{b}} + \overline{\tilde{b} \tilde{x}^{-1} \tilde{N} \tilde{X}^{-1} \tilde{x}_0 \tilde{x}} + \overline{\tilde{x}^{-1} \tilde{N} \tilde{X}^{-1} \tilde{x}_0 \tilde{x} \tilde{b}} \\ &\quad + \overline{\tilde{x}^{-1} \tilde{N} \tilde{X}^{-1} \tilde{x}_0 \tilde{x} \tilde{x}^{-1} \tilde{N} \tilde{X}^{-1} \tilde{x}_0 \tilde{x}} \end{aligned} \quad (\text{III-40})$$

Subtracting equation (III-40) from equation (III-39)

$$\begin{aligned} \sigma_{b^*}^2 &= \overline{\tilde{b}^* \tilde{b}^*} - \bar{\tilde{b}^*} \bar{\tilde{b}^*} = \overline{\tilde{b} \tilde{b}} - \bar{\tilde{b}} \bar{\tilde{b}} \\ &\quad + \overline{(\tilde{x}_0 \tilde{x}^{-1} \tilde{N} \tilde{X}^{-1} \tilde{x}^{-1} \tilde{N} \tilde{X}^{-1} \tilde{x}_0 \tilde{x})} - \overline{\tilde{x}^{-1} \tilde{N} \tilde{X}^{-1} \tilde{x}_0 \tilde{x} \tilde{x}^{-1} \tilde{N} \tilde{X}^{-1} \tilde{x}_0 \tilde{x}} \end{aligned}$$

$$+ \overline{(\tilde{\underline{b}} \underline{X}^{-1} \underline{N} \underline{X}^{-1} \underline{x}_0 \underline{x})} - \overline{\tilde{\underline{b}} \underline{X}^{-1} \underline{N} \underline{X}^{-1} \underline{x}_0 \underline{x}} \\ + \overline{(\tilde{\underline{b}} \underline{X}^{-1} \underline{N} \underline{X}^{-1} \underline{x}_0 \underline{x})} - \underline{X}^{-1} \underline{N} \underline{X}^{-1} \underline{x}_0 \underline{x} \underline{\tilde{b}} = \sigma_{\underline{b}}^2 + \sigma_{\underline{P}}^2 + 2\Delta$$

where $\underline{P} = \underline{X}^{-1} \underline{N} \underline{X}^{-1} \underline{x}_0 \underline{x}$ (III-42)

and Δ is the covariance between \underline{b}_j and \underline{P} .

From equations (III-20), (III-29), and (III-30),

$$\underline{P} = \underline{b}^* - \underline{b} = -\underline{Y}^{-1} \underline{b}^* = -(\underline{I} + \underline{Y})^{-1} \underline{b} \quad (\text{III-43})$$

$$\sigma_{\underline{P}}^2 = \overline{\tilde{\underline{P}} \underline{P}} - \tilde{\underline{P}} \underline{\tilde{P}} = \overline{\tilde{\underline{b}} (\underline{I} + \underline{Y})^{-1} (\underline{I} + \underline{Y})^{-1} \underline{b}} - \tilde{\underline{b}} (\underline{I} + \underline{Y})^{-1} (\underline{I} + \underline{Y})^{-1} \underline{b} \\ = \overline{\tilde{\underline{b}} (\underline{I} + \underline{Y})^{-1} (\underline{I} + \underline{Y})^{-1} \underline{b}} - \tilde{\underline{b}} (\underline{I} + \underline{Y})^{-1} (\underline{I} + \underline{Y})^{-1} \underline{b} \quad (\text{III-44})$$

If only one parameter of \underline{b}^* is adjusted, equations (III-43) and (III-44) can be simplified as

$$\underline{P} = -\underline{b} \frac{1}{1 + \gamma} \quad (\text{III-45})$$

$$\sigma_{\underline{P}}^2 = \sigma_{\underline{b}}^2 \left\{ \left(\frac{1}{1 + \gamma} \right)^2 \right\} \quad (\text{III-46})$$

Then the variance is

$$\sigma_{\underline{b}^*}^2 = \sigma_{\underline{b}}^2 \left\{ 1 + \frac{1}{(1 + \gamma)^2} \right\} + 2\Delta \quad (\text{III-47})$$

Now let us consider the covariance Δ .

$$\underline{P} = \underline{X}^{-1} \underline{N} \underline{X}^{-1} \underline{x}_0 \underline{x} = (\underline{N}^{-1} \underline{X})^{-1} \underline{X}^{-1} \underline{x}_0 \underline{x} = \underline{Y}^{-1} \underline{X}^{-1} \underline{x}_0 \underline{x} \quad (\text{III-48})$$

$$\Delta = \overline{(\tilde{\underline{b}} \underline{Y}^{-1} \underline{X}^{-1} \underline{x}_0 \underline{x})} - \tilde{\underline{b}} (\underline{Y}^{-1} \underline{X}^{-1} \underline{x}_0 \underline{x}) \\ = \underline{Y}^{-1} \left[\overline{(\tilde{\underline{b}} \underline{X}^{-1} \underline{x}_0 \underline{x})} - \tilde{\underline{b}} (\underline{X}^{-1} \underline{x}_0 \underline{x}) \right] \quad (\text{III-49})$$

Δ will approach zero, as $\gamma \rightarrow \infty$.

$$\lim_{\gamma \rightarrow \infty} \Delta = 0 \quad (\text{III-50})$$

Therefore, σ_{bj}^{2*} approaches σ_{bj}^2 when $\gamma \rightarrow \infty$.

$$\lim_{\gamma \rightarrow \infty} \sigma_{b*}^2 = \lim_{\gamma \rightarrow \infty} \sigma_b^2 \left\{ 1 + \frac{1}{(1 + \gamma)^2} \right\} + \lim_{\gamma \rightarrow \infty} 2\Delta = \sigma_b^2. \quad (\text{III-51})$$

Contrails

Unclassified
Security Classification

FDCL - Capt. Rankine

DOCUMENT CONTROL DATA - R&D		
(Security classification of title, body of abstract and indexing annotation must be entered when the overall report is classified)		
1. ORIGINATING ACTIVITY (Corporate author) North American Aviation, Inc. Space & Information Systems Division Downey, California 90241	2a. REPORT SECURITY CLASSIFICATION Unclassified	
	2b. GROUP N/A	
3. REPORT TITLE SELF-ADAPTIVE FLIGHT CONTROL BY MULTIVARIABLE PARAMETER IDENTIFICATION		
4. DESCRIPTIVE NOTES (Type of report and inclusive dates) Final		
5. AUTHOR(S) (Last name, first name, initial) Shipley, P. P. Engel, A. G., Jr. Hung, J. W.		
6. REPORT DATE May 1965	7a. TOTAL NO. OF PAGES 146	7b. NO. OF REFS 13
8a. CONTRACT OR GRANT NO. AF33(615)-1882 b. PROJECT NO. 8225 c. Task 822501 d.	9a. ORIGINATOR'S REPORT NUMBER(S) AFFDL-TR-65-90 9b. OTHER REPORT NO(S) (Any other numbers that may be assigned this report) N/A	
10. AVAILABILITY/LIMITATION NOTICES Qualified requesters may obtain copies from DDC or the sponsor, FDCL, Wright-Patterson AFB, Ohio. CFSTI and foreign distribution is limited because of report contents identifiable with DOD strategic embargo list.		
11. SUPPLEMENTARY NOTES N/A	12. SPONSORING MILITARY ACTIVITY AF Flight Dynamics Laboratory FDCL Wright-Patterson AFB, Ohio 45433	
13. ABSTRACT <p>An approach to adaptive flight control is described which uses outputs from a relatively simple parameter tracking computer to adjust flight control system parameters. A unique characteristic of the parameter tracking mechanism is the ability to function with almost any type of disturbance as an input, including normal pilot activity, wind turbulence, and oscillations due to control loop instability. This may be accomplished without special test inputs or limit cycles.</p> <p>The ability to function with almost any type of input is a direct consequence of the fact that the airframe is represented in its true form as a multivariable system, thereby accounting for all inputs and outputs. One of the most common reasons for failure of adaptive flight control systems to function properly is that wind turbulence is ignored in performing identification of airframe dynamics. Even if this problem could be ignored, many approaches would still be limited in application because of the difficulty involved in extending basic concepts to coupled axes, such as the lateral axes of an airframe.</p> <p>Stability of the parameter adjustments is verified analytically, and simulation results show that convergence is smooth and fast (about five seconds) in all axes.</p>		

DD FORM 1473
1 JAN 64

Unclassified
Security Classification

Unclassified

Security Classification

14.	KEY WORDS	LINK A		LINK B		LINK
		ROLE	WT	ROLE	WT	ROLE
	Flight Control Self-Adaptive Multivariable Airframe Dynamics Parameter Identification Constant Gain-Times-Control-Surface- Effectiveness Parameter Tracking Computer					

INSTRUCTIONS

1. **ORIGINATING ACTIVITY:** Enter the name and address of the contractor, subcontractor, grantee, Department of Defense activity or other organization (*corporate author*) issuing the report.
- 2a. **REPORT SECURITY CLASSIFICATION:** Enter the overall security classification of the report. Indicate whether "Restricted Data" is included. Marking is to be in accordance with appropriate security regulations.
- 2b. **GROUP:** Automatic downgrading is specified in DoD Directive 5200.10 and Armed Forces Industrial Manual. Enter the group number. Also, when applicable, show that optional markings have been used for Group 3 and Group 4 as authorized.
3. **REPORT TITLE:** Enter the complete report title in all capital letters. Titles in all cases should be unclassified. If a meaningful title cannot be selected without classification, show title classification in all capitals in parenthesis immediately following the title.
4. **DESCRIPTIVE NOTES:** If appropriate, enter the type of report, e.g., interim, progress, summary, annual, or final. Give the inclusive dates when a specific reporting period is covered.
5. **AUTHOR(S):** Enter the name(s) of author(s) as shown on or in the report. Enter last name, first name, middle initial. If military, show rank and branch of service. The name of the principal author is an absolute minimum requirement.
6. **REPORT DATE:** Enter the date of the report as day, month, year, or month, year. If more than one date appears on the report, use date of publication.
- 7a. **TOTAL NUMBER OF PAGES:** The total page count should follow normal pagination procedures, i.e., enter the number of pages containing information.
- 7b. **NUMBER OF REFERENCES:** Enter the total number of references cited in the report.
- 8a. **CONTRACT OR GRANT NUMBER:** If appropriate, enter the applicable number of the contract or grant under which the report was written.
- 8b, 8c, & 8d. **PROJECT NUMBER:** Enter the appropriate military department identification, such as project number, subproject number, system numbers, task number, etc.
- 9a. **ORIGINATOR'S REPORT NUMBER(S):** Enter the official report number by which the document will be identified and controlled by the originating activity. This number must be unique to this report.
- 9b. **OTHER REPORT NUMBER(S):** If the report has been assigned any other report numbers (*either by the originator or by the sponsor*), also enter this number(s).
10. **AVAILABILITY/LIMITATION NOTICES:** Enter any limitations on further dissemination of the report, other than those

imposed by security classification, using standard statements such as:

- (1) "Qualified requesters may obtain copies of this report from DDC."
- (2) "Foreign announcement and dissemination of this report by DDC is not authorized."
- (3) "U. S. Government agencies may obtain copies of this report directly from DDC. Other qualified DDC users shall request through _____."
- (4) "U. S. military agencies may obtain copies of this report directly from DDC. Other qualified users shall request through _____."
- (5) "All distribution of this report is controlled. Qualified DDC users shall request through _____."

If the report has been furnished to the Office of Technical Services, Department of Commerce, for sale to the public, state this fact and enter the price, if known.

11. **SUPPLEMENTARY NOTES:** Use for additional explanatory notes.
12. **SPONSORING MILITARY ACTIVITY:** Enter the name of the departmental project office or laboratory sponsoring (publishing for) the research and development. Include address.
13. **ABSTRACT:** Enter an abstract giving a brief and facsimile summary of the document indicative of the report, even though it may also appear elsewhere in the body of the technical report. If additional space is required, a continuation sheet may be attached.

It is highly desirable that the abstract of classified reports be unclassified. Each paragraph of the abstract shall end with an indication of the military security classification of the information in the paragraph, represented as (TS), (S), (C), or (U).

There is no limitation on the length of the abstract. However, the suggested length is from 150 to 225 words.

14. **KEY WORDS:** Key words are technically meaningful words or short phrases that characterize a report and may be used as index entries for cataloging the report. Key words must be selected so that no security classification is required. Identifiers, such as equipment model designation, trade name, model project code name, geographic location, may be used as key words but will be followed by an indication of technical content. The assignment of links, rules, and weights is optional.

Unclassified

Security Classification